APPLICATIONS OF NEW THERMOPLASTIC CFRP REBARS AND MECHANICALLY ANCHORED CARBON FIBRE SHEETS IN REINFORCING AND STRENGTHENING CONCRETE BEAMS

Mossab Wahba W. El-Tahan

A Thesis

in

The Department

of

Building, Civil, and Environmental Engineering

Presented in Partial Fulfillment of the Requirements

for the Degree of Master of Applied Science (Civil Engineering) at

Concordia University

Montréal, Québec, Canada

April 2010

Your file Votre référence
ISBN: 978-0-494-67137-5
Our file Notre référence
ISBN: 978-0-494-67137-5

ABSTRACT

APPLICATIONS OF NEW THERMOPLASTIC CFRP REBARS AND MECHANICALLY ANCHORED CARBON FIBRE SHEETS IN REINFORCING AND STRENGTHENING CONCRETE BEAMS

Mossab Wahba W. El-Tahan

Thermoset fibre-reinforced polymer composite (FRP) rebars and laminates are widely used in reinforcing and strengthening concrete structures due to their advantages such as: corrosion free material, high strength to weight ratio, and electromagnetic resistance. However, thermoset composites have some limitations due to the fact that they cannot be bent once the resin solidifies when used as internal reinforcement (FRP rebars). On the other hand, externally bonded FRP sheets used in strengthening concrete structures is subject to non-ductile failure due to debonding. This emphasizes the need of exploring new methods for reinforcing and strengthening concrete structures.

This thesis evaluates the performance of a new thermoplastic CFRP rebar that can be bent after the resin set and also examines the behaviour of using unbonded mechanically anchored dry carbon fibre (CF) sheets in shear strengthening of concrete T-beams to avoid debonding mode of failure.

Three sets of tests were conducted on the developed CFRP rebars in order to evaluate their mechanical characteristics, minimum development length of the straight rebars, and the tail length of bent rebars. Based on the test results and the modes of failure of the tested specimens, recommendations were proposed to improve the behaviour of the new thermoplastic CFRP rebars. The properties of the newly developed

CFRP rebars were compared to similar thermoset and thermoplastic FRP rebars available in the literature and market.

Three reinforced concrete (RC) T-beams were tested up to failure in four point bending test. One was reserved as control beam, while two beams were strengthened in shear using mechanically anchored dry CF sheets. The tested beams were instrumented with the conventional measuring devices that were connected to a data acquisition system. Moreover, the beam was monitored using acoustic sensors which monitored the acoustic energy activity of the tested beams.

Dedicated to my parents, sister, brothers, and niece.
To my fiancee, with love....

ACKNOWLEDGEMENT

First of all, I wish to express my deepest gratitude and thanks to my supervisors, Dr. K. Galal and Dr. S. Hoa. Their smart questions motivated me to achieve higher level of understanding of my work. Without their encouragement, academic and financial support, this research would not have been completed. Their efforts in reviewing the thesis in a very short time are really appreciated and acknowledged.

I would also like to acknowledge the assistance and technical support during my experimental work of J. Payer, J. Hrib, J. Yeargans, and T. Aldea. Their help, support, and assistance are appreciated.

The AE monitoring part of my experimental work would not have been possible without the collaboration with WavesInSolids LLC (WINS). Their equipments, efforts, and contribution are acknowledged.

I would like to thank Dr. M. Ali for his valuable suggestions and contributions in my experimental work.

I wish to express my acknowledgements to my dear colleagues H. El-Sokkary, H. Seif, M. Sharawy, and E. Elwakil for sincerely supporting me throughout this project. Their valuable contributions and extensive help aided me to accomplish this research. I will forget neither their support, nor their advices. I also want to thank Riccardo Gioia for his tremendous help during summer semesters.

I also would like to extend my sincere gratitude to all my other colleagues namely: Alp, Behnam, Hossein, I. Mashhour, Ihab, Navid, and Nima for helping me to complete my work.

My words cannot express my gratitude to my parents. Their continuous and unyielding love, support and prayers made me stronger to encounter my problems that I had during the last years. I hope that my achievement is a source of pride and happiness for them.

At last but not the least, I would like to thank my beloved fiancee who supported and provided me with indefinite source of motivation. Thank you for your love, motivation and prayers. I thank God for having you in my life.

TABLE OF CONTENTS

LIST OF FIGURES

LIST OF TABLES

LIST OF SYMBOLS AND ABBREVIATIONS

ACI	American Concrete Institute
AE	Acoustic Emission
ASTM	American Standard of Testing and Materials
CF	Carbon Fibre
CFRP	Carbon Fibre-Reinforced Polymers
CONCOM	Concordia Center for Composites
CSA	Canadian Standard Association
d_b	Rebar diameter
FRP	Fibre-Reinforced Polymers
F_{ub}	Ultimate strength of the bent rebars
F_{us}	Ultimate strength of the straight rebars
GFRP	Glass Fibre-Reinforced Polymers
NSM	Near Surface Mounted
RC	Reinforced concrete
V_c	Concrete contribution to the shear strength
V_{cf}	Carbon fibre contribution to the shear strength
V_s	Steel contribution to the shear strength

CHAPTER 1

INTRODUCTION

1.1 Background and Problem Definition

Reinforced concrete bridges are subjected to numerous deterioration conditions because they are exposed to aggressive environmental effects (freeze and thaw cycles, alkali-aggregate reactivity, corrosion of reinforcing steel, de-icing salts, and other chemical attacks). These conditions lead to corrosion of the steel reinforcement that affect the strength and the structural integrity of the reinforced concrete (RC) bridges, resulting in a reduction of the life of the structure. This emphasizes the need of using corrosion free materials such as Fibre-reinforced Polymers (FRP) in constructing and strengthening new and existing structures, respectively, to increase their life and reduce the maintenance cost on the long run.

Thermoset rebars and laminates are widely used in reinforcing and strengthening concrete structures due to their advantages such as: corrosion free material, high strength to weight ratio, and electromagnetic resistance. However, thermoset composites have some limitations due to the fact that they cannot be bent once the resin solidifies when used as reinforcement for concrete structures. Moreover, the FRP laminates used in strengthening of concrete structures are bonded to the concrete surfaces with thermoset resin that are subject to non-ductile failure due to debonding.

Thermoset FRP rebars are produced with the exact required lengths and bents in the factory during the manufacturing process before the resin solidify, unlike the steel rebars. The steel rebars are manufactured as straight bars with a standard length where

they can be cut and bent at the construction site or at machine shops to the desired dimensions. Most of the available FRP rebars in the market are made of thermoset resins such as polyester. These rebars have to be produced with the exact required lengths and bents in the factory during the manufacturing process before the resin solidify. The thermoset rebars cannot be bent once the resin sets due to the brittleness of the material. Moreover, there are some extra limitations to the number of bends per rebar, and the maximum spacing between any two successive bends. Accordingly, lap splices are required to overcome such problems which consume more material and time leading to more cost and less productivity.

On the other hand in the case of existing RC bridges, FRP composites are used in shear strengthening of RC girders by bonding the laminates to the concrete surfaces using epoxy. One of the major problems in such strengthening methods is failure due to debonding which occur due to the inadequate bond length that leads to a brittle failure of the beams. In addition, the epoxy bonded composites need significant effort in preparations prior to applying the composites to the RC structure. Most of the proposed strengthening schemes that use unbonded FRP were able to increase the shear capacity of the beams, while the practicality of strengthening methods was not considered.

1.2 Objectives and Scope of work

In an effort to overcome problems of using thermoset FRP rebars in constructing new structures, researchers supervised by Prof. Hoa at Concordia Center for Composites (CONCOM) at Concordia University, developed new thermoplastic CFRP rebars. These rebars could be bent - by heating - several times after the complete solidification of the

thermoplastic resin. The new CFRP rebar is made of carbon fibres, and bonded together with thermoplastic resin. Three sets of tests were conducted on the developed CFRP rebars in order to evaluate their mechanical characteristics, bond properties of straight rebars, the tail length of bent rebars, and assess the overall performance of the new CFRP rebars.

In order to avoid debonding mode of failure of the FRP laminates, the need of using mechanically anchored strengthening schemes was raised. Moreover, it is required to obtain a strengthening scheme that is easier in terms of manufacturing and surface preparation. A new method in shear strengthening of beams was proposed by Galal and Mofidi (2010), in which carbon fiber (CF) sheets were mechanically anchored to the beam to strengthen beams in shear. The proof-of-concept test showed the effectiveness of the strengthening system, yet it showed that a small portion of the CF stretched and contributed to the shear capacity of the beam. In an effort to maximize and fully utilize the benefits of the high modulus dry CF sheets, the anchorage system was improved to insure the uniformity of the fibres prior to loading. The strains of the CF sheets were monitored along the shear span to have better understanding of the behaviour of the CF sheets. Moreover, the effectiveness of using strips with double layers in strengthening of the T-beams was examined. The tested beams were instrumented with the conventional measuring devices that were connected to a data acquisition system. Moreover, the beam was monitored using acoustic sensors which monitored the acoustic energy activity of the tested beams.

1.3 Organization of the Thesis

This thesis comprises of seven chapters, the first one is an introduction which provides the reader with a background of the topics discussed in this thesis. In addition, the scope of work and the objectives of this thesis are presented in this chapter. Chapter two provides a literature review of the research conducted on similar topics. Chapter three shows the experimental work conducted on testing the thermoplastic CFRP rebars. It describes the materials, the preparation and construction of the specimens, the test setup, and instrumentation. Chapter four discusses and interprets the data and observations obtained during testing of the CFRP rebars. Chapter five discusses the experimental work done on testing of the RC T-beams in shear. This chapter explains the materials, preparation and construction of the specimens and anchorage system, the test setup, and instrumentation. Chapter six reports the results and observations of the RC T-beams tested in shear. Figures, sketches, and tables are provided to present the data and the test observations. Conclusions and recommendation for future work are presented in chapter seven.

CHAPTER 2

LITERATURE REVIEW

2.1 General

It was witnessed in the past few decades that a large number of reinforced concrete structures are deficient. The cost of maintenance and renewal of the deteriorated infrastructures in Canada is estimated by $125 billion to bring the existing structures to an acceptable level (Mirza and Haider, 2003). This raises the need of investing in new structures that can better resist the environmental conditions, need less maintenance cost, and have longer life time. This can be achieved by using FRP materials as reinforcement for new structures. The FRP are non-corrodible materials, have high strength to weight ratio, and are magnetic neutral.

Moreover, the existing RC structures need to be rehabilitated or strengthened using corrosion-free materials to increase the life time of the strengthened structures. In addition to the advantages of the FRP, they are lighter in weight compared to the conventional strengthening materials (steel plates and concrete jackets).

2.2 FRP rebars as reinforcement for new concrete structures

FRP composites are widely used as reinforcement rebars for concrete structures. Unlike the steel that has almost same the properties, FRP rebars produced by different companies. Accordingly, the FRP rebars have different properties which depend on the

type and properties of the fibers and resin used in the manufacturing. Thus, many researches were conducted on new rebars to evaluate their properties.

2.2.1 Thermoset FRP rebars

The bond strength of FRP rebars in concrete was examined by Larralde, and Silva-Rodriguez (1993) through pullout tests. The results were compared to the results of steel rebars. For the same diameter, embedment length, and concrete strength, the steel had higher bond strength than the FRP rebars. All the FRP rebars failed by pullout, however the modes of failure could not be identified due to the limited number of the specimens. It was observed that the slip at failure for FRP rebars was greater than that of steel for the same diameter, embedment length, and concrete strength.

Castro F. And Carino N.(1998) carried out a study to support the development of standard test methods that can be used to identify the properties of FRP rebars. This study examined: the effect of the ratio of the free length to rebar diameter on the tensile strength, the possibility of measuring the dynamic modulus using a non destructive test method. It was found that within values of 40 to 70 d_b of the free length to the rebar diameter, there is no effect on the tensile strength of the FRP rebars. It was recommended that the manufacturer of the FRP rebar should provide the value of the ultimate force of the rebar rather than the ultimate stress because the non-uniform cross section of the FRP rebars.

Benmokrane et al. (2002) tested two types of newly developed CFRP rebars: sand coated CFRP rebars, and ribbed CFRP rebars. The new rebars were tested to evaluate their mechanical properties and bond strength throughout tensile tests and pullout tests,

respectively. The properties of the new rebars were compared to the properties of the steel rebars. The tensile strength, modulus of elasticity, and minimum development length of the sand coated rebar was 1536 MPa, 128 GPa, and 20 times the rebar diameter (20 d_b), respectively. While the values were 2138 MPa, 145 GPa, and 30 d_b for the ribbed rebar.

Seventy nine specimens were tested in tension by Micelli and Nanni (2003) to propose an effective tensile test method to characterize the mechanical properties of FRP rebars. Twelve types of FRP rebars with different sizes were tested up to failure to evaluate the proposed method. The rebars were tested in tension by putting the rebars in steel tubes which were filled with expansive grout. The new method depends on bearing forces rather than gripping forces to transmit the machine force to the FRP rebar. Figure 2.1 shows the test setup of the proposed test method. The results and test observations showed that the expansive grout anchors can replace the epoxy resin. No damage in the anchoring steel sleeves was observed due to the gripping forces. There was no effect on the tensile strength when the ratio of the rebar length to diameter less than 36. Moreover, the cross section shape and roughness of the rebars can affect significantly the bond strength between the FRP rebar and the grout.

An exploratory study was conducted by Moon et al. (2007) on new GFRP rebars. The new GFRP rebars were designed to develop better mechanical anchorage with concrete by applying milled glass fibres to the surface of the rebars. Different amounts of milled glass fibres contents were applied ranging from 20% to 50%. The properties of the new rebars were examined by testing the rebars in compression, tension, and pullout. Moreover, the long term durability of the rebars was evaluated. The tensile strength

ranged from 592 to 1000 MPa, while the elastic modulus ranges from 44.5 to 54.8 GPa. The bond strength of the rebars increases with the increase of the amount of milled glass fibres, and 10% less than the bond strength of steel rebars. The long term durability of the GFRP rebars showed that it is not affected by amount of the milled glass fibres.

El-Sayed et al. (2007) conducted experimental tests to develop new CFRP stirrups as shear reinforcement for new structures. Two types of tests were conducted on different CFRP rebars with different fibre content and manufacturing process: the B.12, and B.5 test methods of the ACI 400.3R-04. The first method was used to identify the best type of rebars that can be considered for B.5 tests. The selected type of rebars was tested with different end anchorage types to simulate the behaviour of the CFRP stirrups in concrete. The effect of the tail length, bar diameter, embedment length, and stirrup anchorage were examined. It was found that the continuous anchorage of CFRP stirrups has higher strength than the standard hook anchorage type. A development length of 20 d_b was sufficient to develop the full strength of the CFRP stirrup, while a tail length of 6 d_b was able to develop the stirrup capacity. Moreover, the size of the stirrups had no effect on the performance of the stirrup.

A comparison between the B.12 and B.5 test methods of the ACI 440.3R-04 were examined by Ahmed et al. (2010). Three different sizes of GFRP rebars (No. 10, 16, and 19) and one size (No.10) of CFRP rebars were tested in this study. The results showed that the B.12 test method underestimate the stirrups bend strength compared to the B.5 test method. The bent strength evaluated using the B.5 test method was 30 to 40 % more than the B.12 test method. It was mentioned that the B.12 test method may not be suitable for rebars that have ribs or indentations. The stirrups will bear on the ribs and cause stress

concentration that will alter the bend strength. And thus, it is recommended to use the B.12 test method as a preliminary evaluation of the bent strength.

The available standard test methods simulate behaviour of the stirrups in concrete by embedding the stirrup in two concrete blocks, which were pushed against each other. In such tests, the FRP stirrups are loaded in reality with an inclined force to the fibers directions i.e. the FRP stirrups usually placed perpendicular to the axis of the beam, not to the cracks. Shehata et al. (2000) tested 52 especially designed specimens to examine the effect of the inclination angle of the stirrup, material type, bar diameter, bend radius, the configuration of the stirrup anchorage, and the tail length beyond the bend portion. Figure 2.2 shows the panel specimens. Shehata et al. (2000) concluded that the bend radius of the FRP stirrups should be bigger than or equal to 4 times the rebar diameter, and the tail length after the bent portion should be bigger than or equal to 70mm or 6 d_b whichever is greater. By following the previous conditions, the strength of the bent stirrups should be at least 50 % of the strength of the straight stirrups. The study showed that there is no understandable relation between the change in the crack angle and the strength of the GFRP and CFRP stirrups.

2.2.2 Thermoplastic FRP rebars

Although FRP rebars offer several advantages with respect to corrosion resistance, they still have some limitations. One of the practical problems is rebar bending. In case of steel rebars, they are manufactured as straight bars with a certain length where they can be cut and bent at the construction site or at a local supplier to the desired dimensions. Most of the available FRP rebars in the market are made of

thermoset resins such as polyester. The rebars have to be produced with the exact required lengths and bends in the factory during the manufacturing process before the resin solidifies. The thermoset rebars cannot be bent once the resin sets due to the brittleness of the material. Moreover, there are some extra limitations to the number of bends per rebar, and the maximum spacing between any two successive bends. Accordingly, lap splices are required to overcome such problems which consume more material (Figure 2.3) and time leading to more cost and less productivity. This raises the need of developing bendable rebars that can be used as shear stirrups, or bent to develop the sufficient end anchorage for flexural reinforcement. However a limited number of thermoplastic FRP rebars were developed in the past.

A new thermoplastic GFRP rebar was tested by Mehrabi et al. (2003). Different mechanical, geometrical, and surface treatment were examined. Tensile strength test and bond tests were conducted to evaluate their properties. The tensile strength, modulus of elasticity, and bond strength of the new thermoplastic GFRP rebars were 827 to 1034 MPa, 37.9 to 51.7 GPa, and 8.3 to 15.2 MPa, respectively.

Another thermoplastic FRP rebar was examined by Currier et al. (1994). Two different rebars were examined: Aramid/Nylon, and Carbon/Nylon where the fibre volume was 50 %. Both had a rectangular cross section with dimensions of 2.4 mm x 7.1 mm. The FRP stirrups were bent to dimensions of 560 mm x 75 mm using a heat gun. The bend strength of the thermoplastic FRP stirrups was evaluated by putting the stirrup in two concrete blocks and applying a relative displacement between them. This test method is similar to the B.5 test method of the ACI 440.3R-04 but with two FRP stirrups.

The strength of the bent rebar was 23% the strength of the straight rebar. The reported mode of failure was due to the stress concentration of the bent stirrup.

2.2.3 Summary

One of the practical problems of the thermoset rebars is rebar bending. Moreover, there are some additional limitations regarding the maximum number of bends per rebar, and the maximum spacing between any two successive bends for manufacturing pultruded rebars using thermoset resins. Accordingly, lap splices are required to overcome such problems which consume more material. However, a limited number of thermoplastic FRP rebars were developed in the past.

2.3 Shear Strengthening of beams

Many existing bridges were designed according to the pre-1970s codes in which they overestimated the concrete shear strength (Higgins et al. 2007). Moreover, these bridges have deteriorated because the lack of quality control at that time leading to high permeability concrete. Also, the later old codes recommended a nominal concrete cover of 25mm (Amleh and Mirza 2004). The small cover along with the permeable concrete lead to rapid corrosion of the steel reinforcement of the RC girders (Figures 2.4 and 2.5).

The deteriorated bridges need to be strengthened using non corrosive materials such as FRP laminates. And the shear failure of reinforced concrete beams is brittle and sudden compared to the flexural failure where the RC beams provide sufficient warning before failure. And thus, strengthened RC beams should be designed such that the shear strength is greater than the flexural strength of the RC beam to obtain a ductile failure.

This can be achieved by identifying and understanding the shear modes of failure of the strengthened RC beams. The modes of failure of the beams strengthened in shear using FRP composites are: FRP debonding, FRP rupture, or failure of the concrete.

2.3.1 Shear strengthening using bonded FRP

Christophe and Cheng (2001) conducted an experimental test on eight RC T-beams strengthened in shear using CFRP sheets (Figure 2.6). This study investigated the interaction between the bonded FRP sheets and the internal steel stirrups in the shear carrying capacity. It was found that the contribution of the bonded FRP sheets varies with the intensity of the internal steel stirrups. The higher the internal steel stirrups the less the effectiveness of the FRP sheets. It was noted that the bonded FRP sheets can reduce the shear capacity by changing the crack path.

Zhang and Hsu (2005) examined the shear behaviour of 11 RC rectangular beams strengthened in shear using FRP sheets and strips in different strengthening schemes. It was found that the behaviour of the FRP sheets and strips are totally different. The FRP sheets failed by rupture, while the FRP strips failed by spalling of the concrete cover underneath the epoxy.

Twenty rectangular RC beams were strengthened using two different shear strengthening techniques to investigate their effectiveness (Barros et al. 2007). The beams were strengthened with epoxy bonded reinforcing and Near Surface Mounted (NSM) techniques. The NSM technique was more effective than the epoxy bonded technique, and exhibited better deformation capacity compared to the epoxy bonded

method. It was observed that the shear failure of Epoxy bonded method was brittle compared to the NSM method.

Sundarraja and Rajamohan (2009) investigated the influence of the width, spacing, angle of inclination, and the spacing of the internal reinforcement on the shear capacity of RC rectangular beams strengthened in shear using GFRP sheets. Two different methods were used: U-jacketing and strips of GFRP sheets on the sides of the beam. The results showed that strengthening with strips of U-jackets method was more effective than the strips bonded only to the sides. By increasing the width of the GFRP, the shear strength was increased. The inclined GFRP strips prevented the shear cracks from growing, and a significance influence on the cracking load was observed. Moreover, the beams strengthened using inclined strips exhibited better load-deflection relationship.

Different strengthening schemes were examined by Adhikary and Mutsuyoshi (2004). The study investigated the shear strength of RC rectangular beams strengthened with externally bonded CFRP sheets. The strengthened methods are shown in Figure 2.7. It was noted that the strength of the beam strengthened with full U-jackets with vertical oriented fibres was the greatest strength among the tested beam. The beam strengthened with one and two layers of horizontally aligned FRP sheets increased the shear strength by 28.8 % and 62.2 %, respectively compared to the control beam. It was also observed that strengthening RC beams with FRP sheets with the maximum depth of the concrete section is preferred.

Adhikary et al. (2004) investigated the effect of bonded anchorage of FRP sheets to the shear strength of RC rectangular beams. The bonded anchorage FRP sheets were bonded with different lengths to the top face of the RC beams. The different wrapping

configurations are shown in Figure 2.8. It was found that the proposed bonded anchorage method was more effective than the U-jackets method. Moreover, the interface bond strength was reduced and the strain in the FRP sheets was increase allowing the beam to fail at higher shear strengths.

Cao et al. (2005) investigated the strain distribution of the FRP sheets, which were bonded to pre-cracked rectangular RC beams tested in shear. The strain gauges were mounted on FRP sheets in the location of the shear crack. It was concluded that the strain distribution was uneven, and hence need more investigation for the bonded FRP sheets.

Leung et al. (2007) investigated the size effect on shear strength of RC beams strengthened with FRP jackets and full wrapping. Three different sizes of thickness were tested: 180 mm, 360 mm, and 720 mm. The results showed that beams with beams with different depths of 360 and 720 mm strengthened using U- jackets had increase in the shear strength lower than beams with thickness of 180 mm. While the complete wrapping showed similar increase in the shear capacity of the different sizes. Figure 2.9 shows the debonding failure of beams tested by Leung et al.

2.3.2 Shear strengthening using anchored bonded FRP

Eshwar et al. (2008) examined the performance concrete T-beams strengthened using bonded FRP with two anchor systems. Eshwar et al. studied the different variables that can affect the strength of the two proposed anchors. Figure 2.10 shows the two anchoring systems.

2.3.3 Shear strengthening using dry unbonded FRP

Shear strengthening using bonded FRP composites show good results, however in practice the bonded FRP composites will debond due to the weak concrete cover of the deteriorated structures. The bonded FRP methods are efficient in strengthening relatively new structures where the concrete cover did not deteriorate yet.

In an effort to avoid that, Lees et al. (2002) investigated the effectiveness of strengthening RC T-beams using dry unbonded external prestressed CFRP straps. As shown in Figure 2.11 the CFRP straps were wounded around the concrete beams passing through pre-grooved holes in the concrete. The outer layer was bonded to the second outermost layer, and then the straps were prestressed. The strengthened beams failed at higher loads than the unstrengthened ones.

Kees and Lees (2007) extended the research above mentioned by testing 12 RC cantilever beams. The study examined the effect of prestress level, the numbers of layers of the dry CFRP straps, and the strap spacing. The test results indicated that there is a relation between the studied factors, and more beams need to be tested for better understanding of the behaviour of the new system. Kees and Lees mentioned that if the proper initial prestress level, the numbers of layers of the CFRP straps, and the strap spacing were chosen; the ultimate capacity of the beams would have reached 90 % higher than the control beam.

Hoult and Lees (2009) investigated the shear behaviour of the RC T-beams strengthened in shear using the similar methods of Kees and lees (2007) and Lees et al. 2002). The method was improved to allow installing the strengthening system from underneath the concrete slab. The new method is shown in Figure 2.12. According to the

test observations, it was found that the FRP strap should be as close as possible to the concrete flange otherwise the shear cracks can pass above the straps. It was noticed that when the loading pads were smaller than the width of the beam, a premature failure occurred. Moreover, the cracks started from the unfilled holes in the compression flanges.

2.3.4 Shear strengthening using anchored unbonded dry Carbon Fibres

Galal and Mofidi (2010) proposed a new method for shear strengthening by using mechanically anchored unbonded dry CF sheets. The new method exhibited a satisfactory manner up to failure. However a small portion of the CF sheets were activated and contributed to the shear strength of the beam. Figure 2.13 shows the new method used by Galal and Mofidi (2010).

2.3.5 Summary

Shear strengthening using bonded FRP composites show good results, however in practice the bonded FRP composites will debond due to the weak concrete cover of the deteriorated structures. The bonded FRP methods are efficient in strengthening relatively new structures where the concrete cover did not deteriorate yet.

The unbonded shear strengthening methods proposed by Lees et al. (2002, 2007, and 2009) are unpractical and harder to install than the conventional bonded FRP systems. In an effort to solve such problem, researchers led by Dr. Galal at Concordia University proposed a new method that is easier to install, require less surface preparation and adhesive, and eliminates the peel-off and debonding modes of failure. Only one beam

was tested as proof of concept. Therefore more specimens need to be tested to evaluate the new strengthening method.

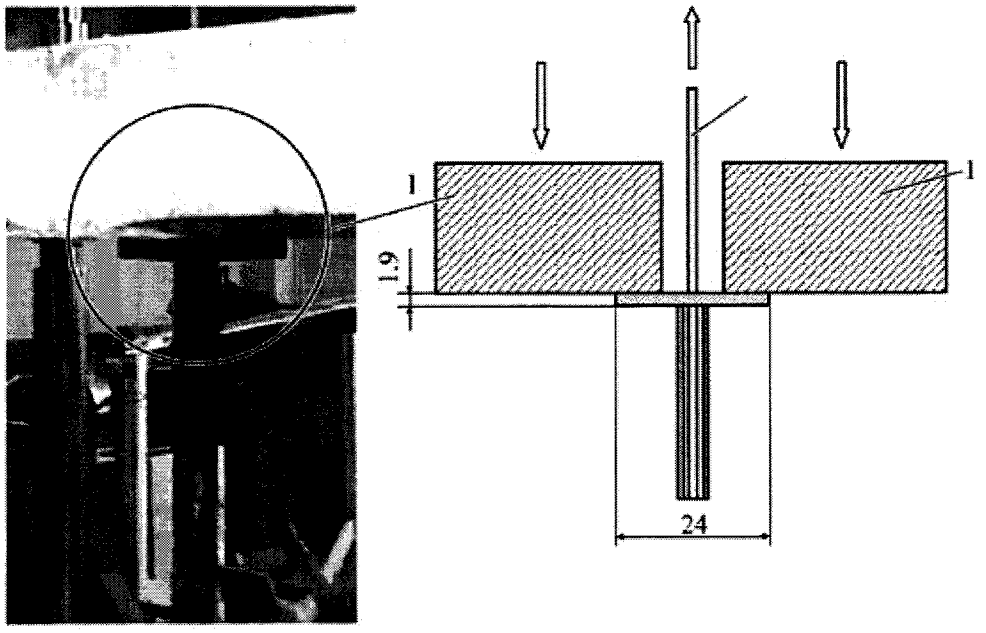

Figure 2.1 Proposed test method by Micelli and Nanni (2003)

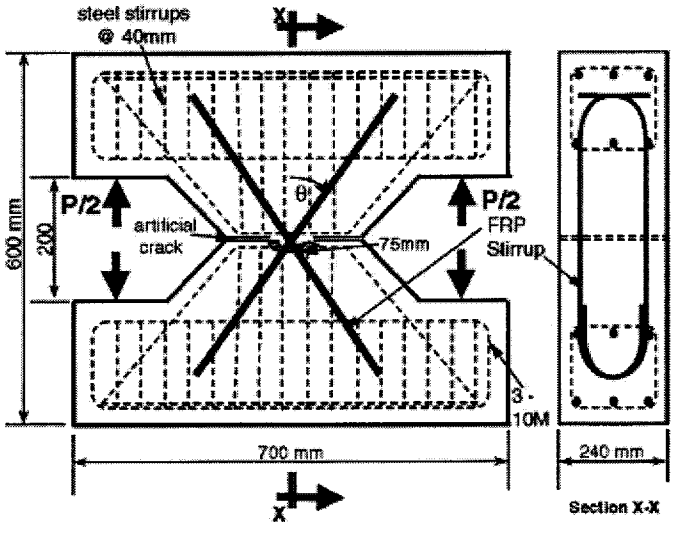

Figure 2.2 Concrete panels tested by Shehata et al. (2000)

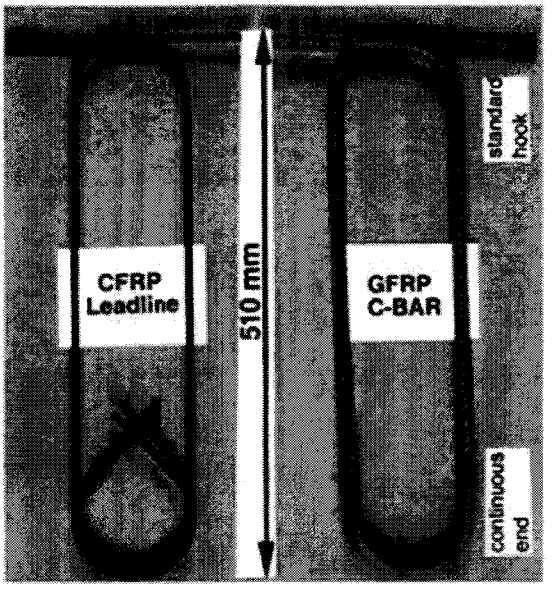

Figure 2.3 Overlapped FRP stirrups (Shehata et al., 2000)

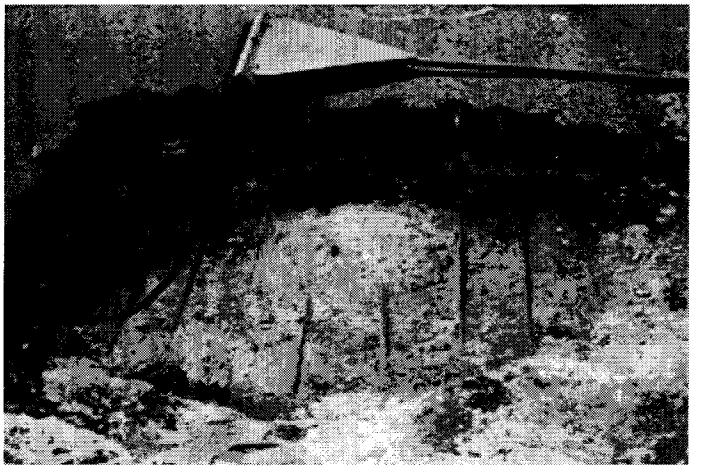

Figure 2.4 Deteriorated concrete cover (Amleh and Mirza, 2004)

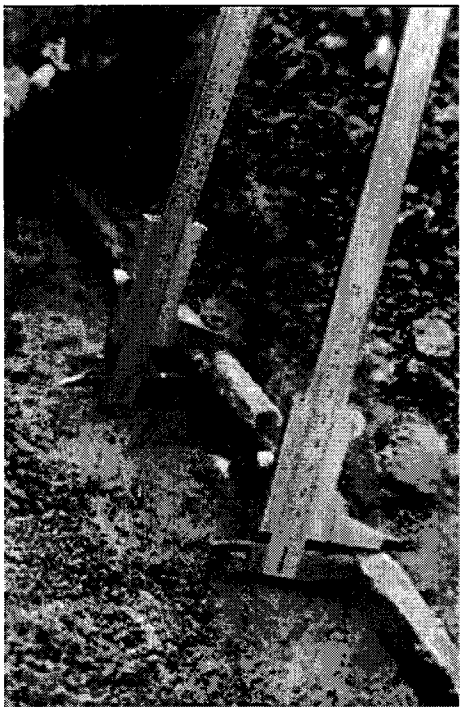

Figure 2.5 Corrosion of steel reinforcement in concrete bridge (Amleh and Mirza, 2004)

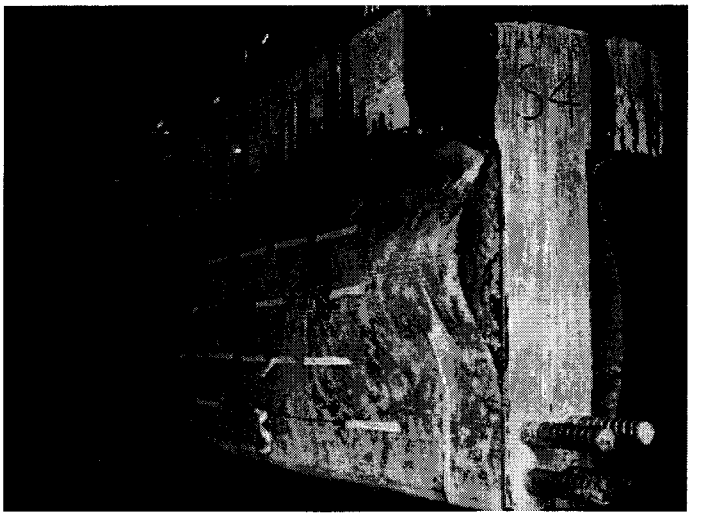

Figure 2.6 Debonded FRP sheets (Daniaud and Cheng, 2001)

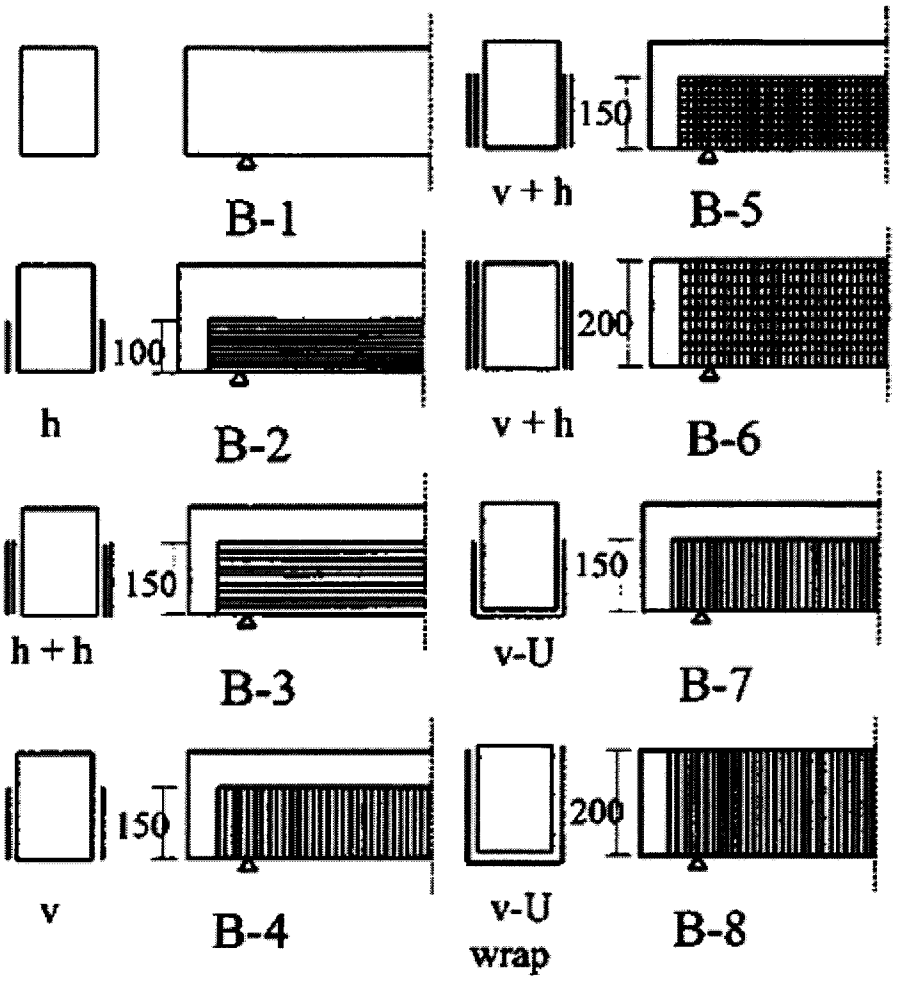

Figure 2.7 Strengthening schemes tested by (Adhikary and Mutsuyoshi, 2004)

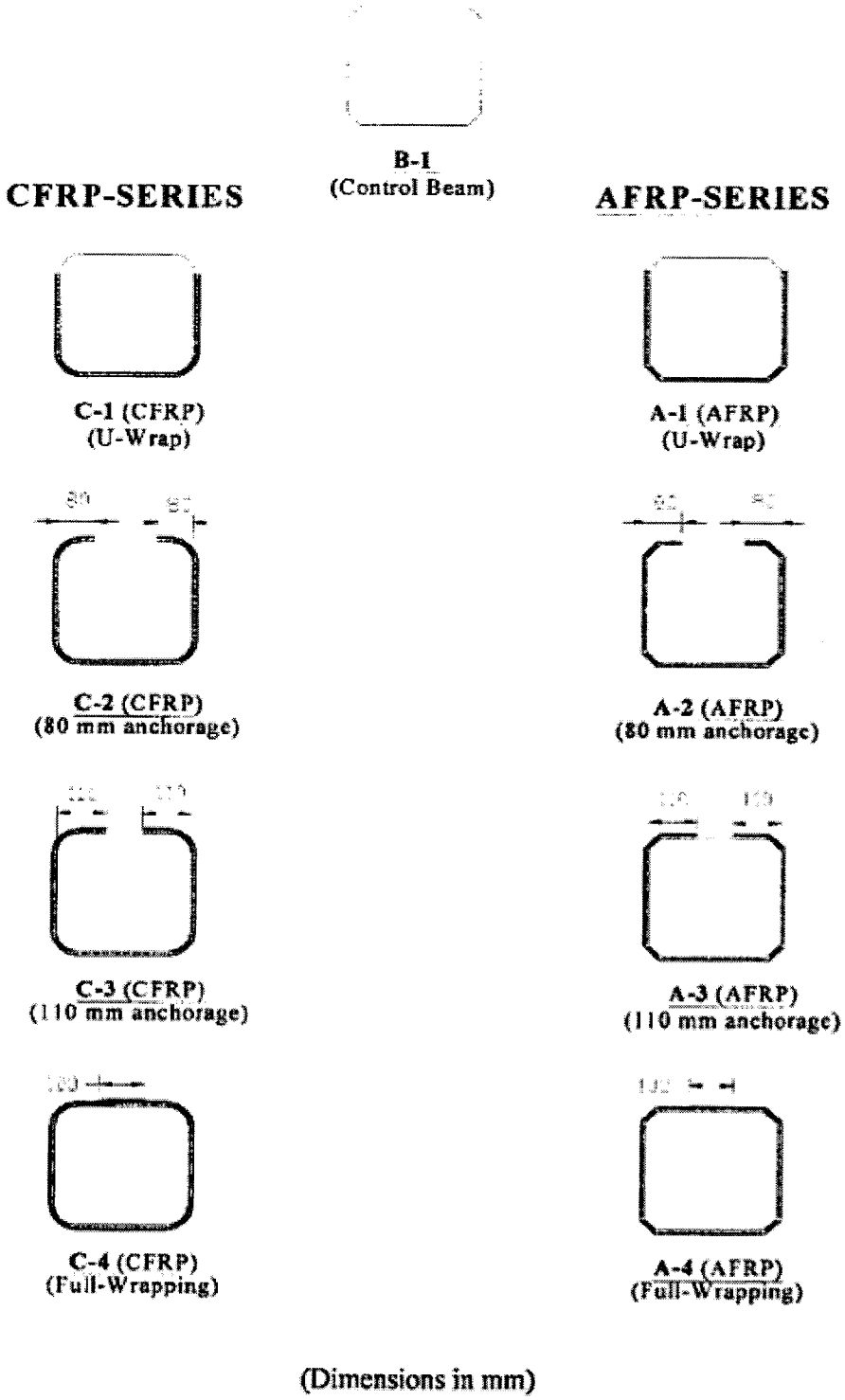

Figure 2.8 Strengthening schemes tested by (Adhikary et al., 2004)

Figure 2.9 Debonding failure of beam strengthened by U-jacket CFRP strips (Leung et al., 2007)

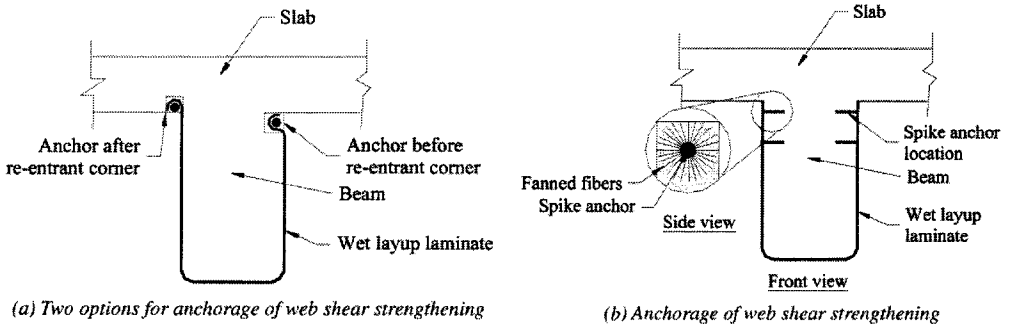

Figure 2.10 Different anchor systems (Eshwar et al., 2008)

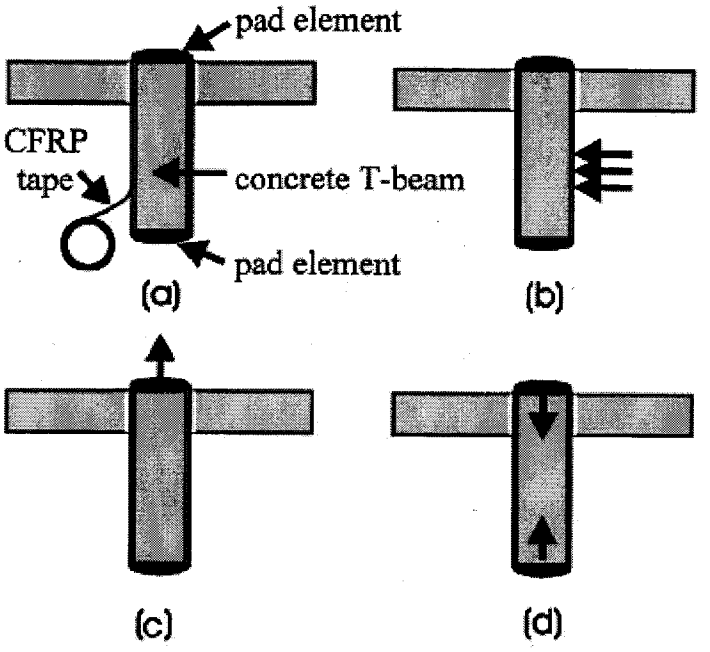

Figure 2.11 External unbonded prestressed CFRP straps (Lees et al., 2002)

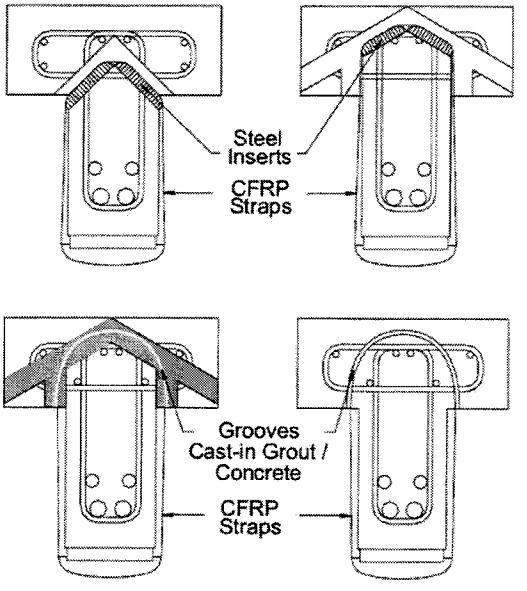

Figure 2.12 Method for external unbonded CFRP straps (Hoult and Lees, 2009)

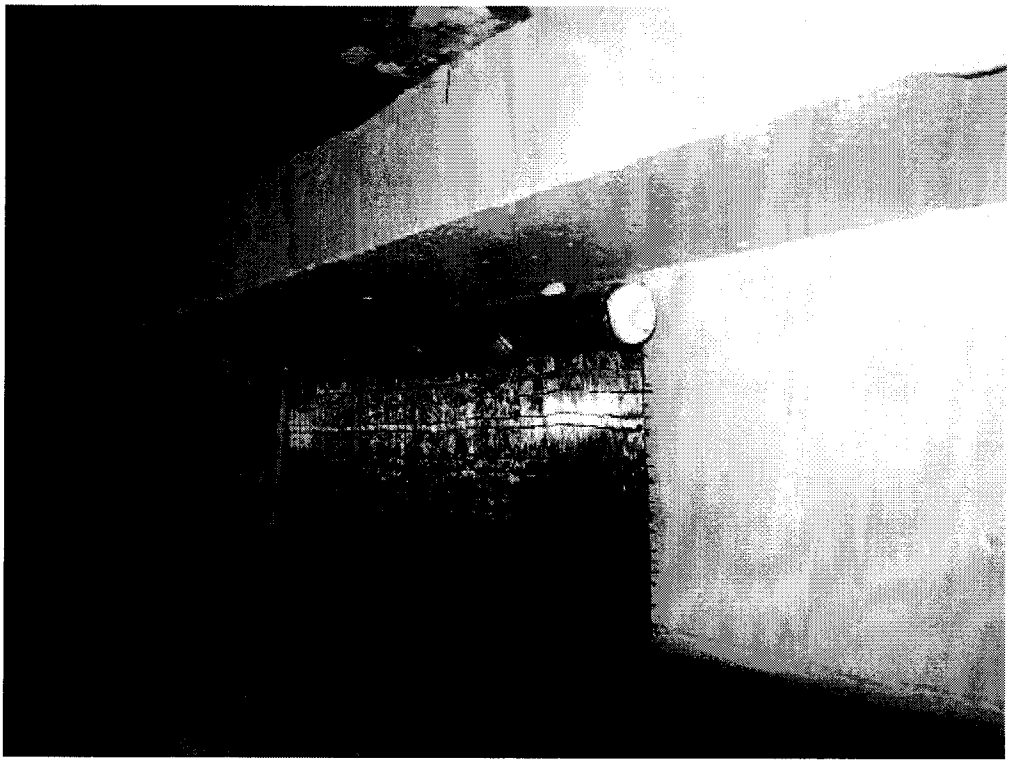

Figure 2.13 Mechanically anchored dry CF sheets (Galal and Mofidi, 2010)

CHAPTER 3

EXPERIMENTAL WORK FOR THE NEW THERMOPLASTIC CFRP REBARS

3.1 Test program

This chapter presents test results of three sets of tests for new thermoplastic carbon fibre-reinforced polymer (CFRP) rebars used as reinforcement for concrete structures. The three sets of tests were conducted on the newly developed CFRP rebars in order to evaluate their mechanical characteristics, bond properties of straight rebars, and the strength of bent rebars. The new CFRP rebar is made of carbon fibres bonded together with thermoplastic resin. The thermoplastic resin allows bending of the rebar -by heating- several times after the complete solidification of the thermoplastic resin.

All the CFRP straight and bent rebars that were used in this study were manufactured and supplied by Concordia Center for Composites (CONCOM) at Concordia University.

3.2 Materials

3.2.1 Thermoplastic CFRP rebars

The new thermoplastic CFRP rebars were manufactured with a diameter of 12.7 mm (1/2″). Each rebar consists of 150 yarns where each yarn has 12,000 non-continuous broken fibers. The diameter of each fiber is ranging from 7 to 10 microns. The new CFRP rebar is made using carbon fibres and thermoplastic resin. The newly developed

thermoplastic rebar can be bent - by heating - several times after the complete solidification of the thermoplastic resin. The carbon fibers are broken and non-continuous to allow the rebar to be bent, otherwise the bent part of the rebar will have some bulges. The yarns chosen for constructing this rebar is pre-wounded with a nylon resin which penetrates all the fibers (with application of heat) to insure the uniformity of the resin all over the rebar section.

Unlike most of the ribbed rebars where the fibers are wound to the rebar or grooved, the new CFRP rebars were designed to have integral ellipsoidal ribs. The new ribs were formed by the longitudinal fibers of the rebar which are expected to provide better mechanical interlock between the concrete and the rebar, and to eliminate the failure of the ribs due to debonding. The new CFRP rebars were also designed to exhibit better bond strength and shorter development length.

The new CFRP rebars were made by compression molding technique. The mold length is 380 mm (15″) plus a 3 inch piece that protrudes out of the mold to give the loose yarns a straight profile to help with the continuity process. For rebar longer than 380 mm (15″), the loose yarns were cut and prepared to the desired length of the rebar, then the rebar was manufactured in sections. To ensure the straightness of the rebar, each section consists of 127mm (5″) of the old solidified section, plus 254 mm (10″) inches of loose yarns. Otherwise the rebar can have a bend between each two successive sections. Since the composite materials are very sensitive to any slight change in the temperature, pressure, and time of applying pressure and temperature; all the conditions were kept the same during manufacturing.

Figure 3.1(a) shows the mold used in manufacturing the rebars, Figure 3.1(b) shows a finished rebar, Figure 3.2 shows bent CFRP rebars, while Figure 3.3 shows schematic elevation and longitudinal cross section of the rebar.

3.2.2 Concrete

The concrete used for constructing the specimens for this research was ordered from a local supplier in Montreal. Concrete with compressive strength of 31 MPa at age of 28 days and maximum aggregate size of 12mm (½") was used.

3.2.3 Steel reinforcement

All steel rebars used in this research were supplied by a local supplier in Montreal. Two sizes of steel rebars were used; 10M deformed rebars and 8 mm undeformed rebars.

3.2.4 Epoxy

Sikadur® 35 Hi-Mod LV epoxy was used in this research for the sleeve anchor. Sikadur® 35 Hi-Mod LV epoxy is a two-component, low-viscosity, high-strength, epoxy resin adhesive. The selected epoxy can develop as high early-strength as 19MPa in two days where the curing temperature is the room temperature.

The two-component epoxy can be mixed together with a ratio of 1 part of component B to 2 parts of component A. A mixer was used to mix the two components thoroughly for three minutes with speed of 550 rpm. Since the epoxy has a short pot life,

a small quantity was mixed each time before the epoxy starts to react. The properties of the epoxy are summarized in Table 3.1.

3.3 Mechanical properties test

The objective of this test is to obtain the tensile strength, modulus of elasticity, and the maximum elongation of the new CFRP rebars. In order to obtain the mechanical characteristics of the new innovative CFRP rebars, three identical specimens were tested according to the CSA-S806-02. Two anchoring grips were prepared for each end of each rebar. Each anchor is 620 mm in length, and the distance between the two anchors is 510 mm (40 d_b, where d_b is the rebar diameter) as recommended by Manav (2002), and Castro and Carino (1998). The total length of each specimen is 1750 mm

3.3.1 Specimens fabrication

Since the FRP rebars cannot sustain griping forces, two griping anchors had to be prepared. Each anchor consists of a steel tube, epoxy resin, and silicon caulking. The steel tube is 600 mm in length with an outer diameter of 33.34 mm (1 5/16") and a wall thickness of 4.78 mm (0.188"). The tube was cleaned from inside to remove any dust or debris that can affect the bond strength between the steel tube and the epoxy.

A wooden alignment stand was prepared to insure the verticality of the rebars while the epoxy is being poured and to fix the rebars until the epoxy hardens. In order to insure the alignment between the rebar and the steel tube, wooden caps and plugs were prepared for that purpose.

The CFRP rebars were fixed to the wooden plugs using fast setting epoxy, and then plugged to the steel tube. Silicon was applied to seal the tube. Epoxy was mixed, prepared, and poured inside the steel tubes. The epoxy was left for at least 24 hours to insure its solidification before the second anchor was prepared. The anchors were left for 14 days as recommended by the manufacturer before testing. Figure 3.4 shows the prepared anchors.

Specimens were designated with letters and numbers to reflect the test name, and specimen number. Specimen MP-1 is the first CFRP rebar tested in mechanical properties test.

3.3.2 Test set-up and instrumentation

The 1750 mm rebars were instrumented with four foil strain gauges and two high accuracy displacement transducers (potentiometers). The strain gauges have a gauge length of 5 mm, and a maximum measurable strain of 15,000 με.The high accuracy potentiometers have a gauge length of 160 mm, maximum stroke of 25 mm, and an accuracy of 0.05 mm. Each two strain gauges were mounted on the same section of the CFRP rebar (back to back), while each group of the strain gauges and the two high accuracy potentiometers were mounted at two different sections. The four strain gauges and the high accuracy potentiometers were used to obtain the average strains / elongation at two different sections of the CFRP rebar.

In order to obtain the load readings from the universal testing machine in a digital format, a pressure transducer was installed on the hydraulic circuit of the machine while

the original load indicator was kept to double check the readings. The machine was calibrated according to the ASTM E4 by the manufacturer representative.

The four strain gauges, the two potentiometers, and the pressure transducer were connected to the data acquisition system which records and saves the data each one second. Figure 3.5 shows the test setup and instrumentation of the mechanical properties test, while Figure 3.6 shows schematic drawings of the specimen details, test setup and instrumentation.

3.3.3 Test procedure

The 1750mm CFRP specimen was mounted in the universal testing machine, and the grips was tightened prior to loading. The load was applied by the manually controlled valve gradually with a constant rate up to failure. The readings were monitored on the computer during the test, while the data are being recorded for further analysis.

3.4 Pullout and bond strength test

In order to determine the maximum bond stress and the optimum development length required to transfer the force of the new CFRP to the concrete without having slip or debond, ten specimens were prepared and tested according to the CSA-S806-02. Each specimen consists of 1950 mm CFRP rebar which was embedded in a concrete block with dimensions of 650 mm x 150 mm x 150 mm from one side and while the other side is anchored using steel anchoring grip.

The variables of the tested specimens were the embedment length which varied from 15 to 35 the bar diameter. For the embedment lengths 15, 20, 25, and 30 d_b two

specimens were tested for each, one specimen were tested for the embedment length of $35d_b$, while one specimen with steel rebar was tested as a control specimen with an embedment length of 80 mm. The debonded part of the embedded CFRP and steel rebars was created and secured using plastic PVC pipes, high strength silicon, and duct tape.

Specimens were designated with letters and numbers to reflect the test name, embedment length, and specimen number of the same embedment length. For example specimen PL-25-2 is a CFRP rebar tested in pullout and bond strength test, have an embedment length of $25d_b$, and it is specimen number 2 of the same embedment length. Table 3.3 summarize the tested specimens in details with corresponding designation.

3.4.1 Specimens fabrication

3.4.1.1 Anchor

One griping anchor had to be prepared at one side of the rebar because the FRP rebars cannot sustain griping forces. The anchor consists of a steel tube, epoxy resin, and silicon caulking. The steel tube is 600 mm in length with an outer diameter of 33.34 mm (1 5/16"), and a wall thickness of 4.78 mm (0.188"). The tube was cleaned from inside to remove any dust or debris that can affect the bond strength between the steel tube and the epoxy.

Wooden alignment stand was prepared to insure the verticality of the rebars while the epoxy is being poured and to fix the rebars until the epoxy is being hardened. Wooden caps and plugs were prepared in order to inure the alignment between the rebar and the steel tube. The wooden caps and plugs were drilled in the center with the

diameter of the rebar, and having circular shaving with the diameter of the steel tube. Both the hole and the circular shaving are concentric.

The CFRP rebars were fixed to the wooden plugs using fast setting epoxy, and then plugged to the steel tube. Silicon was applied to seal the steel tube and the wooden plugs. Epoxy was mixed, prepared, and poured inside the steel tubes. The anchors were left for 14 days as recommended by the manufacturer before testing.

Figure 3.7 shows the prepared anchor and the wooden alignment stand.

3.4.1.2 Wooden forms and steel cages

Wooden forms are manufactured using 19 mm thick (¾") plywood. In order to support the overhanging CFRP rebars which contain a grip anchor at the other end of each rebar, a wooden support was constructed. The wooden forms were painted with oil base primer to ease their removal after the concrete harden.

Two different sizes of steel rebars were used: 10M used for longitudinal reinforcement, and 8 mm undeformed rebars used for confining stirrups. The 10M deformed rebars and the 8 mm undeformed rebars were cut and bent to the desired dimensions. Figure 3.8 shows the wooden forms and steel cages for the pullout specimens.

3.4.1.3 Concrete pouring and curing

A slump of 60 mm was measured prior to the concrete pouring to insure the workability of the fresh concrete. An electrical concrete vibrator was used to vibrate the

concrete and to remove any air pockets. The concrete was surfaced with steel trowels to obtain smooth surface. Six cylinders (100 mm x 200 mm) were cast simultaneously with the specimens. After the concrete hardened, wet burlap sheets were used to cover the concrete and moistened regularly. The cylinders were cured along with the specimens. Figure 3.9 shows the pullout specimens after pouring.

3.4.2 Test set-up and instrumentation

The 50 kg specimen was mounted on top of the machine (2.5m high) using the overhead crane. Moreover the specimen was secured using chains and nets. The specimen was mounted to the universal testing machine such that the concrete block is sitting on a bearing steel plate which in turn is sitting on top of the movable head of the machine. The CFRP rebar which is extending from the concrete block is passing through the top part, while the steel anchoring sleeve is gripped to the bottom fixed head of the machine.

Plaster bags were used between the concrete and the bearing steel plate to overcome any imperfection of the concrete surface and to insure the verticality of the specimen. The specimen was mounted concentrically with the machine to eliminate any bending stress on the rebar that may affect the results.

The specimens were instrumented with two foil strain gauges and two high accuracy displacement transducers (potentiometers). The strain gauges have a gauge length of 5 mm, and a maximum measurable strain of 15,000 με.The high accuracy potentiometers have a gauge length of 160 mm, maximum stroke of 25 mm, and an accuracy of 0.05 mm. The two strain gauges were installed at the same section of the

CFRP rebar (back to back), while the two potentiometers were placed at two different sections.

A pressure transducer was installed on the hydraulic circuit of the machine in order to obtain the load readings from the analog universal testing machine. The machine was calibrated according to the ASTM E4 by the manufacturer representative to insure the accuracy of the machine. Figure 3.10 shows the test setup and instrumentation of the pullout test, while Figure 3.11 shows the concrete dimensions, reinforcement details, test setup and instrumentation of the pullout test.

3.4.3 Test procedure

The loading was applied gradually by a manually controlled valve with a constant rate up to failure. The readings were monitored on the computer during the test, while the data were being recorded on the data acquisition system for further analysis.

3.5 Bent bars and stirrups test

In order to evaluate the performance and the strength capacity of the CFRP bent rebars used as stirrups, four specimens were tested according to the CSA-S806-02. The CFRP stirrup was embedded in two concrete blocks and tested by pushing the two blocks away from each other by applying a relative displacement between the two blocks using a hydraulic jack. The test variable was the tail length after the bent part of the rebar, while the bend radius was kept constant at a value of four times the rebar diameter ($4d_b$). Four specimens having tail lengths of 3 d_b, 6 d_b, 9 d_b , and 12 d_b with a standard hook end

anchorage type were tested up to failure to evaluate the effect of the tail length on the capacity of the bent bar.

This test simulates the case where the stirrups are perpendicular to the cracks, i.e. the stirrups are inclined at 45 degrees to the longitudinal center line of the beam. The debonded part of the embedded CFRP stirrup was created and secured using plastic PVC pipes, high strength silicon, and duct tape.

Each specimen consisted of one 12.7mm diameter CFRP rebar with a total length of 3200 mm which was bent at four locations to form a stirrup as shown in Figure 3.2.

Specimens were designated with letters and numbers to reflect the test name, and tail length. For example specimen STR-9 is a CFRP stirrup tested in bent bars and stirrups test, and has a tail length of 9 d_b. Table 3.3 summarize the tested specimens in details with corresponding designation.

3.5.1 Specimens fabrication

Each specimen consists of one CFRP rebar with a length of 3200 mm which was bent into four bents to form a stirrup. The CFRP stirrup was embedded in two concrete blocks each is 450 mm x 750 mm x 400 mm.

3.5.1.1 Wooden forms and steel cages

Wooden forms are manufactured using 19 mm thick (¾") plywood. In order to prevent the sides of the wooden forms from bulging along the 750 mm side, wooden stiffeners were used to strengthen the form. The wooden forms were painted with oil base primer to ease their removal after the concrete harden.

The CFRP stirrup is very delicate and can be distorted due to the handling or moving of the specimen prior to the test. Thus, the base of each wooden form was strengthened using two longitudinal square timbers 4" x 4" in order to prevent any relative torsion or movement of the wooden form during the handling or moving of the specimens.

The concrete blocks were reinforced longitudinally and laterally to prevent any failure of the concrete by crushing or splitting using 10M steel rebars. The 10M deformed rebars were cut and bent to the designed locations, and assembled together using steel ties. Figure 3.12 shows the concrete dimensions and steel reinforcement details. While Figure 3.13 shows a wooden form and steel cages of the stirrups and bent bars specimen.

3.5.1.2 Concrete pouring and curing

Slump test was done prior to the pouring to insure the workability of the fresh concrete. The measured slump was 60 mm. Electrical concrete vibrator was used to vibrate the concrete and to remove any air pockets. The concrete was surfaced with steel trowels to obtain smooth surface. Six cylinders (100 mm x 200 mm) were casted simultaneously with the specimens. After the concrete hardened, wet burlap sheets were used to cover the concrete and moistened regularly. The cylinders were cured along with the specimens. Figure 3.14 shows the specimens after pouring.

3.5.2 Test set-up and instrumentation

A hydraulic jack with a capacity of 1500 kN was used to apply a displacement between the two concrete blocks. Steel plates were used between the jack and the

concrete surfaces to distribute the load. Plaster bags were used between the steel plates and the concrete surfaces to cover any imperfection of the surface. A load cell was placed between the jack and the steel plate to measure the load applied by the jack.

In order to concentrically align the specimen with the hydraulic jack, the load cell, and the steel plates, the load cell and the jack were connected together using a threaded rod. Moreover, the hydraulic jack and the connected load cell were seated on wooden seats and shims to support it and to keep it centered vertically. The steel plates were mounted on the concrete surfaces concentrically with the CFRP stirrup, then the hydraulic jack is centered horizontally by hand with respect to the CFRP stirrups.

Each specimen was instrumented with six strain gauges, and four linear measuring devices (potentiometers). The strain gauges have a gauge length of 5 mm, and a maximum measurable strain of 15,000 με, while the potentiometers have a maximum stroke of 317 mm (12.5"), and an accuracy of 0.9 mm. The four potentiometers were used to measure the relative displacement between the two concrete blocks.

Three strain gauges were mounted on three different sections on each leg of the stirrup while the four potentiometers were mounted on each corner of one of the block and connected to the adjacent corner of the other block. Figures 3.15, 3.16, and 3.17 show the test setup, instrumentation of the bent bars and stirrups test, and a schematic drawing showing the test setup and instrumentation details of the stirrups and bent bars test, respectively.

3.5.3 Test procedure

The loading was applied gradually by a manually controlled pump with a constant rate up to failure. The readings were monitored on the computer during the test, while the data are being recorded using the data acquisition system for further analysis.

Table 3.1 Properties of Sikadur 35 Hi-mod LV epoxy at curing time of 14 days

Typical dry fibre properties	Value
Tensile strength	58 MPa
Modulus of elasticity	2.8 GPa
Ultimate elongation	4.20 %
Bond strength	19 MPa
Shear strength	35 MPa

Table 3.2 Test matrix of the CFRP rebar tested in the pullout and bond strength test

	Specimen number	Embedment length (mm)
steel	PLS-30-1	339 ($30d_b$)
Batch #1	PL-15-1	191 ($15d_b$)
	PL-15-2	191 ($15d_b$)
	PL-20-1	254 ($20d_b$)
Batch #2	PL-20-2	254 ($20d_b$)
	PL-25-1	318 ($25d_b$)
	PL-25-2	318 ($25d_b$)
Batch #1	PL-30-1	381 ($30d_b$)
	PL-30-2	381 ($30d_b$)
	PL-35-1	445 ($35d_b$)

Table 3.3 Test matrix of the CFRP rebar tested in the best bars and stirrups test

Specimen number	Tail length (mm)
STR-3	38 ($3d_b$)
STR-6	76 ($6d_b$)
STR-9	114 ($9d_b$)
STR-12	154 ($12d_b$)

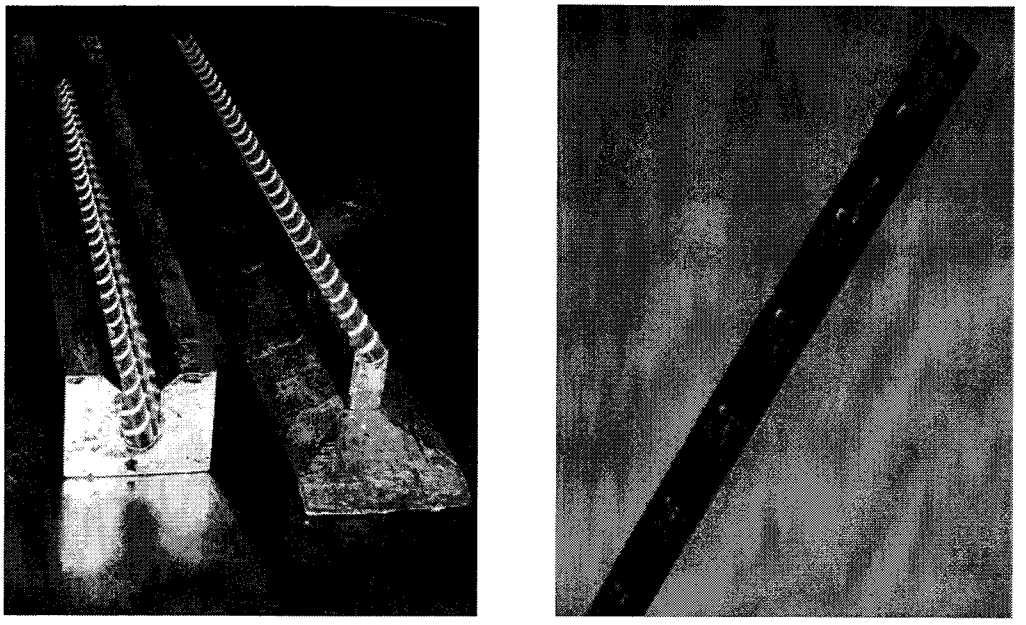

(a) **(b)**

Figure 3.1 (a) The mold used in manufacturing the CFRP rebars; (b) A finished CFRP straight rebar

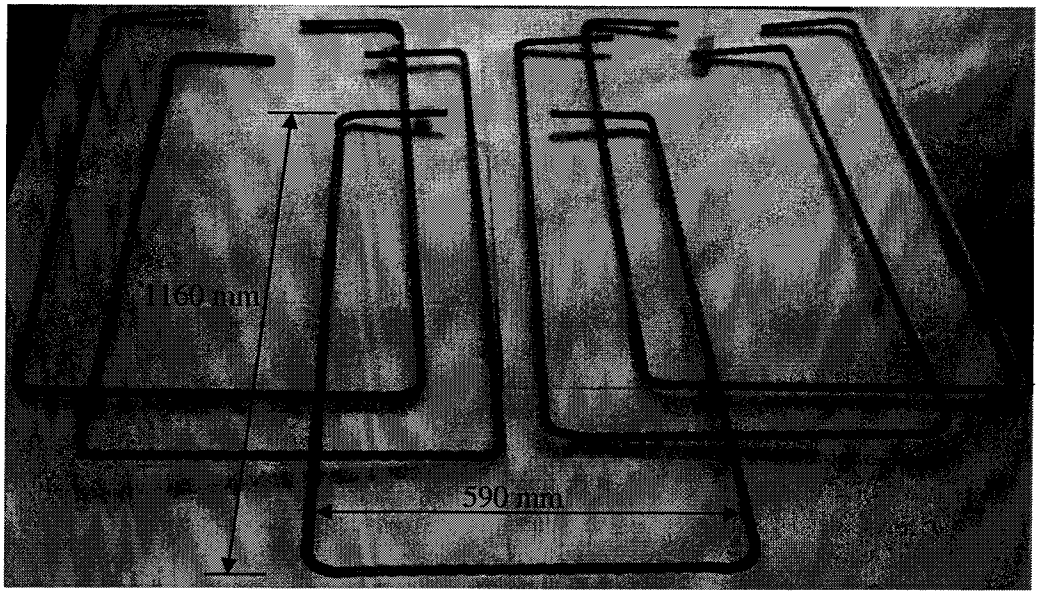

Figure 3.2 Bent CFRP rebars

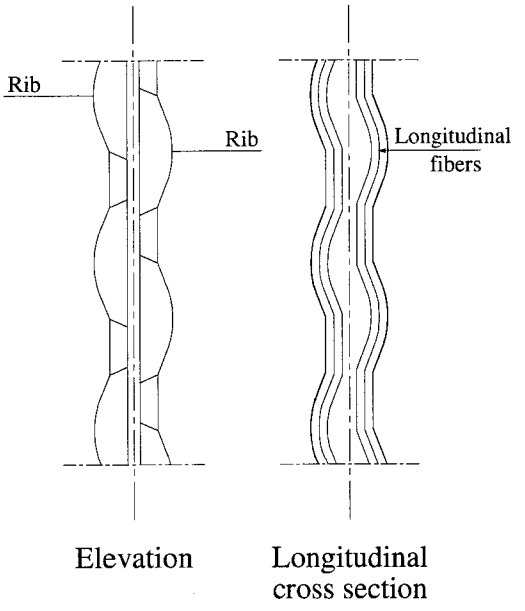

Figure 3.3 Schematic elevation and longitudinal cross section of the rebar

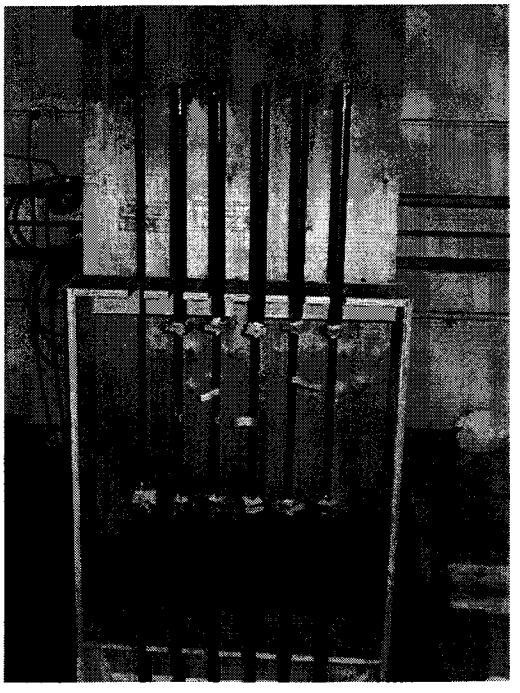

Figure 3.4 Prepared anchors for mechanical properties specimens

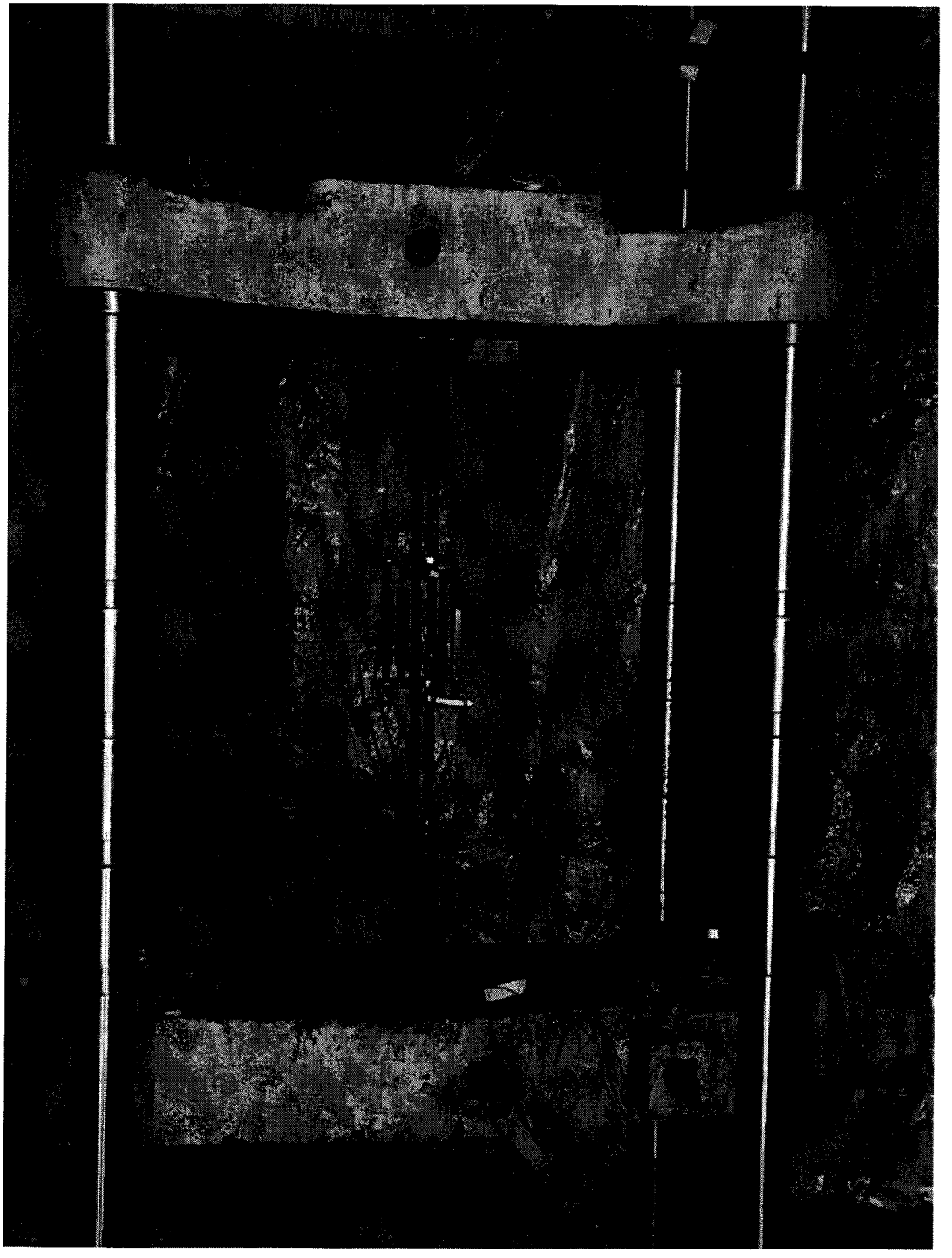

Figure 3.5 Test setup, and instrumentation for mechanical properties test

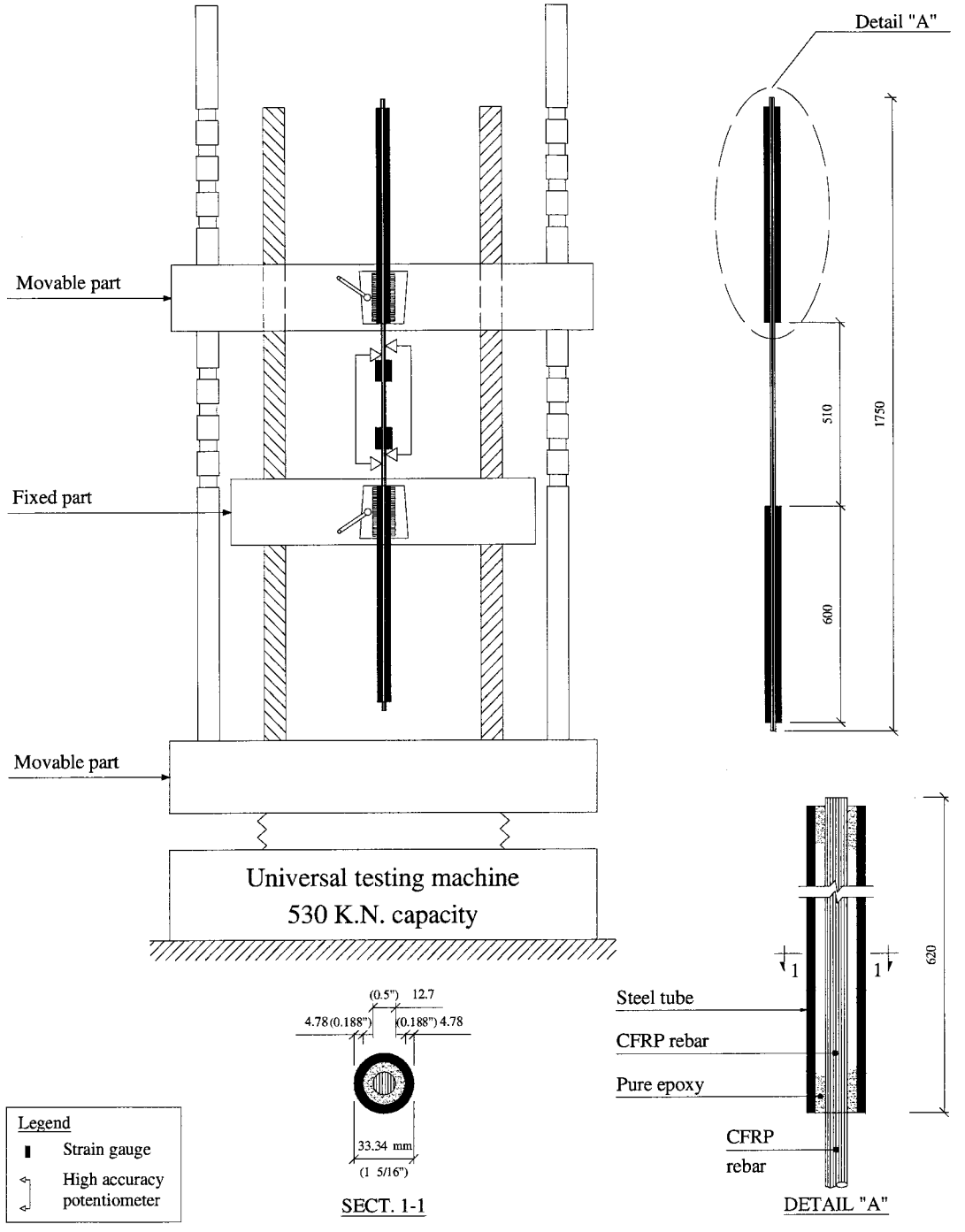

Figure 3.6 Specimen details, test setup, and instrumentation of mechanical properties test

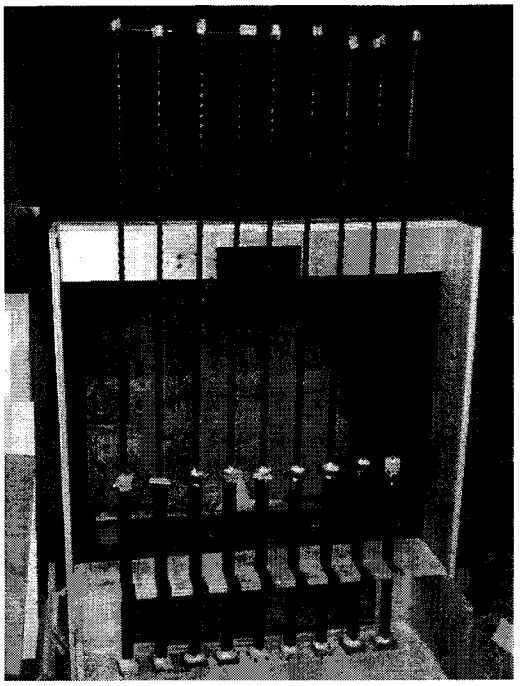

Figure 3.7 Prepared anchors for pullout and bond strength test

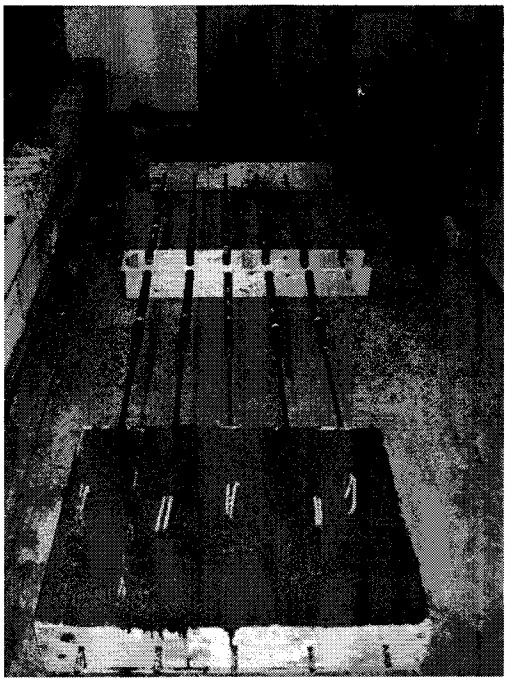

Figure 3.9 Pullout and bond strength specimens after pouring

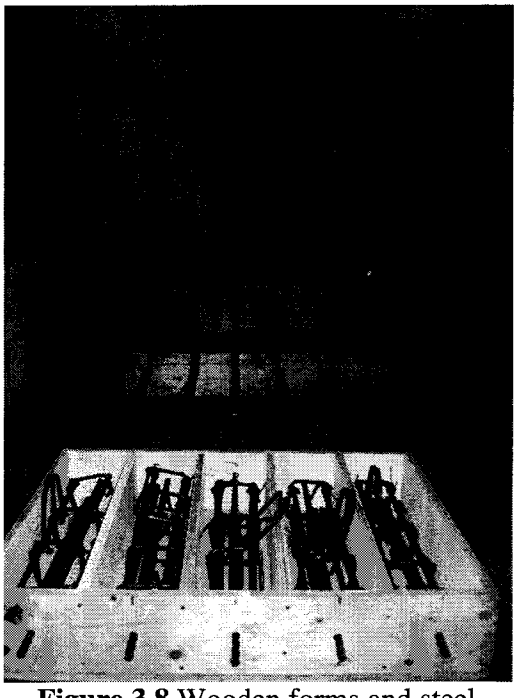

Figure 3.8 Wooden forms and steel cages for pullout and bond strength specimens

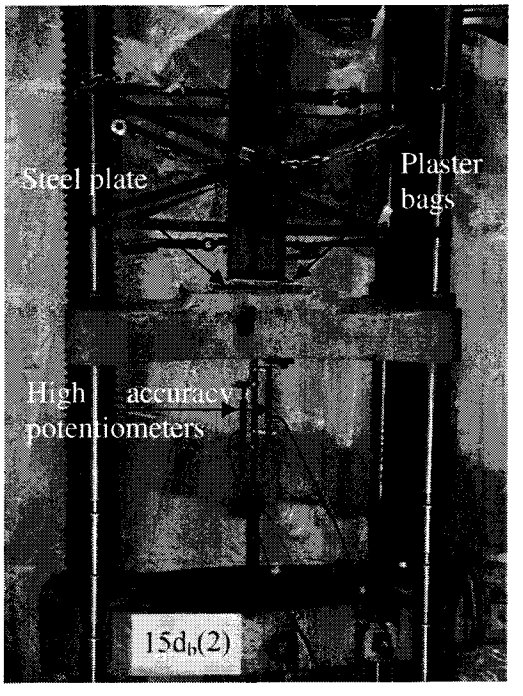

Figure 3.10 Test setup and instrumentation of pullout test

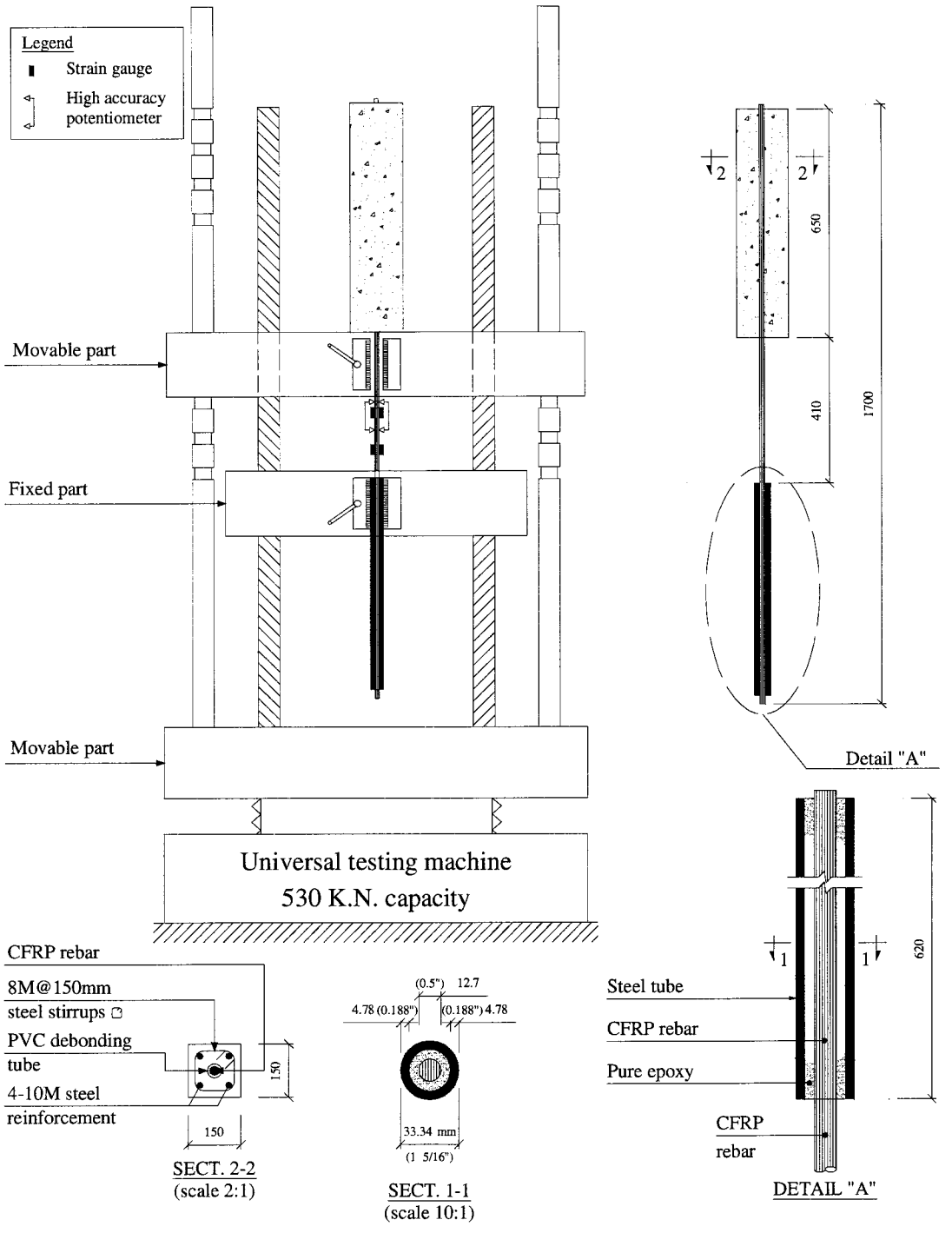

Figure 3.11 Concrete dimensions, reinforcement details, test setup, and instrumentation of pullout test

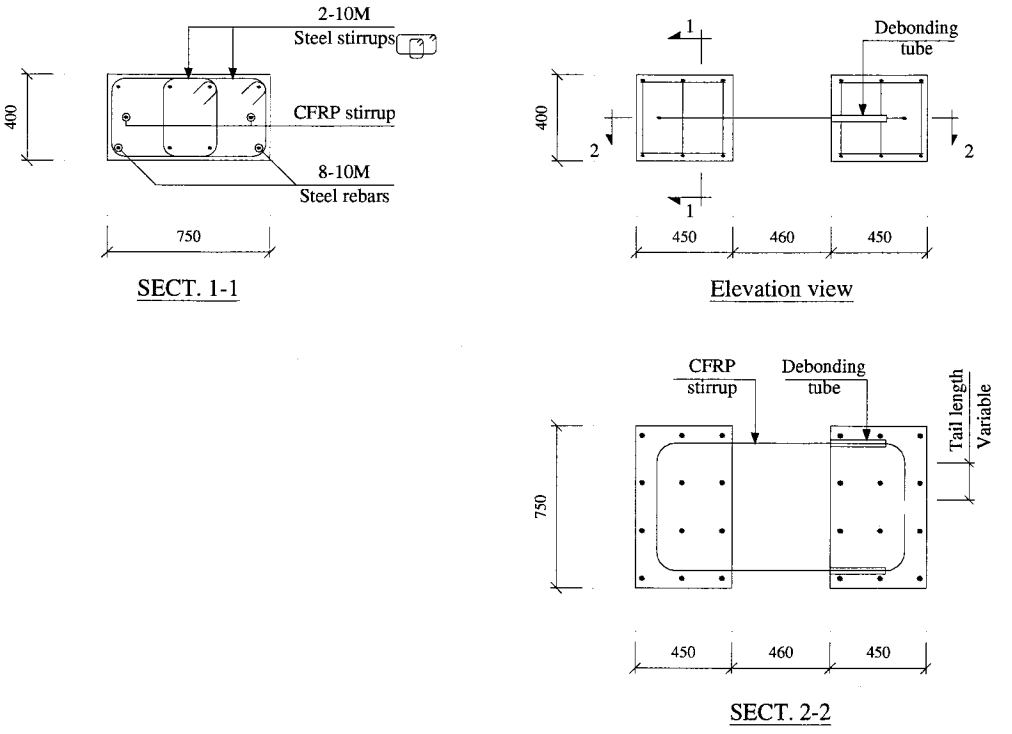

Figure 3.12 Concrete dimensions and reinforcement details of stirrups and bent bars specimens

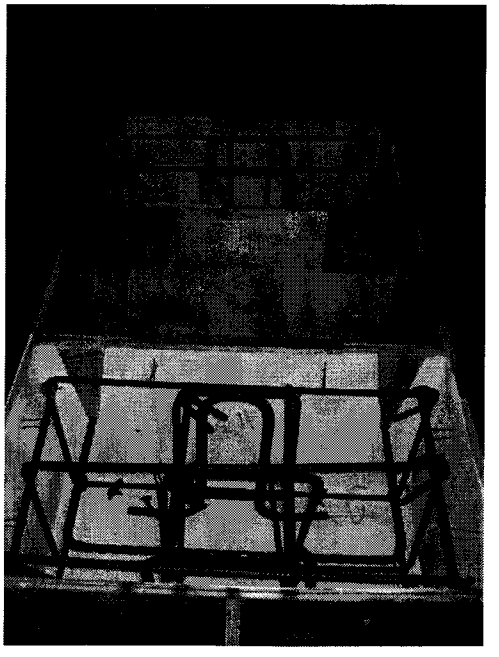

Figure 3.13 Wooden form and steel cage for bent bars and stirrups test

Figure 3.14 Bent bars and stirrups specimens after pouring

Figure 3.15 Bent bars and stirrups test setup

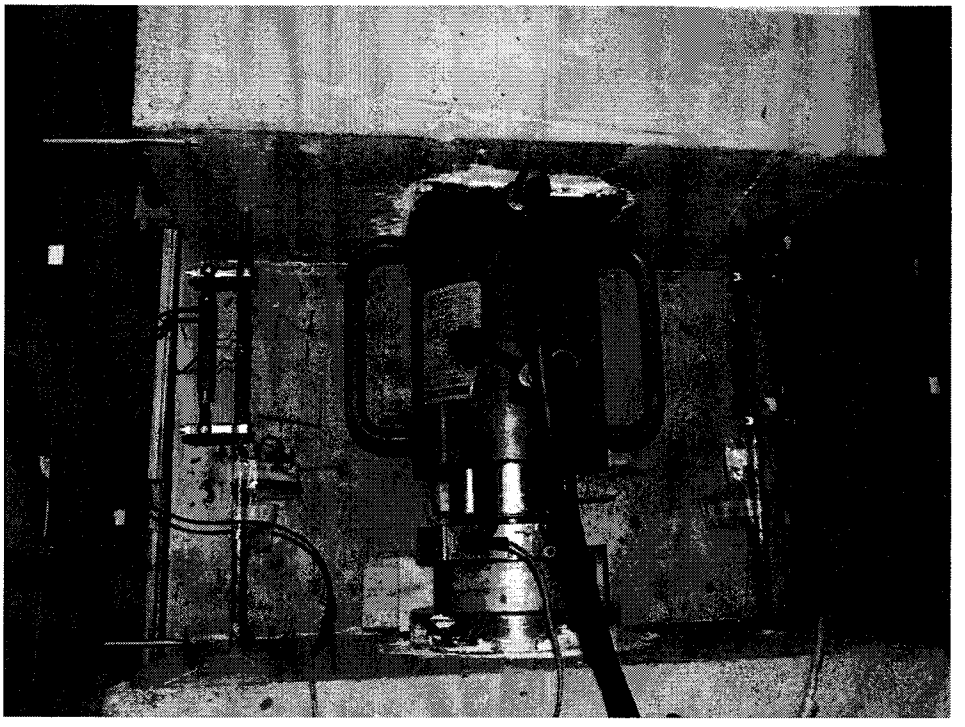

Figure 3.16 Bent bars and stirrups instrumentation

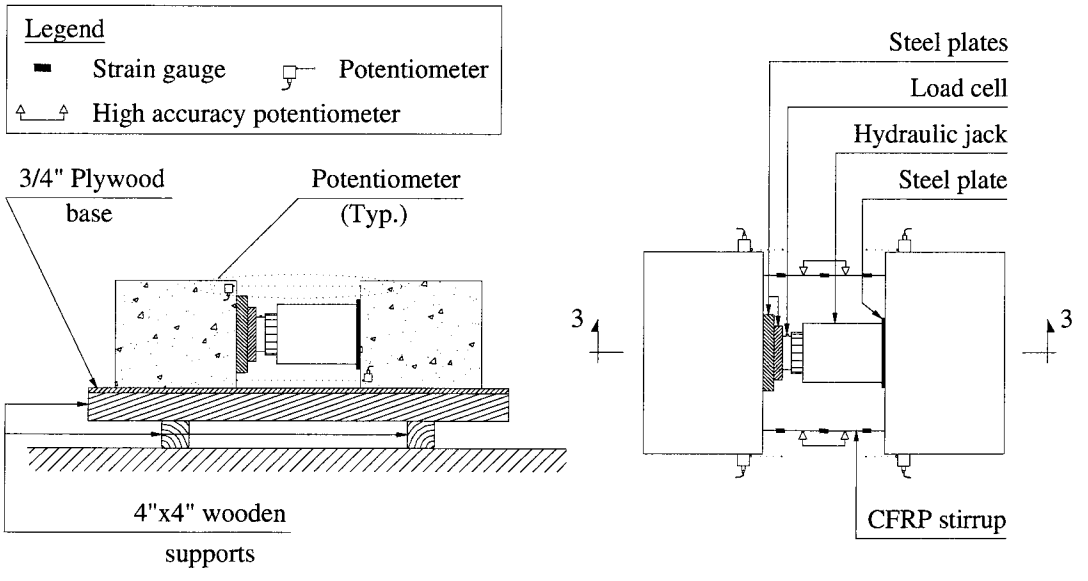

Figure 3.17 Test setup and instrumentation of stirrups and bent bars test

CHAPTER 4

EXPERIMENTAL RESULTS AND DISCUSSION FOR THE NEW THERMOPLASTIC CFRP REBARS

4.1 Introduction

This chapter explains the results and the observations that were monitored during the three sets of tests: mechanical properties test, pullout and bond strength test, and stirrups and bent bars test. Observations on different modes of failure were discussed after each set of tests.

4.2 Mechanical properties test

The stress-strain relationship of the new CFRP rebars exhibited a linear behaviour up to failure. The modulus of elasticity was obtained using the stress and the corresponding strain at 50 % of the ultimate load, and the stress and the corresponding strain at 25 % of the ultimate load (CSA-S806-02). Table 4.1 summarizes the tensile properties of the three tested rebars, while Figure 4.1 shows the stress-strain relationship of the tested specimens.

The test results show that specimens: MP1, MP2, and MP3 failed at a stress of 825, 800, and 710 MPa; while the corresponding strains were 9000, 8500, and 8050 microstrain. The average modulus elasticity of the tested CFRP rebars is 91 ± 2.6 GPa, the maximum tensile strength is 825 MPa, and the corresponding maximum ultimate strain is 9000 microstrain.

4.2.1 Discussion on the performance and different modes of failure of the new CFRP rebars

A rupture with a splitting between the two sides of the rebar was the typical mode of failure for specimens MP1, and MP3; while specimen MP-2 had a rupture plane normal to the fibers orientation and at the intersection of the rib and the smooth part of the CFRP rebar as shown in Figure 4.2.

The splitting mode of failure occurred in three planes: perpendicular to the fibers direction in one half of the rebar, parallel to the fibers between the two halves of the rebar for a length of two to three bar diameters, and perpendicular to the fibers orientation in the other half of the rebar as shown in Figure 4.3.

The geometry of the rebar was designed such that at each section of the rebar a rib exists at each side of the rebar to allow transferring the bond stresses to concrete. Accordingly, at any section of the rebar the ribs are not symmetrical around the center line of the rebar, which in turn created an extra force to the rebar. Consequently, a splitting force was created in the rebar lead to the typical splitting failure (MP-1, and MP-3). Figure 4.4 shows a schematic drawing showing the unsymmetrical ribs along the rebar and a longitudinal cross section showing the splitting forces that lead to the typical failure mode of the rebars.

Due to the splitting forces, a variation of 115 MPa in the tensile strength of the rebars was observed although the variation in the modulus of elasticity was less than ±2.6 %. It was believed that if the rebar had a symmetrical cross section, the rebar would have reached its desired strength (1500 MPa).

4.3 Pullout test

The nine CFRP rebars were manufactured in two different batches, each batch was manufactured separately. All the nine CFRP specimens failed in premature tension failure, no signs of debonding were observed. The results of the nine specimens were used to collect more tensile properties and to obtain the maximum recorded bond strength of the premature failed specimens.

The steel rebar of the control specimen PLS-30-1 failed in tension, and no sign of debonding was observed. As shown in Figure 4.5, the stress strain curve of the control specimen was a typical stress-strain relationship of a steel rebar: linear up to yielding stress of 485 MPa, yielding plateau until the strains reached 27,100 microstrain, strain hardening up to ultimate stress of 582 kN and corresponding strain of 115,700 microstrain, then necking and failure occurred at a stress of 475 MPa. The two potentiometers were removed at stress of 580 MPa in order not to damage them during the rupture of the steel rebars.

For specimens PL-15-1, PL-15-2, PL-20-1, PL-20-2, PL-25-1, PL-25-2, PL-30-1, PL-30-2, and PL-35-1; the stress-strain relationship of the CFRP rebars exhibited a linear behaviour up to failure. The modulus of elasticity was obtained using the load and the corresponding strain at 50 % of the ultimate load, and the load and the corresponding strain at 25 % (CSA-S806-02). Table 4.2 summarizes the tensile properties and the maximum recorded bond stress of the tested rebars, while Figure 4.6 shows the stress-strain relationship of the nine tested specimens. The results show that the average modulus of elasticity of the new CFRP rebars is 118.5 ± 2.0 GPa and 90.3 ±5.0 GPa for

batches 1 and 2, respectively. The maximum tensile strength was 693 MPa, and the maximum observed bond strength was 9 MPa.

4.3.1 Discussion on the performance and different modes of failure of specimens tested in pullout and bond strength test

Three modes of failure were observed: (S) rupture with a splitting between the two sides of the rebar; (S-W) splitting failure with wavy fibers at the location of the failure; and (R) rupture. The splitting mode of failure (S) occurred in three planes: perpendicular to the fibers direction in one half of the rebar, parallel to the fibers between the two halves of the rebar for a length of two to three bar diameters, and perpendicular to the fibers orientation in the other half of the rebar. The rupture mode of failure had a plane of failure normal to the fibers orientation and located at the intersection of the rib and the smooth part of the CFRP rebar.

Specimen PL-20-2 failed with (S) mode of failure; specimens PL-15-1, PL-20-1, PL-25-1, PL-30-1, and PL-30-2, and PL-35-1 failed with (S-W) mode of failure; while specimens PL-15-2, and PL-25-2 had (R) mode of failure. Figures 4.7, 4.8, and 4.9 show failed specimens with S-W, R, S modes of failure respectively.

The geometry of the rebar was designed such that at each section of the rebar a rib exists at each side of the rebar to allow transferring the bond stresses to concrete. Accordingly, at any section of the rebar the ribs are not symmetrical around the center line of the rebar, which in turn created an extra force to the rebar. Consequently, a splitting force was created in the rebar lead to the splitting failure mode. Figure 4.4 shows a schematic drawing showing the unsymmetrical ribs along the rebar and a longitudinal

cross section showing the splitting forces that lead to the splitting failure mode of the rebars.

Due to the splitting forces, a variation of 377 MPa in the tensile strength of the rebars was observed although the variation in the modulus of elasticity was less than ± 5 % for group1 and ± 2 % for group 2. The authors believe that if the rebar was having a symmetrical cross section, the rebar would have reached its desired strength (1500 MPa).

Although the rebar was designed with smooth ellipsoidal ribs, the specimen PL-20-2 indicates that there is stress concentration at the intersection of the ribs and the smooth part of the rebar.

4.4 Bent bars and stirrups test

The results of the three tested specimens are summarized in Table 4.3. All the tested specimens exhibited a linear stress-strain relationship up to failure as shown in Figure 4.10. Specimens STR-3, STR-6, STR-9, and STR-12 failed at stress of 219, 204, 306, and 199 MPa; while the corresponding strains were 2265, 2425, 3120, 3260 microstrain respectively. The average modulus of elasticity was 91.1 ± 5 GPa.

The readings of the four potentiometers indicated that two concrete blocks were moved parallel without rotation. Figures 4.11, 4.12, 4.13, and 4.14 show specimens STR-3, STR-6, STR-9, and STR-12 before and after the test, respectively.

The stirrups of specimens STR-3, STR-6, and STR-9 failed at the bent location, while specimen STR-12 failed in premature splitting tension failure as shown in Figure 4.15.

4.4.1 Discussion on the performance and modes of failure of the specimens tested in the stirrups and bent bars test

The properties of the bent rebars are evaluated with the ratio of the strength of the bent rebars to the strength of the straight rebars (F_{ub}/F_{us}). The capacity of the bent stirrups was 27%, 24%, 37%, and 24% of the capacity of the straight rebars for specimens with tail length of $3d_b$, 6db, 9db, and $12d_b$, respectively.

4.5 Comparisons between the new CFRP rebar (CONCOM) and the available FRP rebars

Five rebars available in the market and literature were used to compare the results of the newly developed CFRP rebar (CONCOM rebar). The five rebars can be classified according to the resin type as: thermoset (Pultrall CFRP and GFRP rebars, and Schöck COMBAR) and thermoplastic rebar (FULCRUM and Currier et al.). All the rebars are made of glass fibers except CFRP Pultrall, and Currier et al. rebars.

The properties of the CONCOM rebar and the other five rebars were compared in terms of: mechanical properties, bond strength, and the strength of the bent rebars.

The mechanical properties were compared in terms of the modulus of elasticity and tensile strength. The modulus of elasticity of the CONCOM rebar is 83% of the modulus of elasticity of the Pultrall CFRP rebar, and 15% to 250% the modulus of elasticity of the other rebars. In terms of tensile strength, the test results of CONCOM rebars show that they have less tensile strength compared to Pultrall (CFRP), Schöck COMBAR, and FULCRUM; while it has higher tensile strength than Pultrall (GFRP). The authors believe that with some improvements to the CONCOM rebar, the tensile

strength of the straight rebar will be as high as 1500 MPa with the advantage of being bendable upon heating.

In terms of bond strength, the rebars had a premature failure during the pullout and bond test. Thus, the bond strength was not evaluated through this study.

The properties of the bent rebars are evaluated with the ratio of the strength of the bent rebars to the strength of the straight rebars (F_{ub}/F_{us}). The results shows that the CONCOM bent rebar have better properties compared to the results of the thermoplastic rebars tested by Currier et al. (160%), while it is 62% to 81 % of the GFRP and CFRP Pultrall bent rebars. Moreover, with some improvements to the straight rebars, the properties of the bent rebars are expected to be improved as well.

Table 4.4 shows a comparison between the new CFRP rebar (CONCOM rebar) versus other rebars available in the market.

Table 4.1 Mechanical properties of the tested CFRP rebars

Specimen number	Nominal diameter (mm)	Load at failure (kN)	Tensile strength (MPa)	Ultimate strain (microstrain)	Modulus of elasticity (GPa)	Mode of failure
MP-1	12.7	104.5	825	9000	89.9	S
MP-2	12.7	101.4	800	8500	92.2	R
MP-3	12.7	90.0	710	8050	90.8	S

S: Splitting failure; R: rupture normal to the fibers orientations

Table 4.2 Test results of the CFRP rebar tested in the pullout and bond strength test

	Specimen number	Embedment length (mm)	Ultimate load (kN)	Tensile strength (MPa)	Modulus of elasticity (GPa)	Ultimate bond strength (GPa)	Mode of failure
steel	PLS-30-1	339 ($30d_b$)	58.2	582	212	4	R
Batch #1	PL-15-1	191 ($15d_b$)	45.4	359	120.1	6	S-W
	PL-15-2	191 ($15d_b$)	65.1	514	112.4	9	R
	PL-20-1	254 ($20d_b$)	68.5	544	125.5	7	S-W
Batch #2	PL-20-2	254 ($20d_b$)	75.6	597	91.8	7	S
	PL-25-1	318 ($25d_b$)	47.7	377	91.2	4	S-W
	PL-25-2	318 ($25d_b$)	49.0	387	88.0	4	R
Batch #1	PL-30-1	381 ($30d_b$)	87.7	693	115.9	6	S-W
	PL-30-2	381 ($30d_b$)	40.0	316	123.3	3	S-W
	PL-35-1	445 ($35d_b$)	56.7	448	113.9	3	S-W

R: Rupture; S: Splitting; S-W: Splitting with wavy fibers

Table 4.3 Test results of the CFRP rebar tested in the stirrups and bent bars test

Specimen number	Tail length (mm)	Ultimate load (kN)	Ultimate strength (MPa)	Ultimate strain (microstrain)	Modulus of elasticity (GPa)	Mode of failure
STR-3	38 ($3d_b$)	27.7	219	2265	94.5	R
STR-6	76 ($6d_b$)	25.8	204	2425	85.1	R
STR-9	114 ($9d_b$)	38.8	306	3120	96.4	R
STR-12	154 ($12d_b$)	25.2	199	3260	88.4	S

R: Rupture at the bent part; S: Splitting failure

Table 4.4 Comparison between the new CFRP rebar versus other rebars available in the market

Property	Thermoset FRP rebars			Thermoplastic FRP rebars		CONCOM rebar
	Pultrall		Schöck COMBAR	FULCRUM	Currier et al.	
	GFRP	CFRP	GFRP	GFRP	CFRP	CFRP
Tensile strength (MPa)	675-874	1185	1300-1500	820-1032	NA	825
Modulus of elasticity (GPa)	46-51	109	60	37-51	NA	91
Bond strength (MPa)	14-20	16.5	12-25	8-15	NA	9
F_{ub}/F_{us}	0.46-0.58	0.44-0.57	NA	NA	0.23	0.37

NA: not available information

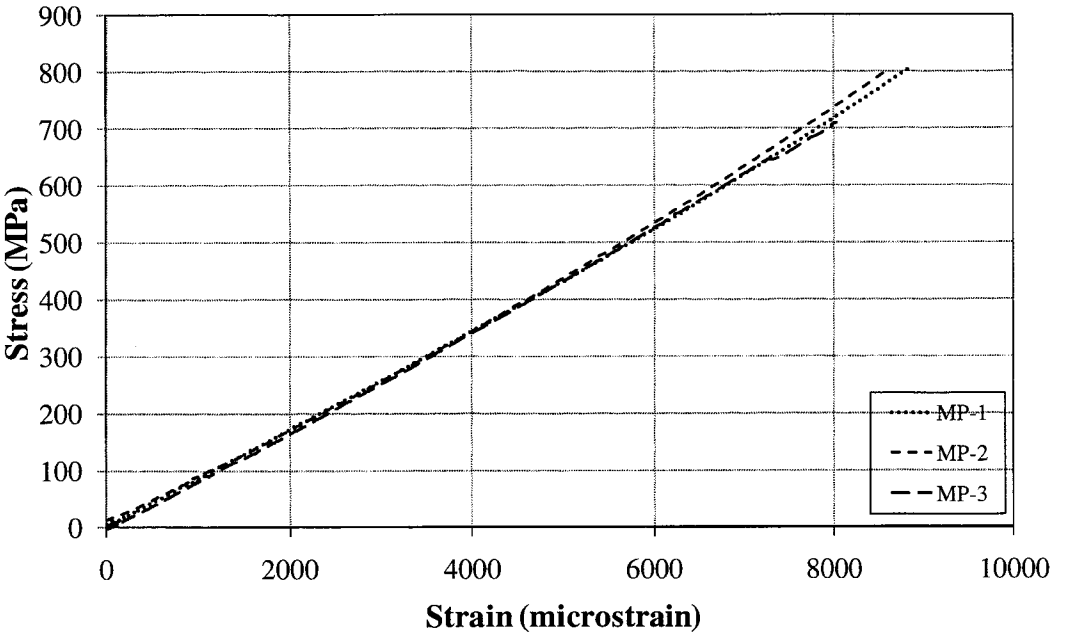

Figure 4.1 Stress-strain relationship of CFRP rebars tested in the mechanical properties test

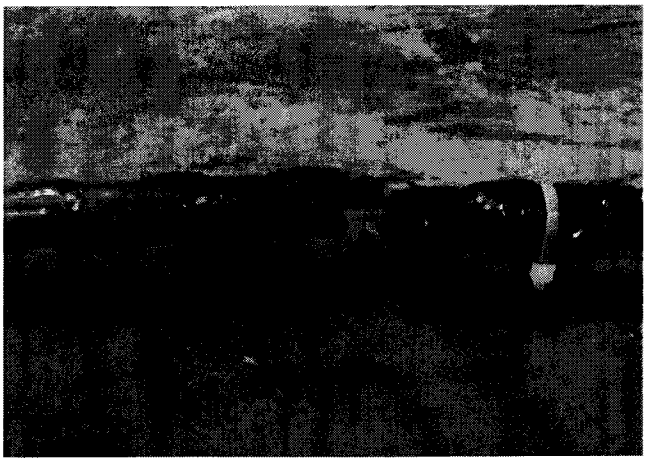

Figure 4.2 Rupture normal to the fibres orientation mode of failure for specimen MP-2

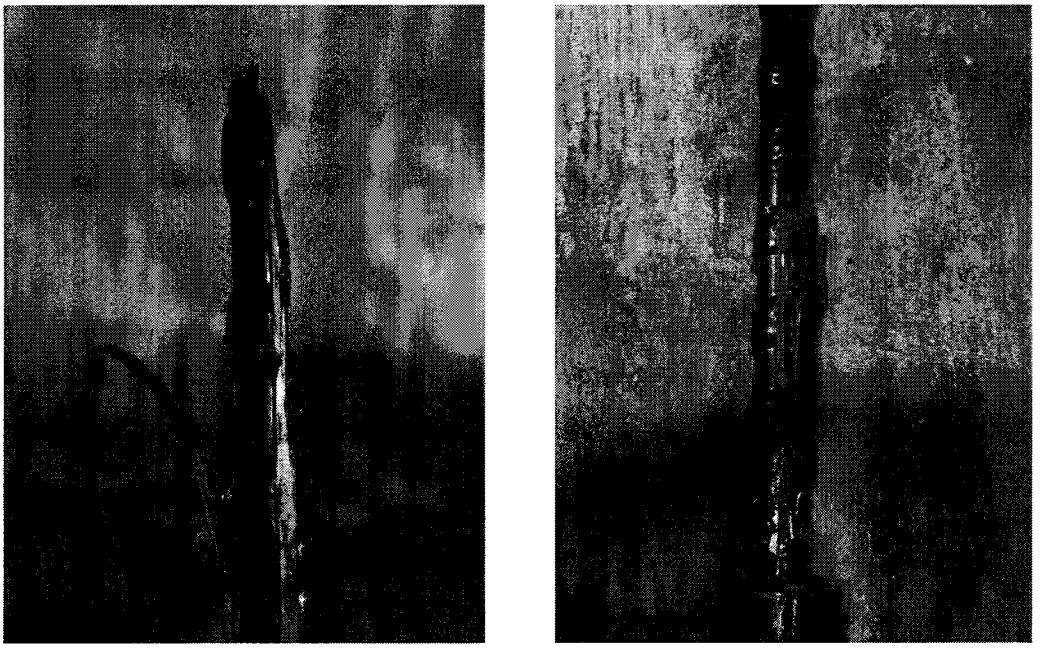

(a) **(b)**

Figure 4.3 Splitting failure mode for specimens: (a) MP-1, (b) MP3

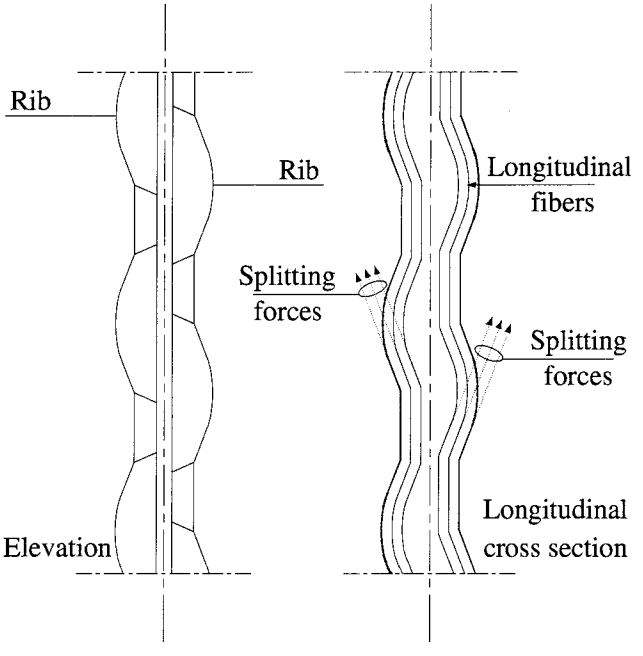

Figure 4.4 Schematic longitudinal cross section, elevation and side view of the new developed CFRP rebar

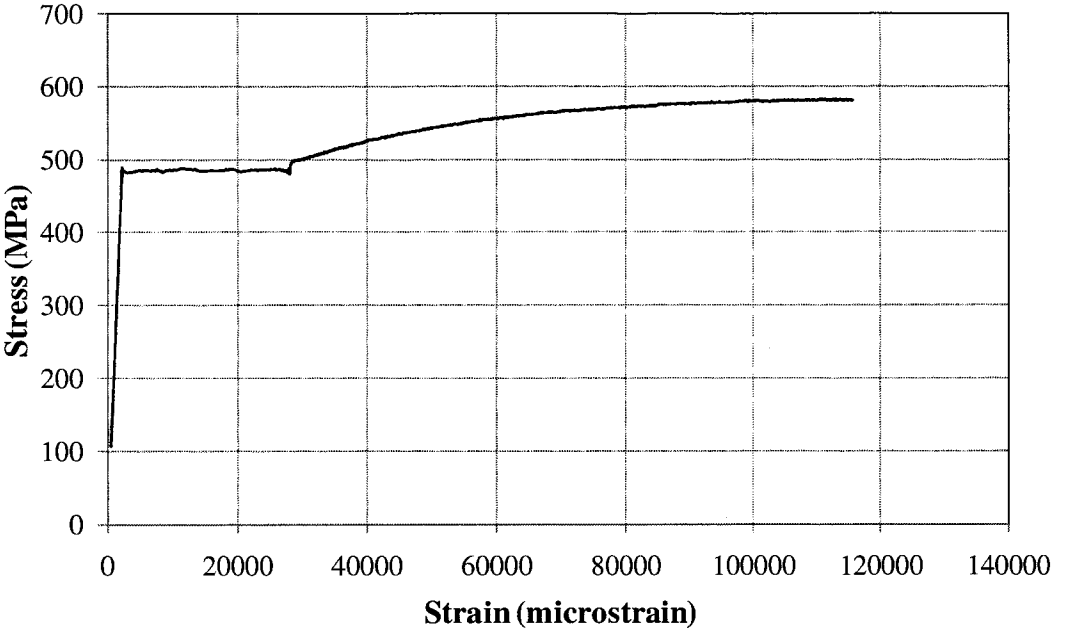

Figure 4.5 Stress-strain relationship of specimen PLS-30-1

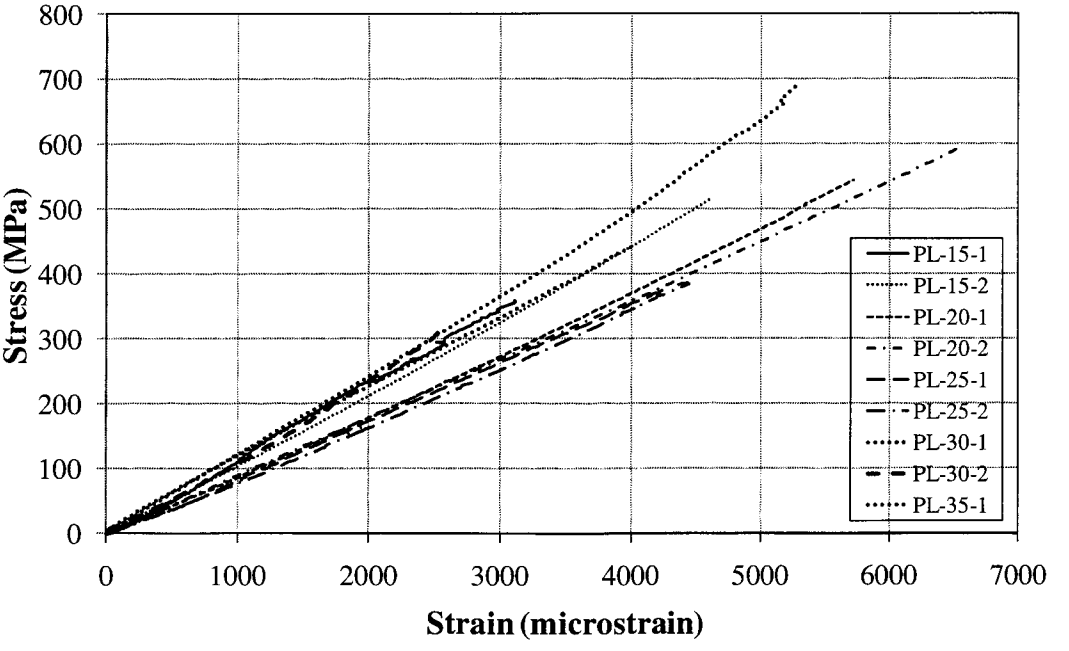

Figure 4.6 Stress-strain relationship of the CFRP rebars tested in the pullout and bond strength test

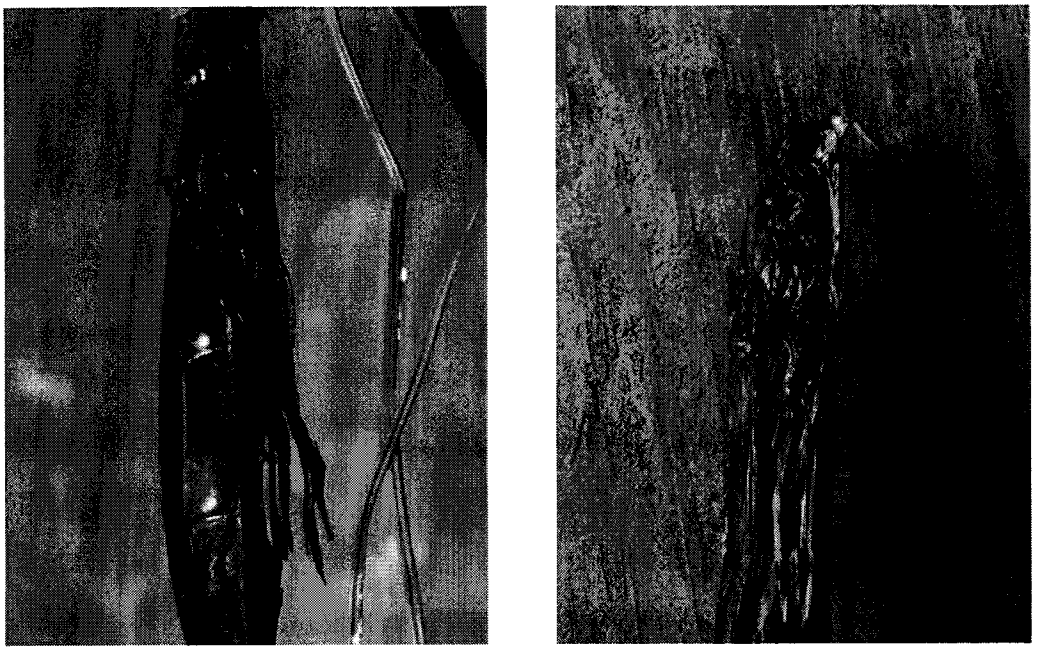

(a)

(b)

(c)

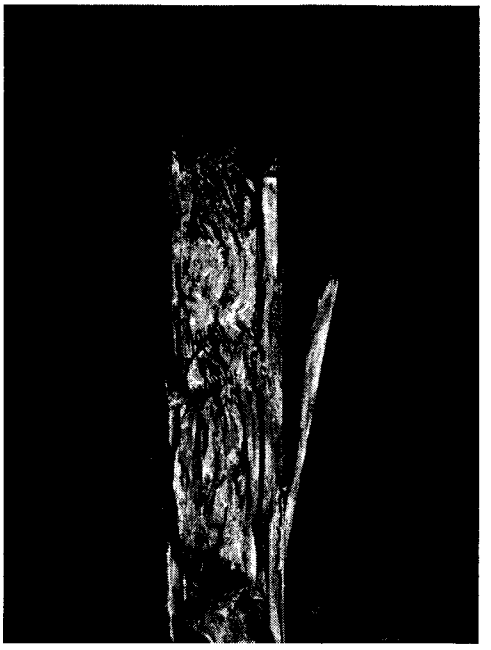

(d)

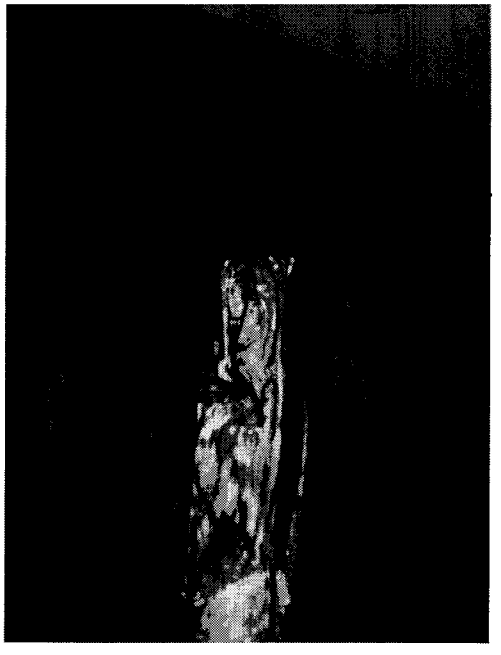

(e)

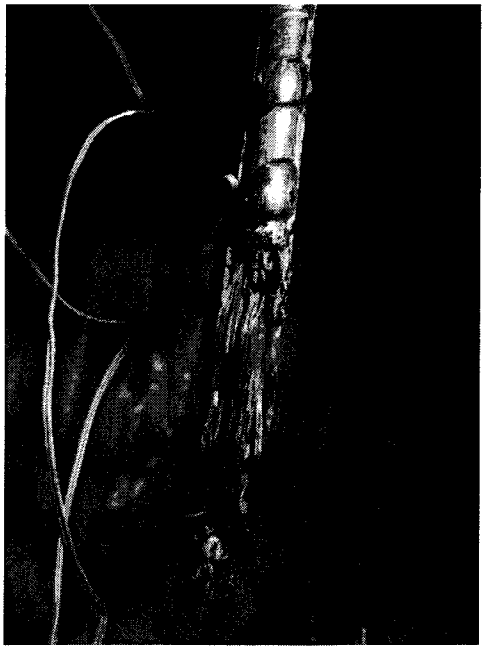

(f)

Figure 4.7 Failure with splitting and wavy fibers of specimens: (a)PL-15-1, (b)PL-20-1, (c) PL-30-1, (d) PL-30-2, (e) PL-25-1, (f) PL-35-1

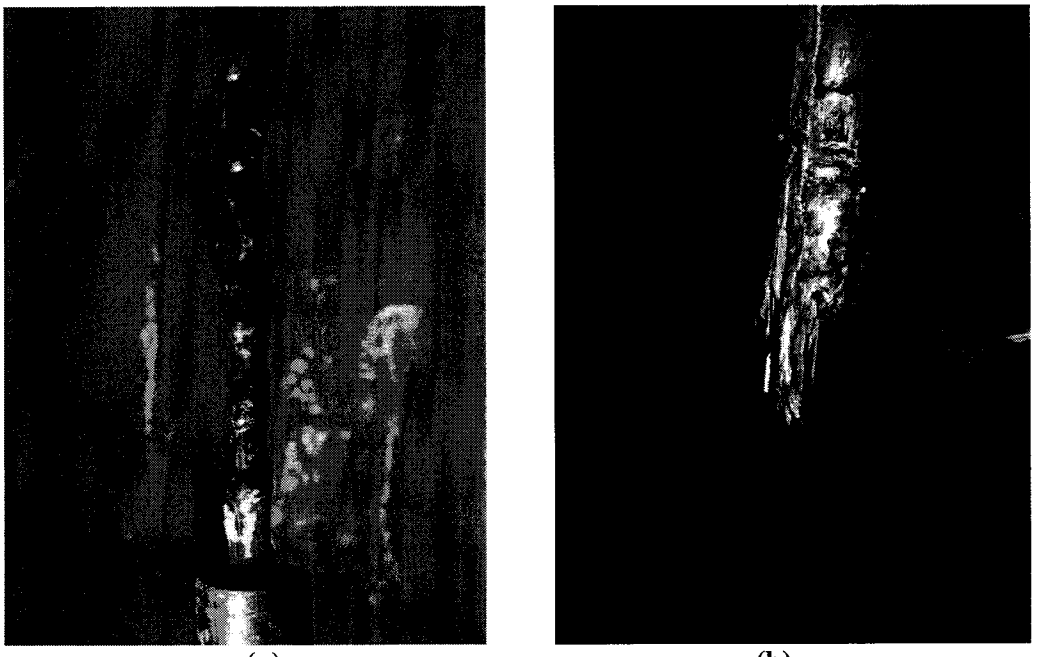

(a) (b)

Figure 4.8 Rupture normal to the fibers orientation mode of failure for specimens: (a)PL-15-2, (b) PL-25-2

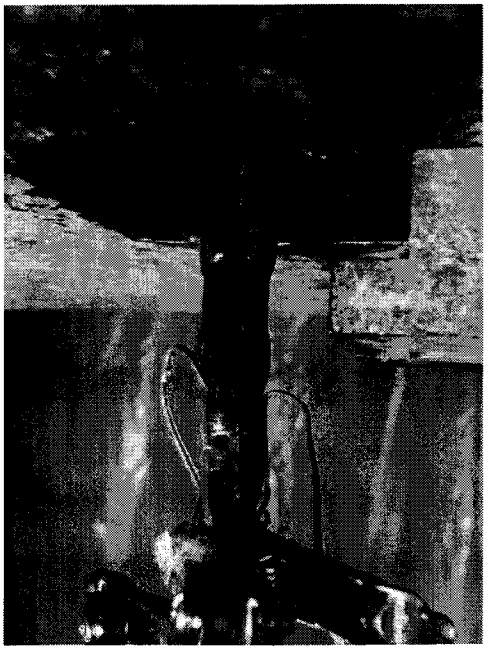

Figure 4.9 Failure with splitting failure of specimen PL-20-2

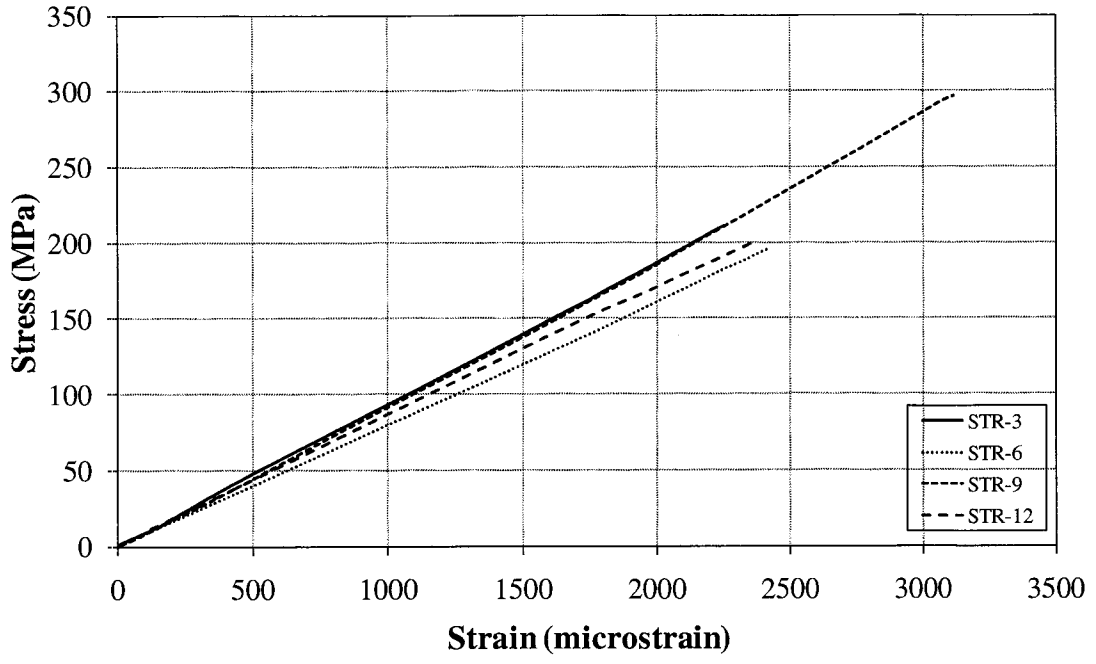

Figure 4.10 Stress-strain relationship of the CFRP rebars tested in the stirrups and bent bars test

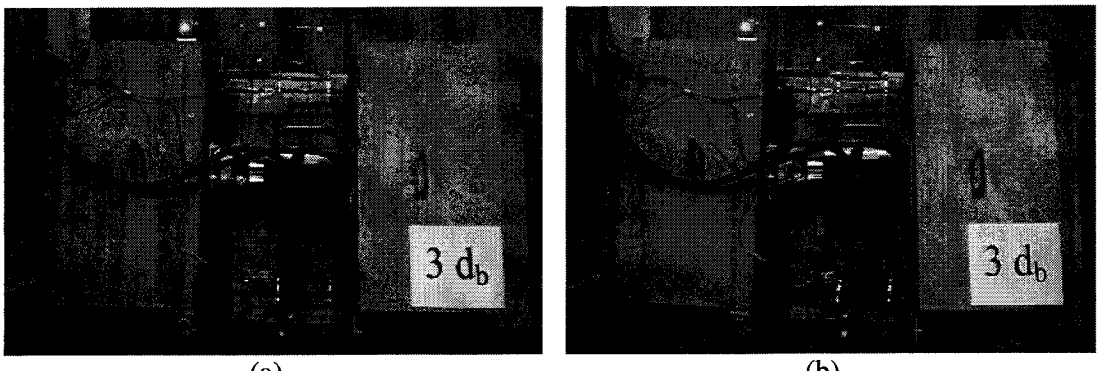

(a) (b)

Figure 4.11 Specimen STR-3: (a) Before loading, (b) After failure

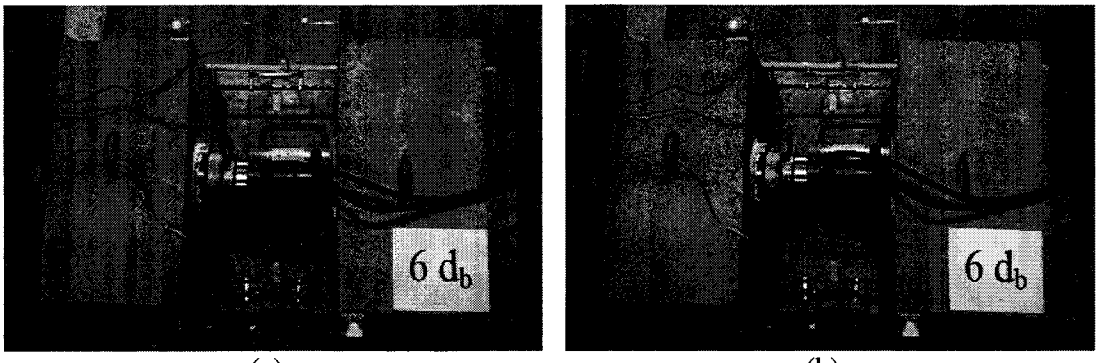

(a) (b)

Figure 4.12 Specimen STR-6: (a) Before loading, (b) After failure

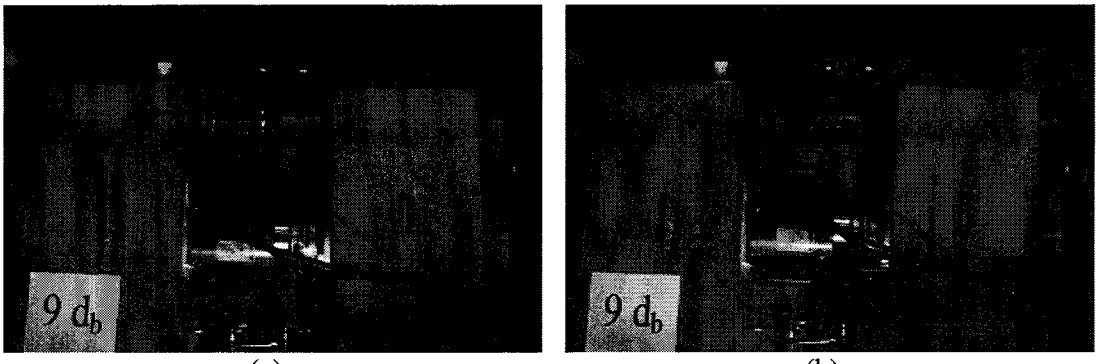

(a) (b)

Figure 4.13 Specimen STR-6: (a) Before loading, (b) After failure

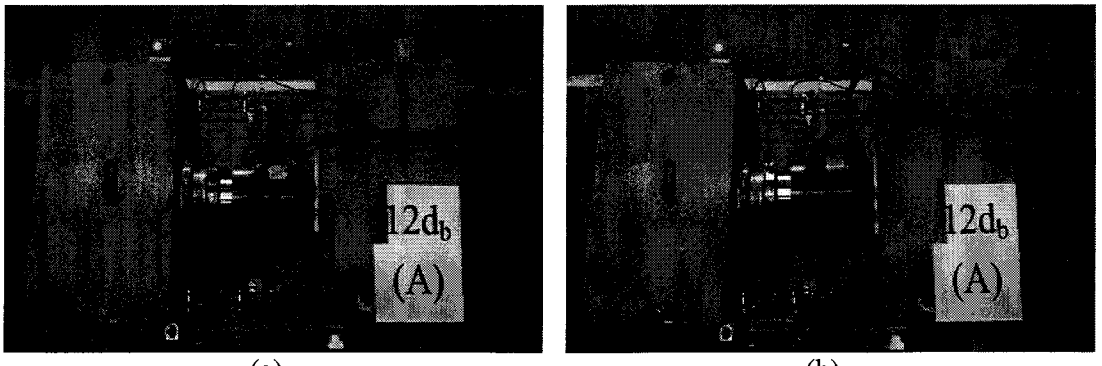

(a) (b)

Figure 4.14 Specimen STR-12: (a) Before loading, (b) After failure

Figure 4.15 Splitting failure of specimen STR-12

CHAPTER 5

EXPERIMENTAL WORK ON STRENGTHENING CONCRETE T-BEAMS IN SHEAR

5.1 Introduction

This chapter describes the test setup and instrumentation of RC T-beams that have deficient shear resistance that does not meet current code requirements thus need to be strengthened. The beams were tested under four-point bending when subjected to monotonically increasing vertical loads up to failure. The specimens were designed to have flexure capacity that is higher than the anticipated capacity of the strengthened beams in order to ensure a shear failure in the shear span zone. The focus of this research is on the use of mechanically anchored dry carbon fiber sheets as means of shear strengthening. Besides conventional data acquisition techniques, i.e. via strain gauges, potentiometers, and load cells, an acoustic emission monitoring of the concrete T-beams was conducted by an industrial partner, WavesInSolids (WINS). The following sections explain the details of the tests on the RC beams.

5.2 Test specimens

The current tests are extension of the previous pilot work by Galal and Mofidi (2010) on a similar anchoring system. Previous tests explored the possibility of strengthening RC beams in shear by wrapping the full shear span zone with a U-shaped dry carbon fibre (CF) sheet that is anchored at its top to the beam. The proof-of-concept

test showed the effectiveness of the strengthening system, yet it showed that a small portion (about 50 mm every 200mm) of the full length of the sheet covering the shear span zone was stretched and contributed to the shear capacity of the beam. In an effort to maximize and fully utilize the benefits of the high modulus dry CF sheets, the mechanical anchoring system was improved in the current experimental program. Moreover, the strains of the CF sheets were monitored along the shear span to explore the behaviour of the CF sheets and to obtain the distribution of the strain along the CF sheet.

Three RC T-beams were tested up to failure: B-0 is a control beam to obtain the contribution of the concrete (V_c) and steel (V_s) to the shear strength; B-1 is a beam strengthened with one layer of dry CF sheet mechanically anchored to the beam; and B-2 is a beam strengthened with double layers of CF sheets which were 150 mm in width.

5.2.1 Beam B-0

Beam B-0 was tested as a control beam to obtain the contribution of the concrete and steel to the shear strength, V_c and V_s, respectively. The control beam was designed such that the flexural yielding capacity is bigger than the shear capacity of the strengthened beams with a sufficient margin above the anticipated capacity of the strengthened beams. Figure 5.1 shows the concrete dimensions and reinforcement details of beam B-0. The dimensions of the tested T-beam were: 445 mm, 90 mm, 290 mm, and 155 mm which are corresponding to the flange width, flange thickness, total high of the beam, and the web width. The beams were tested in four point bending test to create a constant shear zone. The total span between the supports was 1925 mm, the clear shear

span was 575 mm, while the distance between the two concentrated loads was 625 mm. The shear span to depth ratio of the tested beams was 2.05.

The beam was reinforced with 2-35M rebars as a longitudinal web-flexural reinforcement, while two layers of fabric meshes were used in the flange. The web was reinforced with 10M steel rebars spaced at 250 mm. The first stirrup was placed at a distance of 125 mm from the face of the support, and the second was placed 250 mm from the first one and 125 mm from the face of the loading area. The concrete cover was created using plastic seats of 19 mm height (¾").

5.2.2 Beam B-1

Beam B-1 is an identical to the B-0 beam. Both have the same amount and spacing of the flexure and shear reinforcement. Beam B-1 was strengthened with one layer of dry CF sheet mechanically anchored to the beam. The CF sheet had a width of 500 mm and located at a distance of 37 mm from the face of the support and the loading point. The components and details of the improved mechanical anchor system are explained in details in sections 5.3.3 and 5.5, respectively. Figure 5.2 shows the components of the mechanical anchor system, while Figure 5.3 shows the concrete dimensions, reinforcement details, and the mechanical anchor details of beam B-1.

5.2.3 Beam B-2

Beam B-2 has the same amount and spacing of the flexure and shear reinforcement as the other two beams, and was strengthened with two layers of dry CF sheet that were anchored mechanically to the beam. The CF sheets were located between

the two steel stirrups and centered between them. The CF sheet had a width of 150 mm and located at a distance of 175 mm from the face of the support and the loading point. The components and details of the improved mechanical anchor system are explained in details in sections 5.3.3 and 5.5 respectively. Figure 5.4 shows the concrete dimensions, reinforcement details, and the mechanical anchor details of beam B-2.

5.3 Materials

5.3.1 Concrete

The concrete used for constructing the specimens for this research was ordered from a local supplier in Montreal. Concrete with compressive strength of 25 MPa at age of 28 days, and maximum aggregate size of 12 mm (1/2") was ordered.

Six concrete cylinders (100 mm x 200mm) were cast simultaneously with the specimens. The six cylinders were compacted using the standard steel rod. The compressive strength of the concrete cylinders at ages of 14 and 28 days were 35.4 MPa and 41.4 MPa, respectively.

5.3.2 Steel reinforcement

The beams were designed such that the flexural yielding capacity of the strengthened beams was higher than the shear capacity strength of the beam. To achieve this goal, 2-35M steel rebars were used as flexural longitudinal reinforcement for the concrete T-Beams, and 10M stirrups spaced at 250 mm as shear reinforcement. In addition to that, the flange was reinforced with 2 layers of steel fabric meshes of 153x153 18/18.

Samples of the steel rebars were cut from the steel rebars and tested to determine its mechanical properties. The samples were tested up to failure for the 10M rebars, and up to yield for the 35M rebars due to the limitation of the testing machine (530 kN capacity).

The 10M rebars had average yield strength of 465 MPa, yield strain of 2135 microstrain, Young's modulus of 215 GPa, and ultimate strength of 585 MPa. While the 35M rebars had yield strength of 455 MPa.

5.3.3 Mechanical anchor components

The modified mechanical anchor system is composed of round steel rod, steel plate, high strength plaster, heavy duty expansion anchors, and carbon fibre sheets. The steel rod had a diameter of 32 mm (1-¼"), while the steel plate had a thickness of 6 mm (¼") and a width of 63 mm (2-½"). Both the steel rod and the steel plate had a grade of G40.21-44W.

The heavy duty anchors used in this research were Hilti® HSL-3 M10/40 anchors, which provide optimum performance in cracked and non-cracked concrete under large load values. The selected anchor is a torque controlled expansion bolt designed for high performance in static and dynamic load applications. Figure 5.5 shows the Hilti anchor used in this research.

Dry Tyfo® SCH-11UP fibres were chosen to be used in this research as the strengthening material. Tyfo® SCH-11UP is a custom, uni-directional carbon fabric. Tyfo® S Epoxy is used to bond the dry sheets to the steel rods. The Tyfo® S Epoxy is a high elongation material which gives optimum properties as a matrix for the fibres, and

provides a long working time for application. The Tyfo® S epoxy can be mixed together with a ratio of 0.42 part of component A to 1 parts of component B by volume. A slow mixer was used to mix the two components thoroughly for five minutes with speed of 550 rpm. Table 5.1 shows the properties of the dry CF sheets, while Table 5.2 shows the properties of Tyfo® S epoxy.

5.4 Construction of T-beams

Before pouring the three concrete T-beams, wooden forms are designed and constructed, strain gauges are installed on steel rebars, steel cages are prepared. The concrete was poured and cured in the Structure Laboratory of Concordia University, and the formwork was removed after one week.

5.4.1 Preparation of Formwork

Three different wooden forms are manufactured using 19mm thick (¾") plywood. The forms were strengthened with wooden stiffeners which support the concrete flanges and prevent the web to deflect laterally during the concrete pouring. The wooden forms were painted with oil base primer to ease their removal after the concrete harden. Two concaved wooden pieces were placed at the bottom corners of the web to obtain round corners to avoid stress concentration of the CF sheets. Figure 5.6 shows the form work during construction.

5.4.2 Preparations of steel cages

Three sizes of reinforcing steel were used in constructing the concrete T-beams: 10M rebars used as shear reinforcement, 35M rebars used as flexural reinforcement, and 153 x 153 18/18 steel fabric mesh.

The 35M rebars were cut and bent to the designed dimensions by a local supplier, while the fabric meshes and the 10M rebars were cut and prepared at the structures laboratory at Concordia University. The steel rebars were assembled together and tightened together to the wooden form to prevent any movement during the concrete pouring and vibrating. Figure 5.7 shows the wooden forms and steel cages prior to concrete casting.

5.4.3 Concrete pouring and curing

Slump test was done prior to the pouring to insure the workability of the fresh concrete. The measured slump was 60 mm (Figure 5.8). Electrical concrete vibrator was used to vibrate the concrete and to remove any air pockets. The concrete was surfaced with steel trowels to obtain smooth surface. After the concrete hardened, wet burlap sheets were used to cover the concrete and moistened regularly. Six cylinders were prepared and cured along with the concrete beams. Figure 5.9 shows the concrete vibrator used in this research, while Figure 5.10 shows the beams cured using wet burlap sheets.

5.5 Manufacturing of the improved mechanical anchoring system

The mechanical anchor system consists of CF sheet that is wrapped around a steel rod at each end. Each steel rod is restrained against a steel plate that is inclined with a 45°

which is attached on the corner of the web and the flange of the concrete T-beam. Figure 5.2 shows the mechanical anchor components and details used in strengthening of beam B-1.

The system was designed such that none of its elements exceeds its yielding strength, nor the deflection at any location of the steel rod exceeds 10% of the vertical component of the expected shear crack width.

The mechanical anchoring system was prepared in three stages: preparing each individual element, wrapping the CF sheets around the steel rods, and mounting the different parts on the beams.

The concrete beams were drilled in the designed locations with a diameter of 15.8 mm (5/8") drill bit. The holes were cleaned with compressed air to remove any left dust or debris. Matching holes were drilled to the round steel rods and plates. The rods were sand papered to remove any rust particles that may affect the bond with the epoxy. The Carbon Fibre (CF) sheets were cut shorter than the desired length to insure the stretchiness of the fibres.

The CF sheets were wrapped two and half rounds around the steel rods. Two wraps were wet while the half wrap was dry. The reason of wrapping the dry CF sheets half round after the two wet layers is to insure that the joint between the stiff wet fibres and the flexible dry fibres is not in the straight part of the fibres. If the joint exists at such location it may cause stress concentration and lead to early tear off of the flexible dry fibre at that joint location. The excess epoxy which accumulated at this joint was removed. Moreover, plastic sheets were put to protect the dry fibres from the inner wet

fibre layers. The rods were fixed to the table for two to three days with c-clamps until the epoxy set.

The mechanical anchoring system should be pre-stretched (before the beam loading) to be able to carry the load as soon the concrete starts to crack. Thus, the anchor was improved to allow the fibres to self-align and stretch during the tightening of the Hilti anchors. Plaster bags were used for that purpose. In addition to that, steel plate was needed to provide shearing resistance that is needed to sustain the shearing forces created (on the anchors) due to the inclination between the fibres and the Hilti anchors. The plaster and steel plate were put at the intersection of the web and the flange of the concrete beam before mounting the mechanical anchoring system. During the tightening of the anchors, the squeezed plaster was removed from the outer side of the sheets. The inner side of the fibres was protected with plastic sheets to prevent any undesirable contact between the flexible dry fibres and the rough edges of the plaster (after hardening and during loading).

To overcome any non-uniformity of the length of the CF sheets and to ensure that the fibres are stretched with the same amount of force, another plaster bag was needed. The plaster was put in a plastic bag which in turn is placed between the CF sheets and the bottom surface of the concrete beam. This plastic bag is opened from its two sides (along the length of the CF sheets) to allow the plaster to squeeze upon tightening the CF sheets. The Hilti anchors were tightened to the required torque, the squeezed plaster were removed before immediately, and the anchoring system was left at least 90 minutes to allow the plaster to set.

When two layers of CF sheets were prepared, the outer layer was cut longer than the inner one. Before tightening the anchors, third plaster bag were prepared between the first and second layer of the CF sheets to insure the stretchiness of the two layers.

Figure 5.11 shows the anchor used for strengthening beam B-1 during manufacturing, while Figures 5.12 and 5.13 show bottom and elevation views of the anchor after installing them to beam B-1.

Figure 5.14 shows the anchor used for strengthening beam B-2 during manufacturing, while Figures 5.15 shows the anchor after installing them to beam B-2.

5.6 Test setup and instrumentation

The beams were tested in four point bending test to create a constant shear zone. The total span between the supports was 1925 mm, the clear shear span was 575 mm, while the distance between the two concentrated loads was 625 mm. The shear span to depth ratio of the tested beams was 2.05.

A strong reaction frame with a total capacity of 750 kN was designed and constructed to match the expected failure load of the tested (strengthened) beams. Figure 5.16 shows the test setup and the strong reaction frame of the tested beams. Hydraulic cylinder with a capacity of 600 kN and maximum stroke length of 257 mm (10-1/8") was used to apply the load which was connected to a manually controlled hydraulic pump. A load cell was placed between the hydraulic cylinder and the strong reaction frame in order to obtain the readings of the applied load.

Steel plate with a thickness of 50 mm (2") was used as bearing plate between the steel rollers and the concrete T-beam to avoid concrete crushing due to the stress

concentration. Steel channels and hard rubber were used under the two point loads to distribute the applied forces and prevent any stress concentration. Plaster was used between the concrete beam and the steel plates and between the concrete and channels to overcome any surface imperfection.

Each concrete beam was instrumented with 11 strain gauges and five linear position string pots (potentiometers). The strain gauges used in this research had a gauge length of 5 mm, and a maximum measurable strain of 15,000 με, while the potentiometers used had a maximum stroke length of 317 mm (12.5") and an accuracy of 0.9mm.

Three strain gauges were mounted on the flexural reinforcement, and 8 strain gauges were installed on the shear reinforcement (stirrups). One of the flexural strain gauges was located at mid span, and one at each loading point. While one strain gauge installed on each leg of the shear reinforcement stirrups. The potentiometers were located in different locations: three of them were placed at mid span of the beam, and one potentiometer under each loading point.

The strains of the CF sheets were monitored along the shear span to explore the behaviour of the CF sheets and to obtain the distribution of the strain along the CF sheet. For that purpose, 12 strain gauges were mounted on the CF sheets of beam B-1 while 8 strain gauges were installed on beam B-2. Figures 5.17, 5.18, and 5.19 show the instruments of beams B-0, B-1, and B-2, respectively.

The details of the test setup and instruments used to monitor the concrete acoustic emission are explained in Appendix A.

5.7 Test procedure

The loading was applied gradually by a manually controlled pump with a constant rate up to failure. The readings were monitored on the computer during the test, while the data are being recorded each one second using the data acquisition system for further analysis.

Figures 5.20, 5.21, and 5.22 show beams B-0, B-1, and B-2, respectively prior to test.

Table 5.1 Properties of the dry CF sheets

Typical dry fibre properties	Value
Tensile strength	3.79 GPa
Modulus of elasticity	230 GPa
Ultimate elongation	1.60 %
Density	1.8 $\frac{gr}{m^3}$
Weight per sq. Meter	315 $\frac{gr}{m^2}$
Fibre thickness	0.175 mm

Table 5.2 Properties of Tyfo S epoxy

Epoxy properties	Value
Tensile strength	72.4 MPa
Modulus of elasticity	3.18 GPa
Elongation	5.00 %
Flexural strength	123.4 MPa
Flexural modulus	3.12 GPa

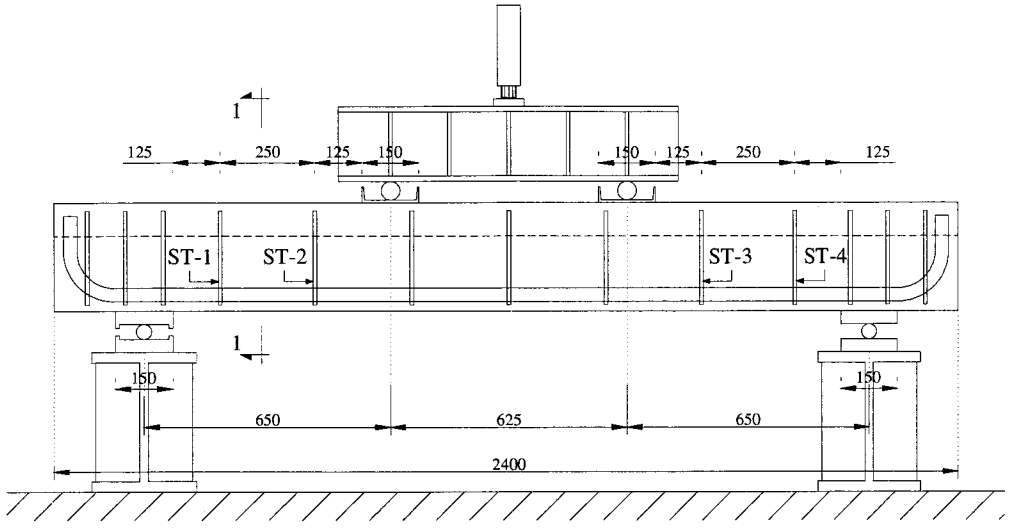

Elevation

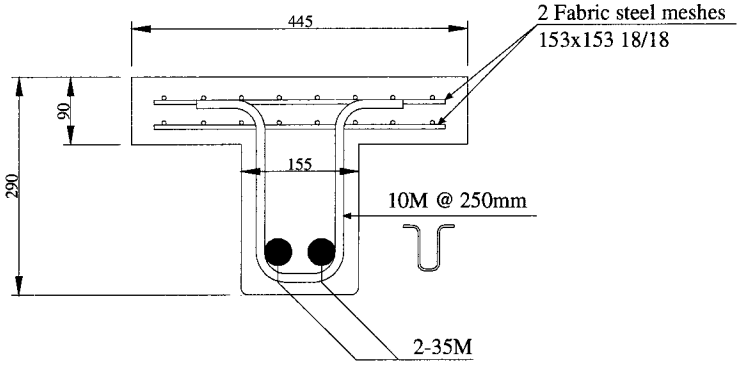

SECT. 1-1

Figure 5.1 Concrete dimensions, reinforcement details, and test setup of beam B-0

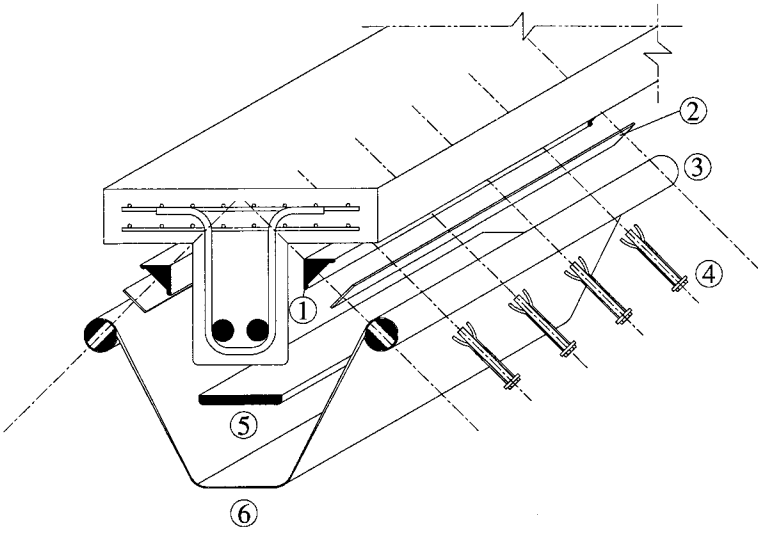

Figure 5.2 Components and details of the improved mechanical anchor system

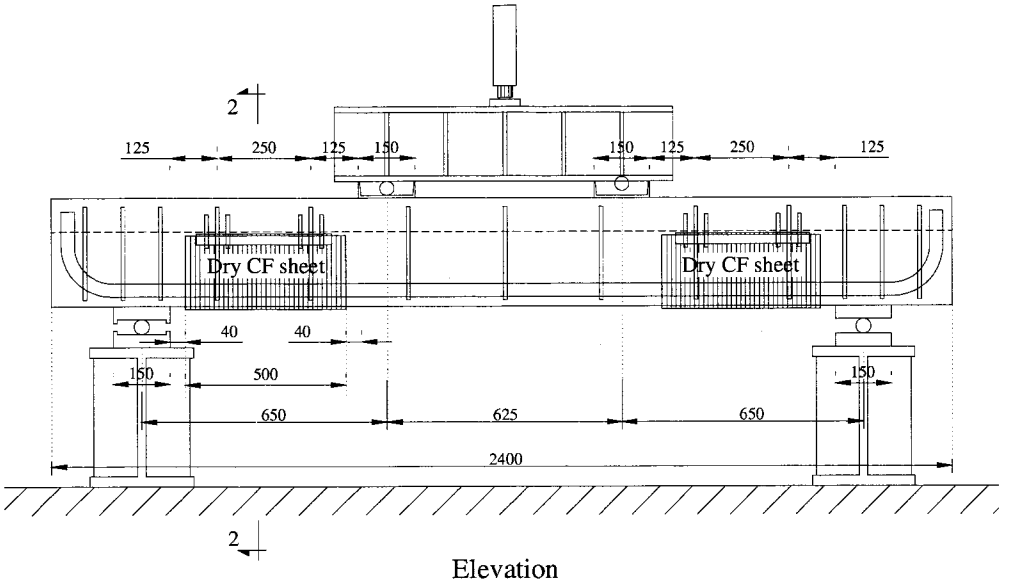

Elevation

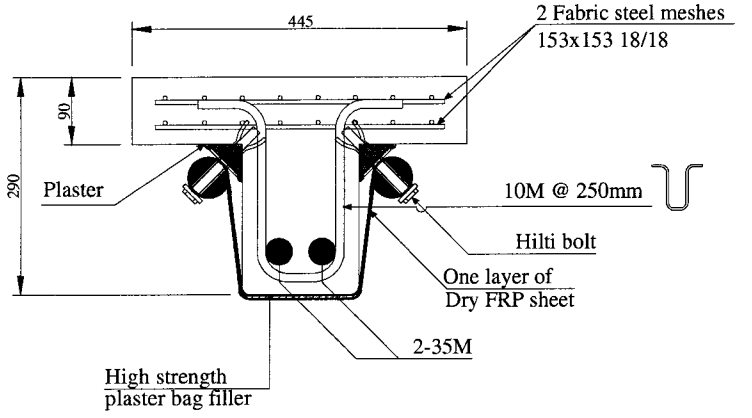

SECT. 2-2

Figure 5.3 Concrete dimensions, reinforcement details, anchor details, and test setup of beam B-1

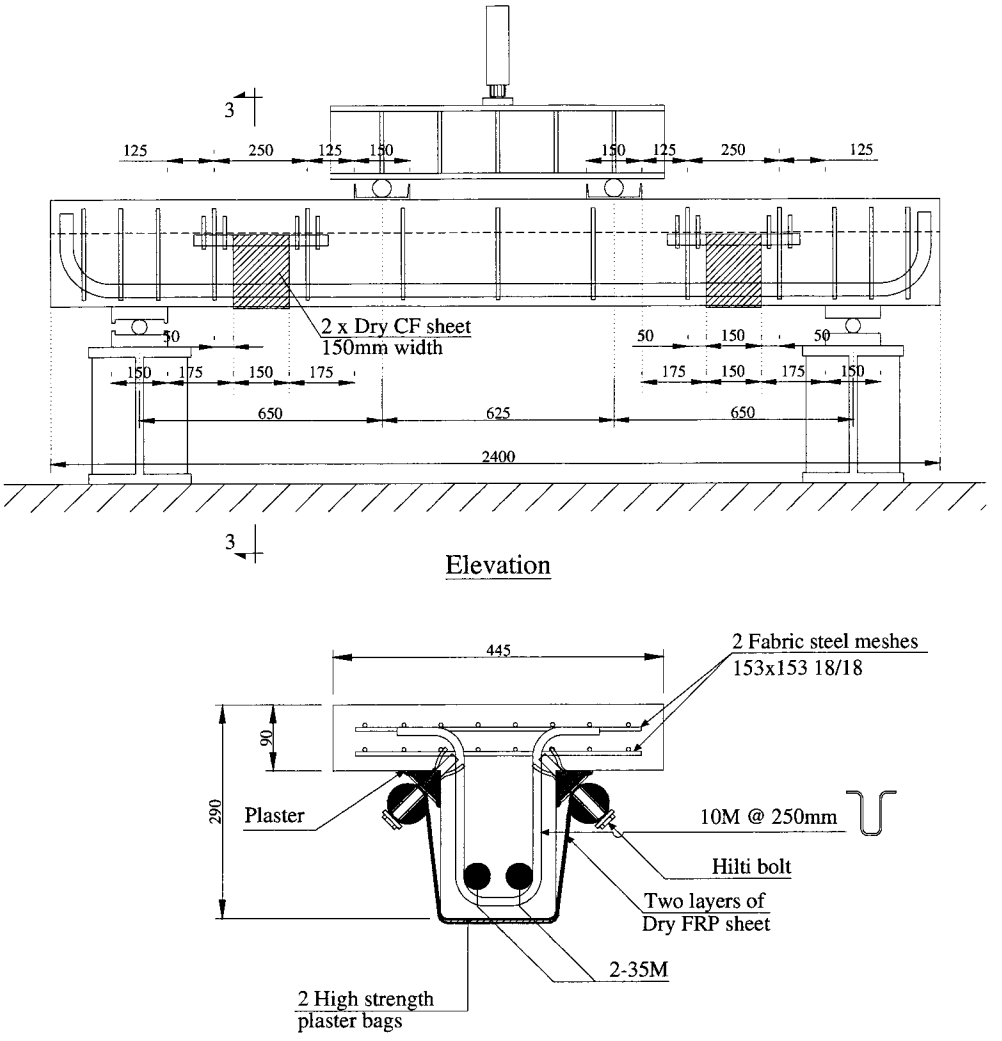

Figure 5.4 Concrete dimensions, reinforcement details, anchor details, and test setup of beam B-2

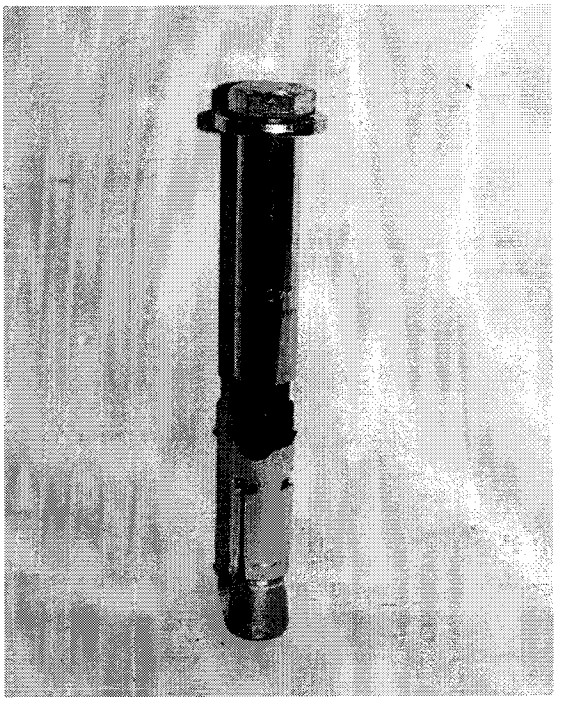

Figure 5.5 The Hilti HSL-3 M10/40 anchor used in this research

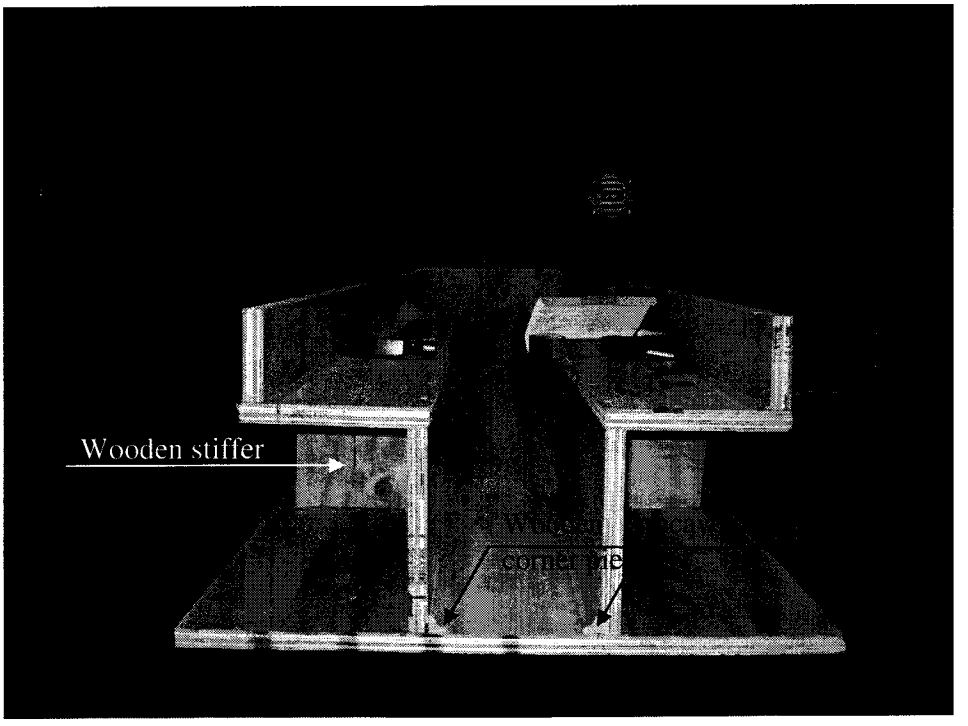

Figure 5.6 Details of the form work during construction

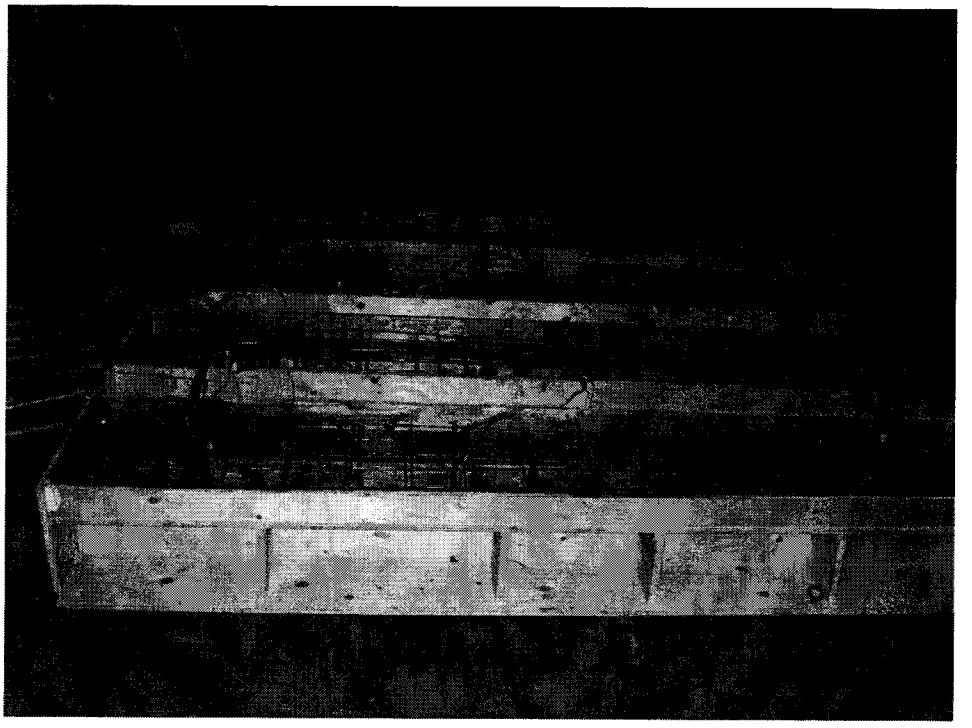

Figure 5.7 Wooden forms and steel cages prior to concrete pouring

Figure 5.8 Slump test

Figure 5.9 Concrete vibrator used in this research

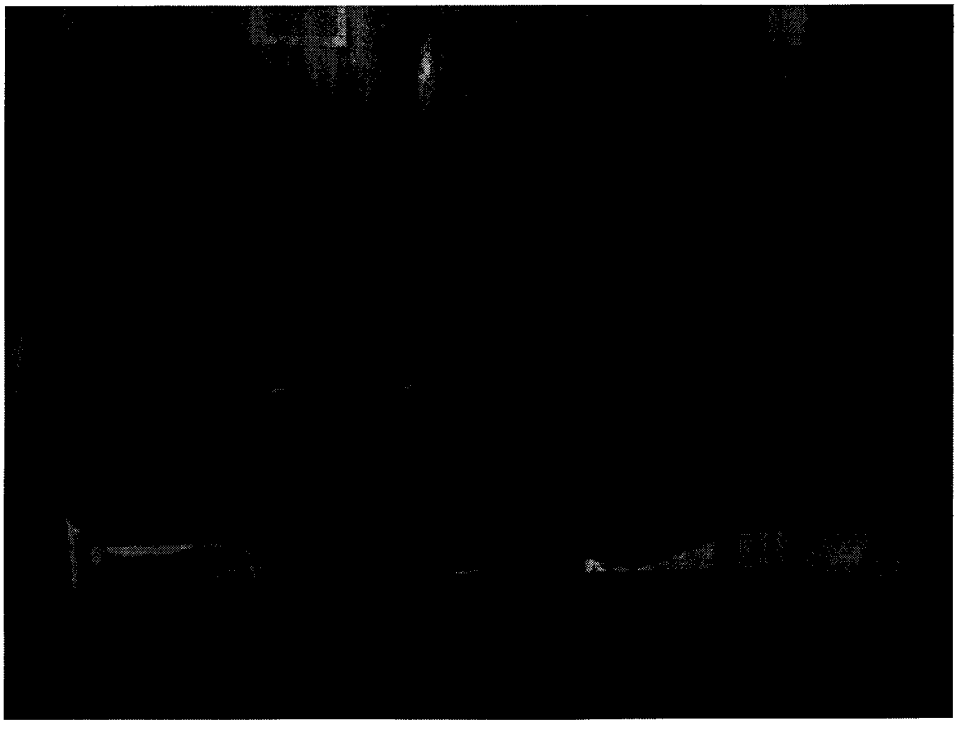

Figure 5.10 Curing of the beams using wet burlap sheets

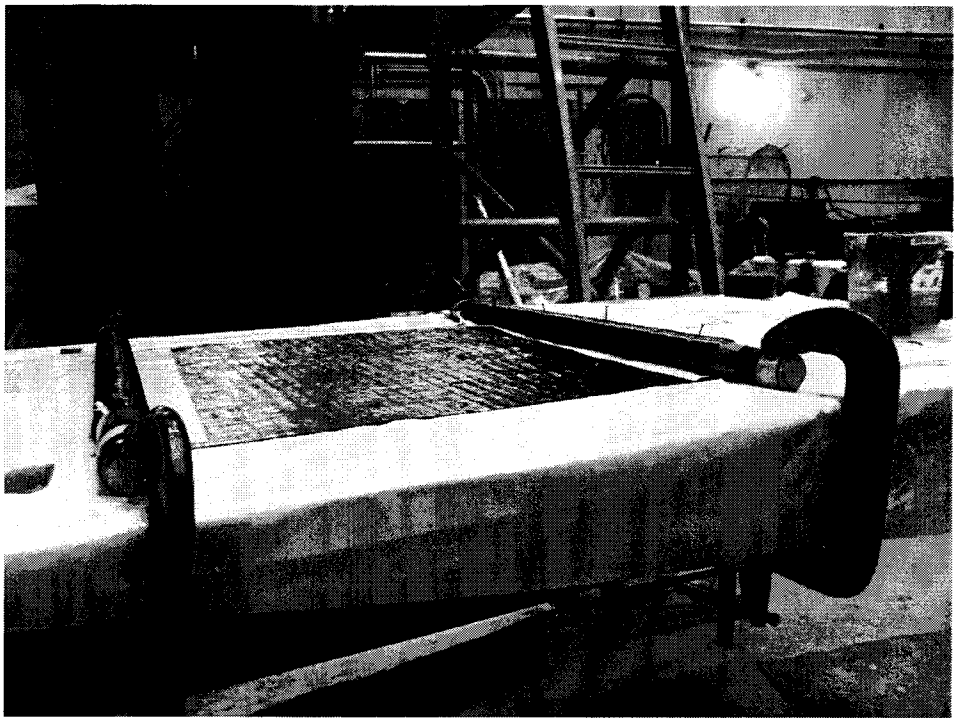

Figure 5.11 Anchor of beam B-1 while being manufactured

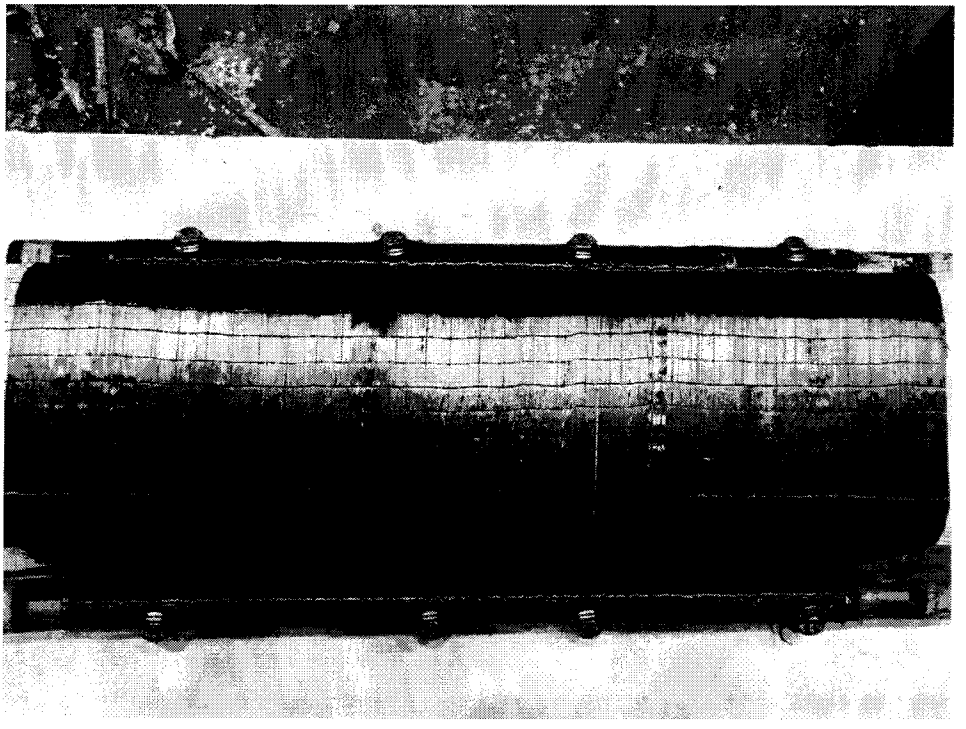

Figure 5.12 Bottom view of beam B-1 after installing the mechanical anchor

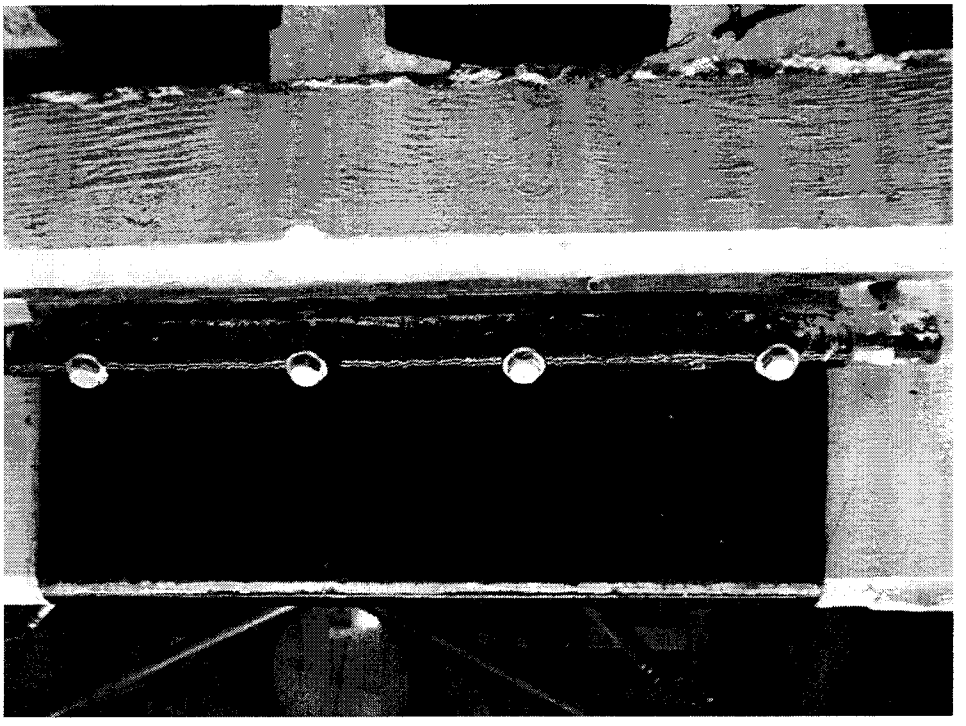

Figure 5.13 Elevation view of beam B-1 after installing the mechanical anchor

Figure 5.14 Anchor of beam B-2 while being manufactured

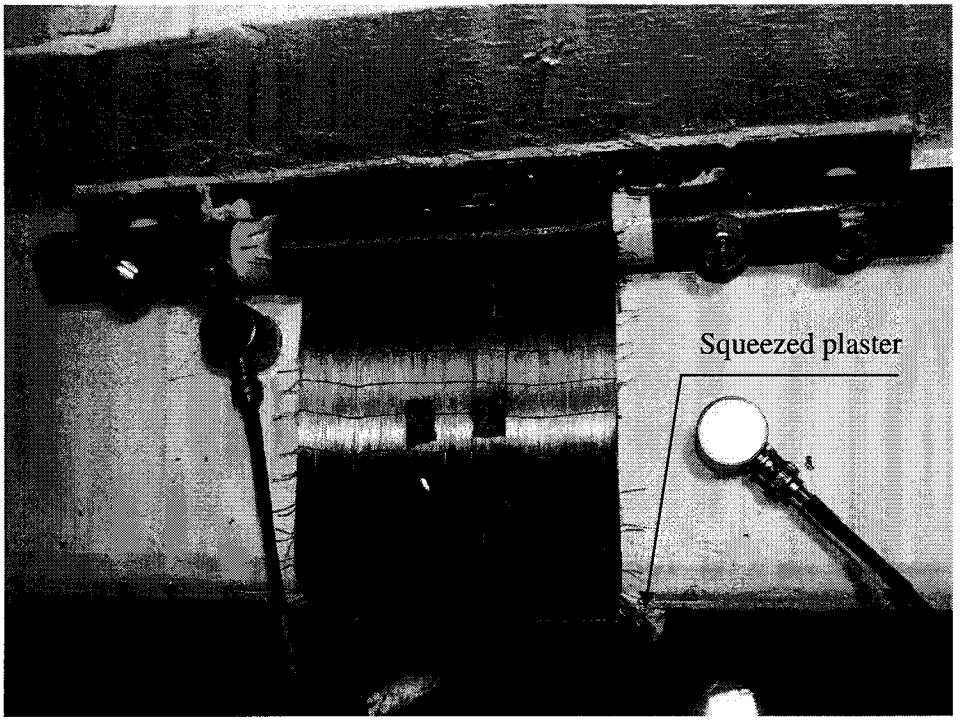

Figure 5.15 Elevation view of beam B-2 after installing the mechanical anchor

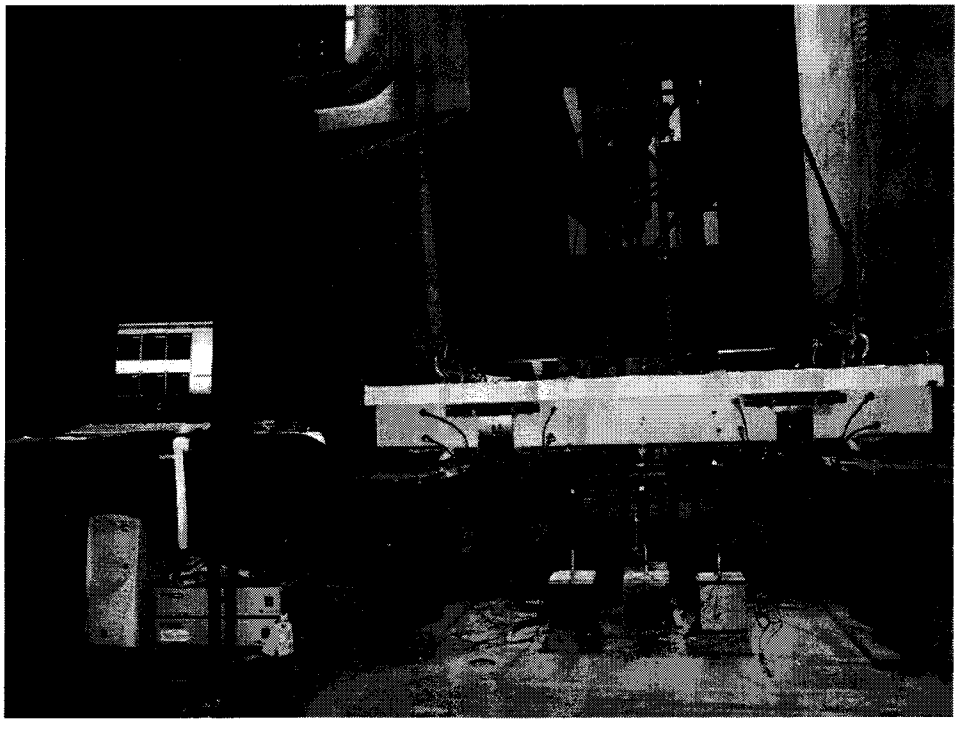

Figure 5.16 Test setup and strong reaction frame

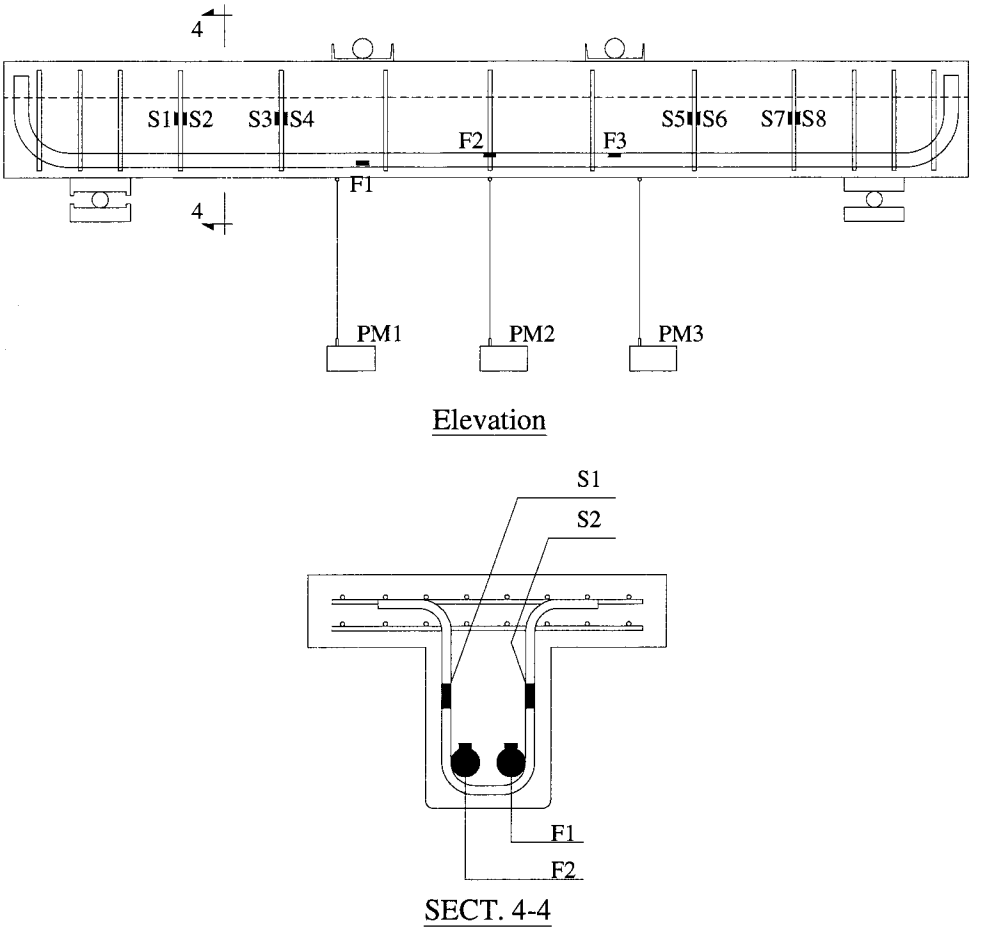

Figure 5.17 Instruments of beam B-0

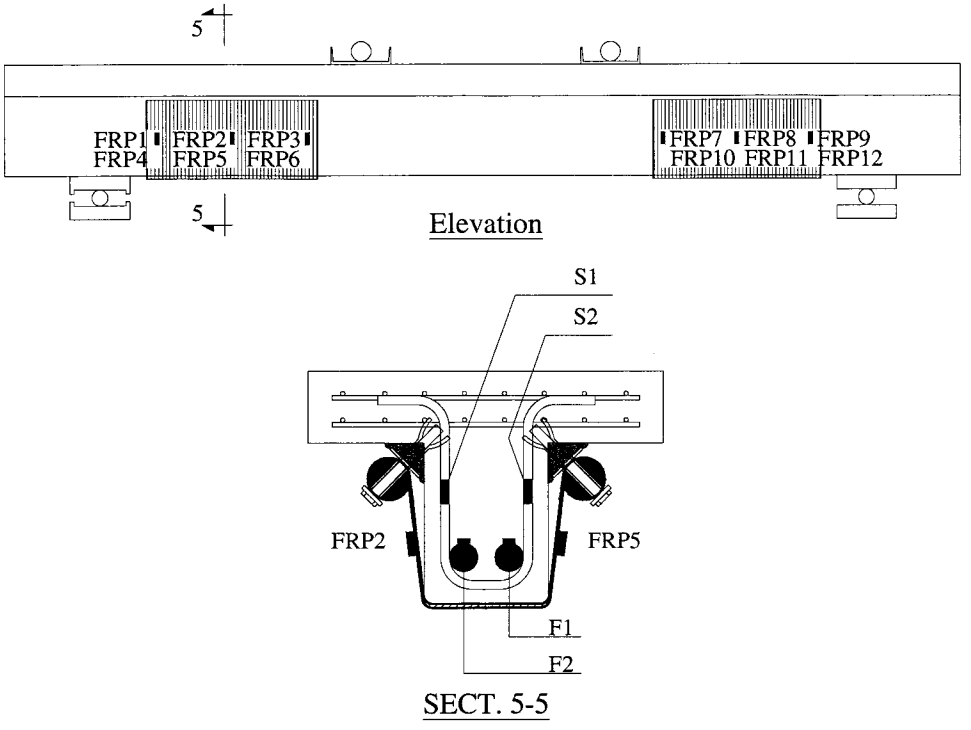

Figure 5.18 Instruments of beam B-1

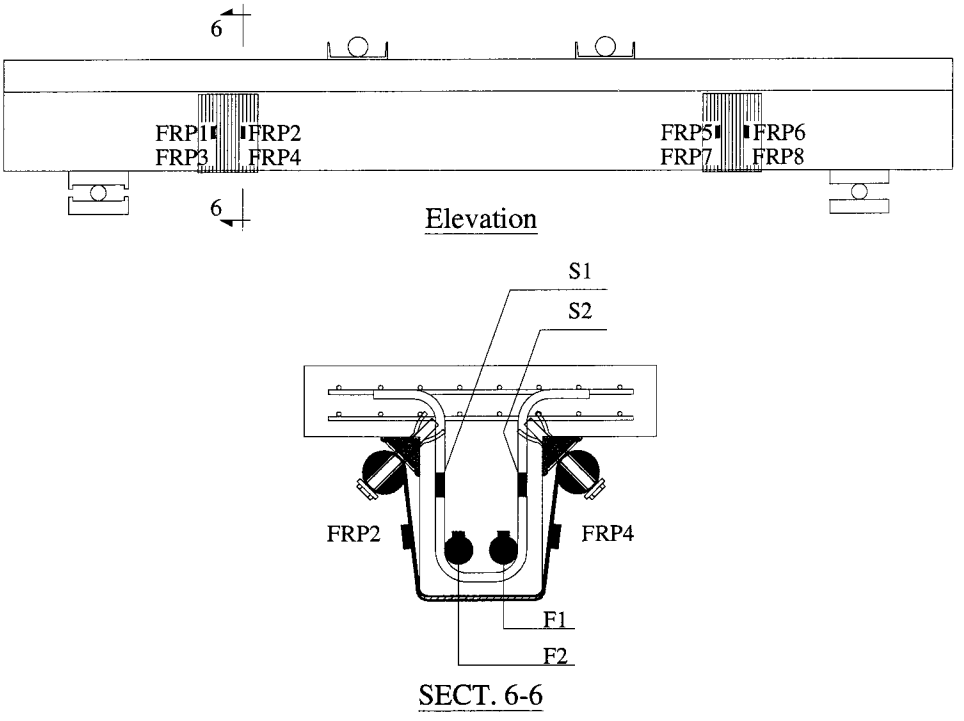

Figure 5.19 Instruments of beam B-2

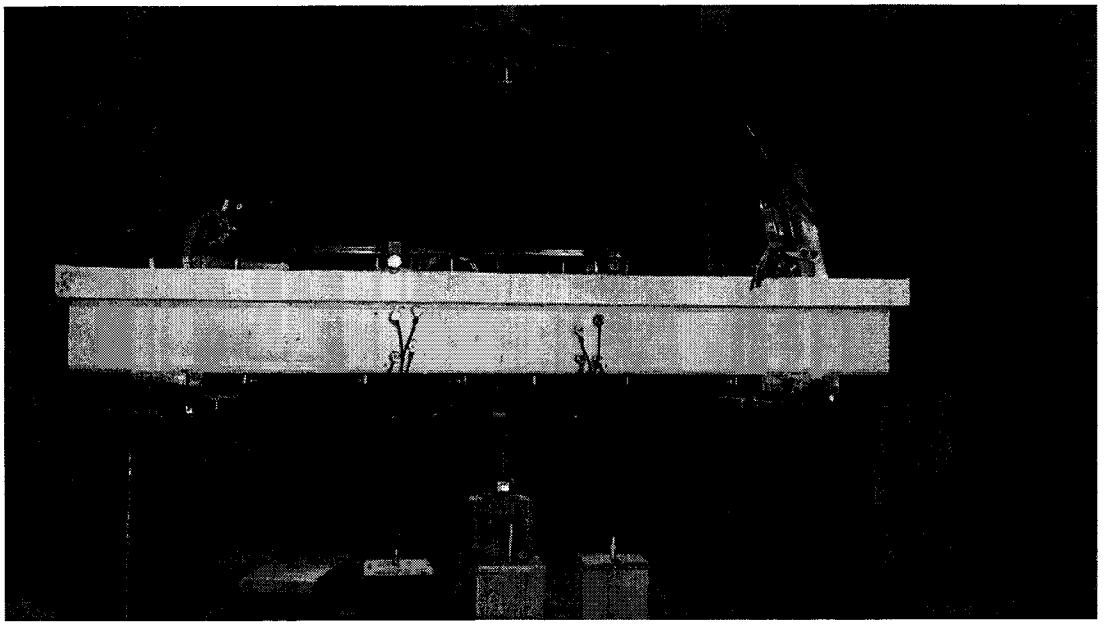

Figure 5.20 Beam B-0 prior to test

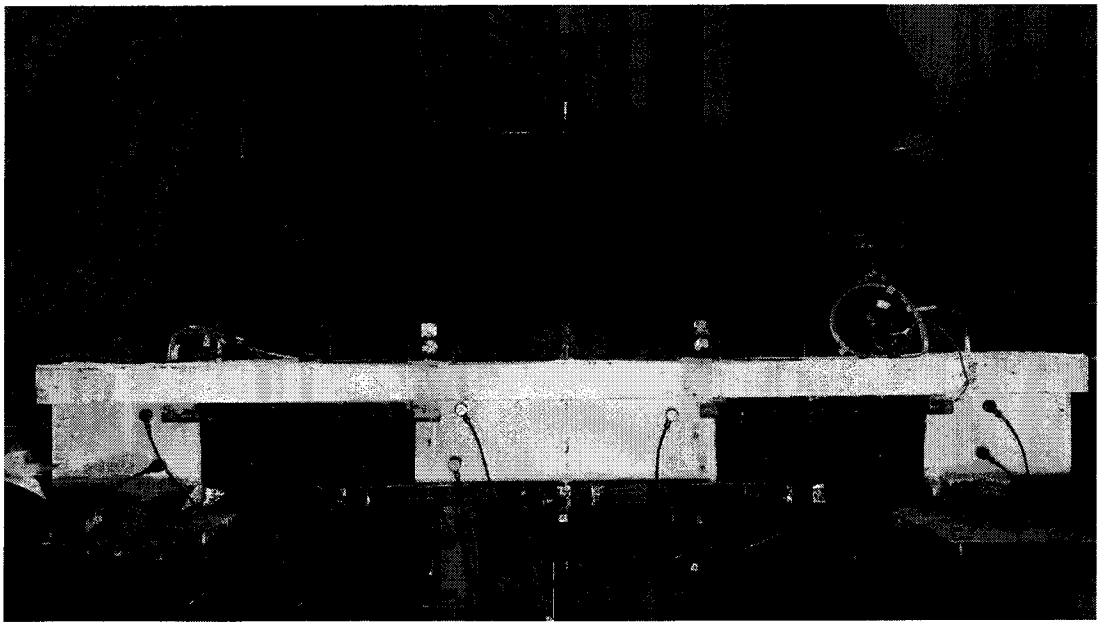

Figure 5.21 Beam B-1 prior to test

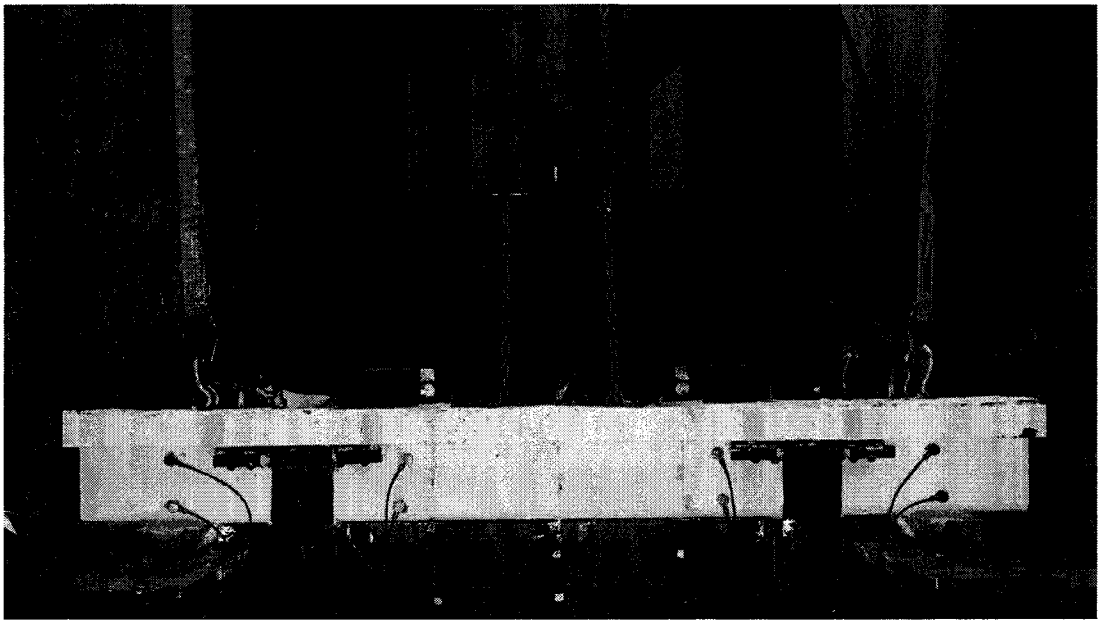

Figure 5.22 Beam B-2 prior to test

CHAPTER 6

EXPERIMENTAL RESULTS OF THE CONCRETE T-BEAMS STRENGTHENED IN SHEAR

6.1 Introduction

This chapter describes the results and the observations during testing the concrete T-beams strengthened in shear. The beams were strengthened using dry CF sheets which were anchored mechanically to the beam. The beams were designed such that the flexural yielding capacity is bigger than the shear capacity of the strengthened beams with a sufficient margin above the anticipated capacity of the strengthened beams. To achieve this goal, 2-35M steel rebars were used as flexural longitudinal reinforcement for the concrete T-Beams, and 10M stirrups spaced at 250 mm as shear reinforcement. The anchoring system was designed such that none of its elements exceeds its yielding strength, nor the deflection at any location of the steel rod exceeds 10% of the vertical component of the expected shear crack width.

Three RC T-beams were tested up to failure: B-0 is a control beam to characterize the contribution of the concrete (V_c) and steel (V_s) to the shear strength; B-1 is a beam strengthened with one layer of dry CF sheet mechanically anchored to the beam with a width of 500 mm; and B-2 is a beam strengthened with double layers of CF sheets which was 150 mm in width.

The loading was applied gradually through a manually controlled pump with a constant rate up to failure. The readings of the load, strains, and deflections were

monitored on the computer during the test, while the data were being recorded each one second using the data acquisition system.

6.2 Behaviour of control beam B-0

The beam was loaded gradually with a constant rate up to failure. Shear cracks started to initiate at a shear load of 75 kN. Another shear crack was observed at a shear load of 98 kN. At a shear load of 219 kN, a shear crack formed in the concrete flange followed by a brittle compression shear failure of the beam. Some flexural cracks were noticed during the test in the constant moment zone. Figure 6.1(a) shows a global view of beam B-0 after failure, Figure 6.1(b) shows a close view to the failed portion of the beam, while Figure 6.1(c) shows a schematic drawing showing the crack patterns of beam B-0 and the locations of the steel stirrups with respect to the cracks.

6.2.1 Strains in steel stirrups

The strains of the steel stirrups were monitored using a strain gauge mounted on each leg of the steel stirrups. Figure 6.2 shows the relation between the average strains in each of the four steel stirrups versus the shear load, where the locations of stirrups ST1, ST-2, ST-3, and ST-4 are shown in Figure 5.1. The strains in the steel stirrups were negligible until the shear load reached 50 kN at which a significant increase in the strains observed. The strains increased gradually and exceeded its yielding strain before the beam failed in shear at a shear load of 219 kN. The maximum average strain in stirrups ST-1, ST-2, ST-3 and ST-4 was 2050, 1850, 2250, and 2160, respectively. It was noticed

that the major shear crack that occurred and caused the shear failure of the beam occurred at stirrups ST-3 and ST-4 which were strained more than stirrups ST-1 and ST-2.

6.2.2 Strains in flexural reinforcement

Figure 6.3 shows the relation between the shear load and the strains in the flexural steel reinforcement. The strains in the flexural steel reinforcement were linear up to the failure of the beam. The ultimate strain in the flexural reinforcement was 1970 microstrain.

6.2.3 Load-deflection relationship

During the test the readings of the deflections of the potentiometers were monitored on the computer screen and checked using an independent dial gauge. Both showed identical deflection values.

Figure 6.4 shows that the relation between the shear load and the mid-span deflection of beam B-0 was linear up to the failure. Moreover, the failure was sudden and brittle. The ultimate deflection of the beam was 8.1 mm occurred at a shear load of 219 kN.

6.2.4 Discussion of the results of beam B-0

Beam B-0 was tested to characterize the contribution of the concrete (V_c) and steel (V_s) to the shear strength. The contribution of the steel stirrups was obtained using the readings of the strain gauges, while the contribution of the concrete was obtained by

deducting the steel contribution from the total shear strength. The steel contribution was 179 kN, while the concrete contribution was 40 kN as summarized in Table 6.1.

6.3 Behaviour of beam B-1

The beam was loaded gradually with a constant rate up to failure. The dry CF sheets covered both shear spans, thus no shear cracks in the concrete web were observed. At a shear load of 220 kN a shear crack was observed in the concrete flange which widened upon increasing the load. The beam failed at a shear load of 235 kN.

After the failure occurred, the dry CF sheets were removed to inspect the shear cracks in the concrete web. Figure 6.5(a) shows a global view of the beam B-1 after failure, Figure 6.5(b) shows a close view to the failed shear span, while Figure 6.5(c) shows a close view of the shear cracks in the concrete web after removing the dry CF sheet. Figure 6.5(d) shows a schematic drawing of the crack patters and the locations of the internal steel stirrups

6.3.1 Strains in steel stirrups

The strains of the steel stirrups were monitored using a strain gauge mounted on each leg of the steel stirrups. Figure 6.6 shows the relation between the average strains in each of the four steel stirrups versus the shear load, where the locations of stirrups ST1, ST-2, ST-3, and ST-4 are shown in Figure 5.1. The strain values in the steel stirrups were very low until the shear load reached 45 kN at which a significant increase in the strains was observed. The strains increased gradually and two of them exceeded their yielding strain until the beam failed in shear at a shear load of 235 kN. The maximum average

strain in stirrups ST-1, ST-2, ST-3 and ST-4 was 2165, 1295, 1935, and 2400 microstrain, respectively. It was noticed that the stirrups ST-2 and ST-3 which are close to the loading points were strained less than ST-1, and ST-3. This is because the CF sheets contributed to the shear strength and reduced the load from the stirrups close to the loading points.

6.3.2 Strains in dry CF sheets

Three strain gauges were mounted on each side of each CF sheet. The locations of the strain gauges are shown in Figure 5.17.

Figure 6.7 shows the relation between the strains in the CF sheets and the shear load. The strains in the CF sheets were negligible till the load reached 40 kN at which the CF sheets were activated. The strains increased linearly until the shear load reached 220 kN at which the CF started to strain significantly at the location of FRP-2 and FRP-5. The maximum recorded strain was 3000 microstrain at FRP-2 and FRP-5, which were located at the middle of the two steel stirrups ST-1, and ST-2. It was noticed that FRP-1, FRP-4, FRP-3, and FRP-6 had an ultimate strain less than 500 microstrain. It was also observed that the strain gauges mounted in the location of the steel stirrup near to the supports (FRP1 and FRP4) had smaller strain values than the ones mounted in the location of the stirrups near the point load (FRP3 and FRP6). The distribution of the strains along the CF sheet is shown in Figure 6.8

6.3.3 Strains in flexural reinforcement

Figure 6.3 shows the relation between the strains in the flexural steel reinforcement and the shear load of beam B-1. The strains in the flexural steel

reinforcement were linear up to the failure of the beam. The ultimate strain in the flexural reinforcement was 2100 microstrain which is still less than the yielding strain of the steel reinforcement.

6.3.4 Load-deflection relationship

During the test the deflections were monitored using an independent dial gauge and the potentiometers. Both showed identical mid-span deflection values.

Figure 6.4 shows the relation between the shear load and the mid-span deflection of beam B-1. The relationship of the load-deflection was linear up to a shear load of 225 kN, at which the beam showed some ductility until failure. The ultimate deflection of the beam was 10.4 mm occurred at a shear load of 235 kN.

6.3.5 Discussion on the behaviour of beam B-1

The contribution of the concrete (V_c), steel (V_s), and the dry CF sheets (V_{CF}) to the shear strength of beam B-1 were 40 kN, 161 kN, and 34 kN, respectively. Thus the increase of the shear strength was 16.9 %. The strains of the CF sheets were minimum at the location of the steel stirrups, and maximum at the middle of the two steel stirrups. The beam showed a semi-ductile behaviour before failure compared to the control beam B-0 as reported by Mofidi (2008).

6.4 Behaviour of beam B-2

As observed in the behaviour of beam B-1, the strains of CF sheets were minimum at the location of the steel stirrups, and maximum at the middle of the two steel

stirrups. To maximize the benefit of the high modulus dry CF sheets, double strips of dry CF sheets were mechanically anchored at the middle of the steel stirrups. Moreover, the effectiveness of using double layers of CF sheets system was investigated and evaluated. The width of the CF sheets is located such that the area under the curve of the strain versus the distance from the face from the support is 70 % of the total area. Accordingly, the double layers of CF sheets are expected to contribute 140 % of the value of the contribution of the CF sheets in beam B-1.

Beam B-2 was loaded gradually with a constant rate up to failure. The dry CF sheets covered a part of the shear span, thus no shear cracks in the concrete web were able to be observed during the test. A shear crack was observed in the concrete flange prior to the failure of the beam failed at a shear load of 267 kN.

After the failure occurred, the mechanically anchored dry CF sheets were removed to inspect the shear cracks in the concrete web. Figure 6.9(a) shows a global view after failure of the beam B-2, Figure 6.9(b) shows a close view to the failed shear span, while Figure 6.9(c) shows a close view of the shear cracks in the concrete web after removing the dry CF sheet. Figure 6.9(d) shows a schematic drawing of the crack patters of beam B-2 and the locations of the internal steel stirrups.

6.4.1 Strains in steel stirrups

A strain gauge mounted on each leg of the steel stirrups was used to monitor the strains of the steel stirrups. Figure 6.10 shows the relation between the average strains in each of the four steel stirrups versus the shear load, where the locations of stirrups ST-1, ST-2, ST-3, and ST-4 are shown in Figure 5.1. The relation between the shear load and

the strains in steel stirrups ST-1 and ST-4 (which were located near to the supports) were linear until the shear load reached 150 kN, and 100 kN respectively. Afterwards, a significant increase in the strains was observed. On the contrary stirrups ST-2 and ST-3 had higher strain values upon loading until the shear load reached 160 kN. After the shear load reached 160 kN, the rate of the change of the strain in stirrup ST-2 was less than the other stirrups. After the shear load reached 250 kN stirrup ST-2 lost part of its strain. As mentioned in section 6.4, a shear crack was observed in the concrete flange. Due to this shear crack, the stirrup ST-2 lost part of its bond strength and cause the observed reduction of its strains.

All of the stirrups except stirrup ST-2 exceeded their yielding strain. The maximum average strain in stirrups ST-1, ST-2, ST-3 and ST-4 was 2635, 1730, 2785, and 2446, respectively.

6.4.2 Strains in the dry CF sheets

Two strain gauges were mounted on each side of each CF sheet. The locations of the strain gauges are shown in Figure 5.18.

It was observed that all the strain gauges at each CF sheet had almost the same strain. The average strain was calculated and plotted in Figure 6.11 for each shear span. The strains in the CF sheets were negligible till the load reached 80 kN at which the CF sheets started to strain. The strains increased until the beam failed at shear load of 267 kN. The maximum recorded strain was 1990 microstrain at strain gauge FRP-5 and FRP-6.

6.4.3 Strains in flexural reinforcement

Figure 6.3 shows the relation between the shear load and the strains in the flexural steel reinforcement. The strains in the flexural steel reinforcement were linear up to failure. Although the ultimate strain in the flexural reinforcement was 2730 microstrain (which is higher than its yielding strain), the relation between the strains in the flexural steel reinforcement and the shear load was linear up to failure.

6.4.4 Load-deflection relationship

During the test the deflections were monitored using an independent dial gauge and potentiometers. Both showed identical deflection values at the mid-span of the beam.

Figure 6.4 shows the relation between the shear load and the mid-span deflection of beam B-2. The relationship of the load-deflection was linear up to a shear load of 150 kN, at which the beam tended to deflect more. At a shear load of 225 the stiffness of the beam was decreased. The ultimate deflection of the beam was 11.1 mm which occurred at a shear load of 267 kN.

6.4.5 Discussion on the performance of beam B-2

The contribution of the concrete (V_c), steel (V_s), and the dry CF sheets (V_{CF}) to the shear strength of beam B-2 were 40 kN, 178 kN, and 48 kN, respectively as summarized in Table 6.1. The mechanically anchored dry CF sheets were able to increase the shear strength by 22 %. Since the strain gauges were mounted in the high strain zone, the strains of CF sheets had almost the same values.

The width of the CF sheets was located such that the area under the curve (obtained from beam B-1) of the strain versus the distance from the face of the support is 70 % of the total area. Accordingly, the double layers of CF sheets are expected to contribute 140 % of the value of the contribution of the CF sheets in beam B-1. As predicted, the contribution of the CF sheets was 48 kN (141%) in beam B-2 while it was 34 kN in beam B-1 (100%).

6.5 Discussion on the performance of the concrete T-beams strengthened in shear

The improved mechanical anchor system was successfully able to increase the shear strength of beams B-1 and B-2 by 16.9% and 22 %, respectively. No signs of problems or deficiencies were observed in the design of the anchoring system of the two tested beams for both the single and double layer systems (i.e. slippage, yielding). The contributions of the concrete, steel, dry CF sheets are summarized in Table 6.1 and Figure 6.12.

One of the main advantages of using CF sheet system in shear strengthening is due to its high modulus of elasticity unlike the wet CFRP. Moreover, strengthening of the concrete T-beams with dry CF sheets using the modified mechanical anchoring system is easier than the conventional strengthening method by using wet CFRP sheets. Strengthening using dry CF sheets needs less surface preparations, less epoxy which affects the productivity of the labour leading to less time and effort in the preparation phase.

Because no epoxy is used to bond the dry CF sheets to the concrete surface, the mechanical anchor can be manufacture in a factory or a work shop, then assembled and installed later in the site. Accordingly, this will result in having better quality controlled strengthening system, unlike the wet laid systems that can be affected by the site conditions and the expertise of the labours.

6.5.1 Strains in steel stirrups

Figure 6.13 shows the relation between the shear load and the average stirrups' strain in all beams tested in shear. It can be observed that the average strain in beam B-2 was less than the average strains in beam B-0 at the same load. The increase rate of the strains was constant for both beams. On the other hand, the average strain in beam B-1 was higher than the values of beam B-0 until the load reached 100 kN. Afterwards, the increase rate of the strain was less than beams B-0 and B-2. At a shear load of 215 kN the increase rate of strains in the steel stirrups was identical for all. It was observed that the average strain in beam B-1 was higher than beam B-2.

6.5.2 Strains in CF sheets

Figures 6.7 and 6.11 show the relation between the shear load and the strains in the CF sheets of beams B-1 and B-2, respectively. The width of the CF sheets in beam B-2 was chosen such that the area under the curve of the strain versus the distance from the face from the support is 70 % of the total area. Accordingly, the double layers of CF sheets are expected to contribute 140 % of the value of the contribution of the CF sheets

in beam B-1. As predicted, the contribution of the CF sheets was 48 kN which was 141% of the contribution of the CF of beam B-2.

The strains of beam B-2 were located in the high strain zone, unlike B-1 were the strain gauges were distributed along the CF sheets. Accordingly, the strains in CF cannot be compared for beams B-1 and B-2.

6.5.3 Strains in flexural steel reinforcement

Figure 6.3 shows the relation between the shear load and the strains in the flexural steel reinforcement of the three beams tested in shear. The strains in the flexural steel reinforcement were linear up to the failure of the beam in the three beams. The ultimate strain in the flexural reinforcement was 1970, 2100, 2730 microstrain in beams B-0, B-1, and B-2, respectively.

6.5.4 Load-deflection relationship

Figure 6.4 shows the relation between the shear load and the mid-span deflection of all beams tested in shear. The ultimate deflection of the beams B-0, B-1, and B-2 were 8.1 mm, 10.4 mm, and 11.1 mm, respectively. Beam B-0 exhibited a brittle failure, while Beam B-1 showed a semi-ductile behaviour before failure. Beam B-2 showed a slight ductile behaviour before failure but yet beam B-1 was the most ductile beam among them.

6.6 AE monitoring of concrete beams

Beam B-0 was used to determine the locations and arrangements of the AE sensors. The failure of beam B-1 was predicted and the the cracks were precisely located using the AE monitoring technique. While the predection of the failure of beam B-2 was not accuratly located as beam B-1.

Table 6.1 Experimental results of all beams strengthened in shear

Beam	V_c (kN)	V_s (kN)	V_{CF} (kN)	V_n (kN)	**Increase** (%)
B-0	40	179	---	217	---
B-1	40	161	34	235	16.9
B-2	40	178	48	267	22

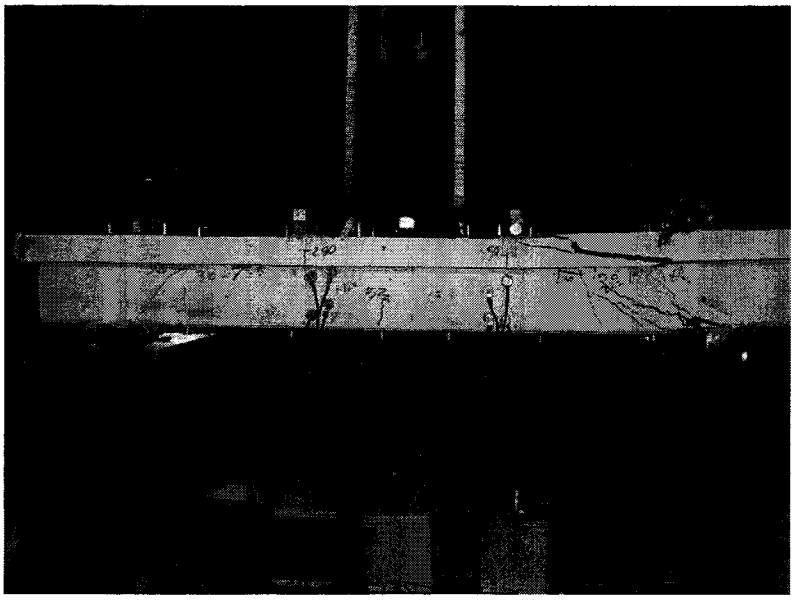

(a)

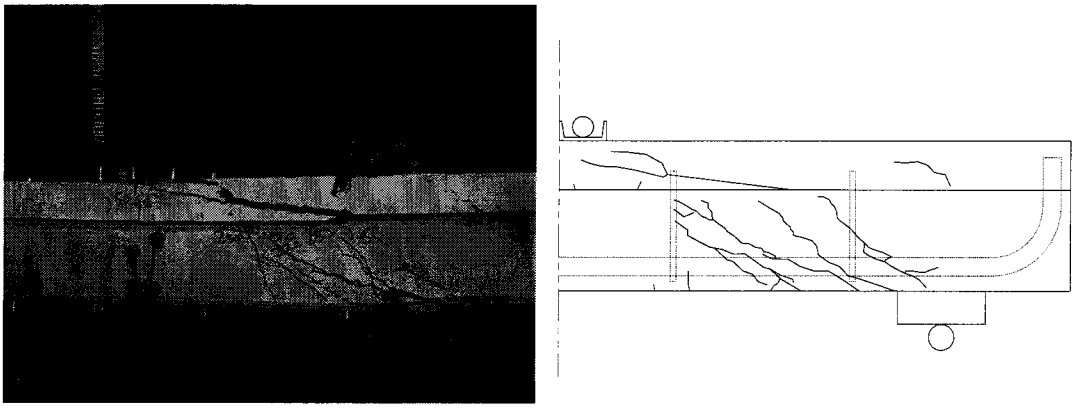

(b) (c)

Figure 6.1 Beam B-0 after failure: (a) Global view, (b) Close view to the beam, (c) Schematic crack patterns showing the locations of the internal steel stirrups

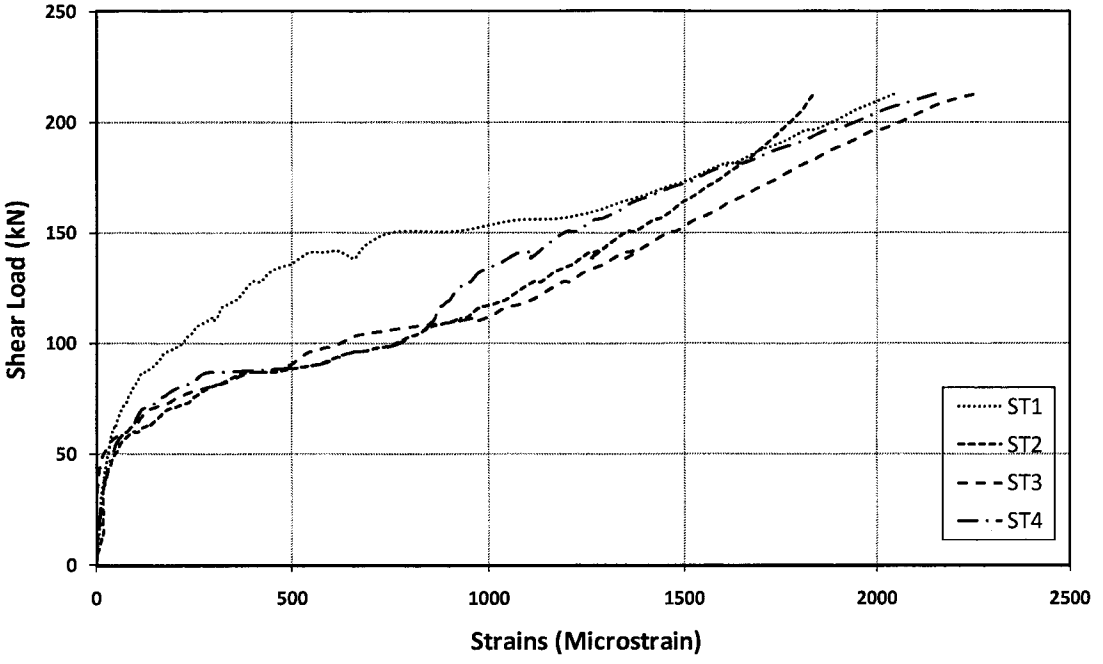

Figure 6.2 Load versus strain in steel stirrups in beam B-0

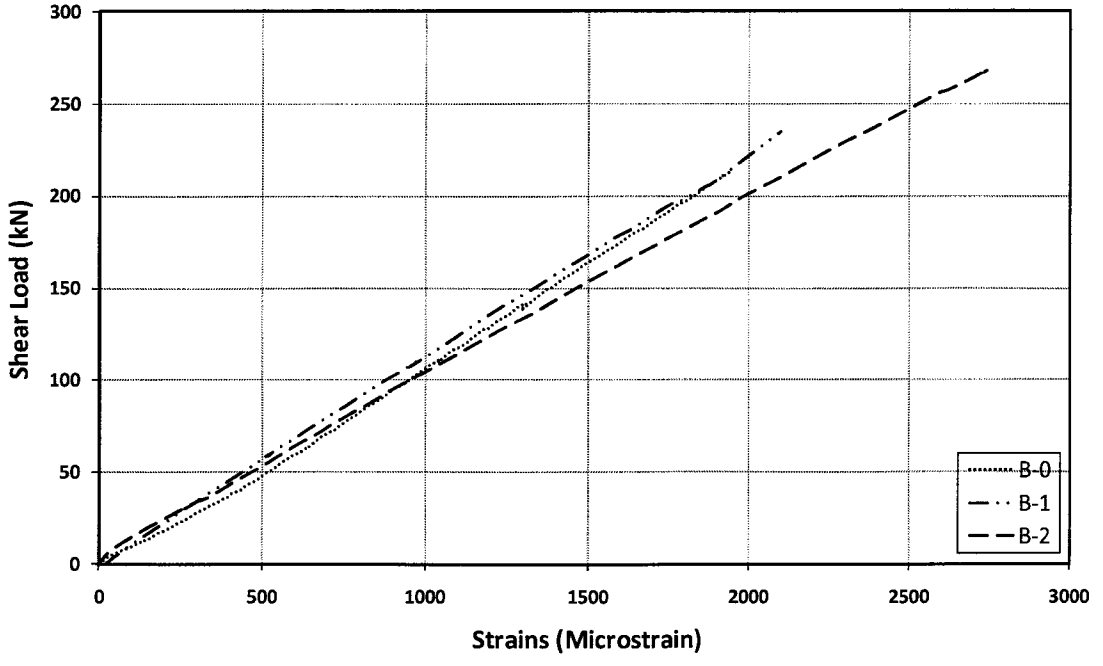

Figure 6.3 Load flexural-strain relationship of all beams strengthened in shear

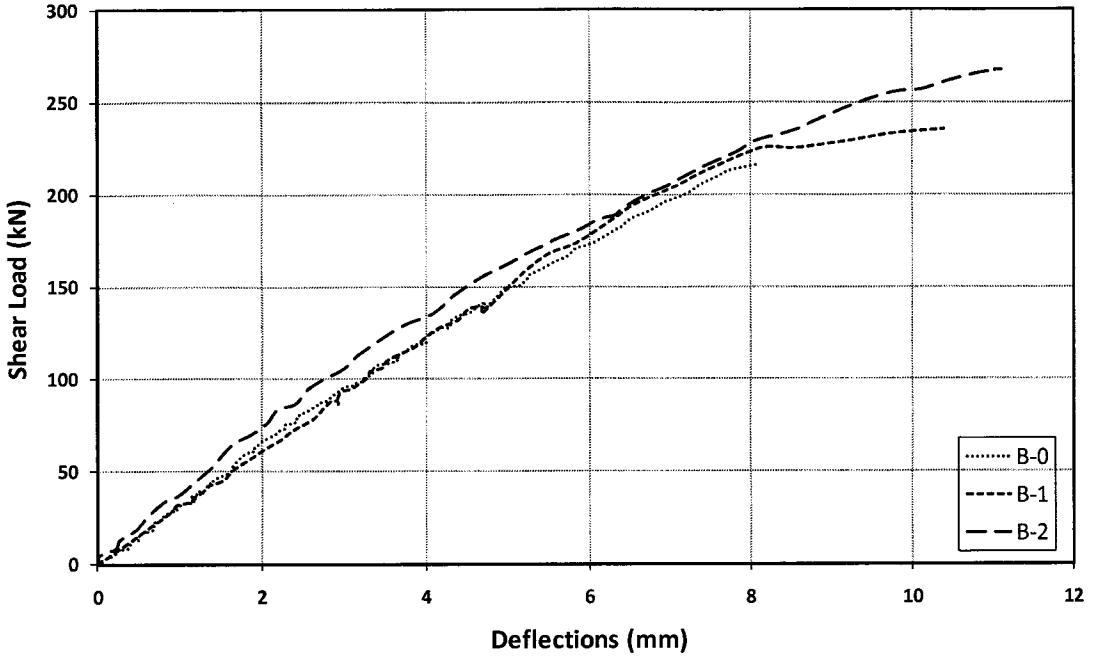

Figure 6.4 Load deflection relationship of all beams strengthened in shear

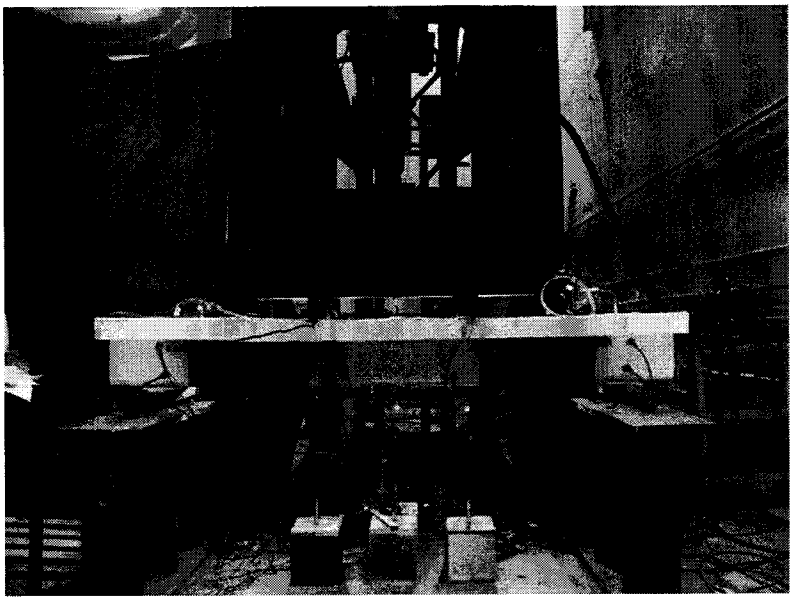

(a)

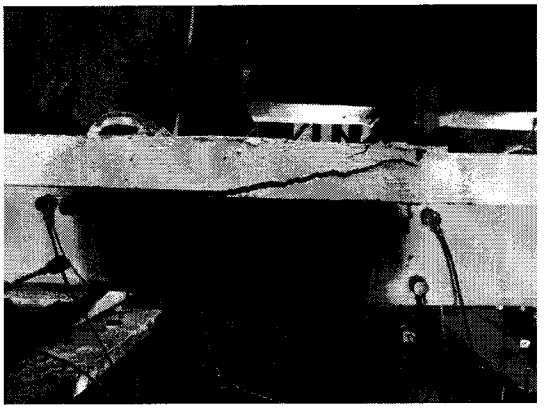

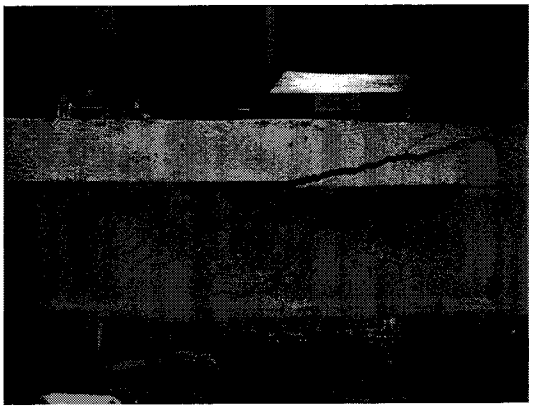

(b) (c)

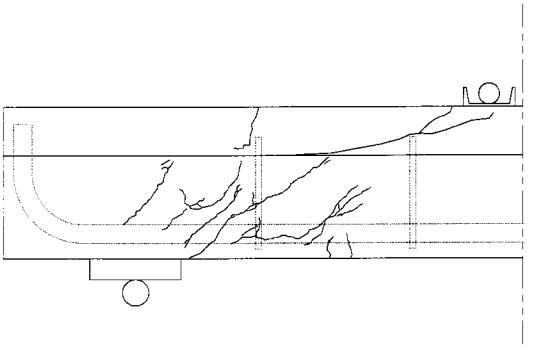

(d)

Figure 6.5 Beam B-1 after failure: (a) Global view, (b) Close view, (c) Failure pattern after removing the CF sheets, (d) Schematic crack patterns

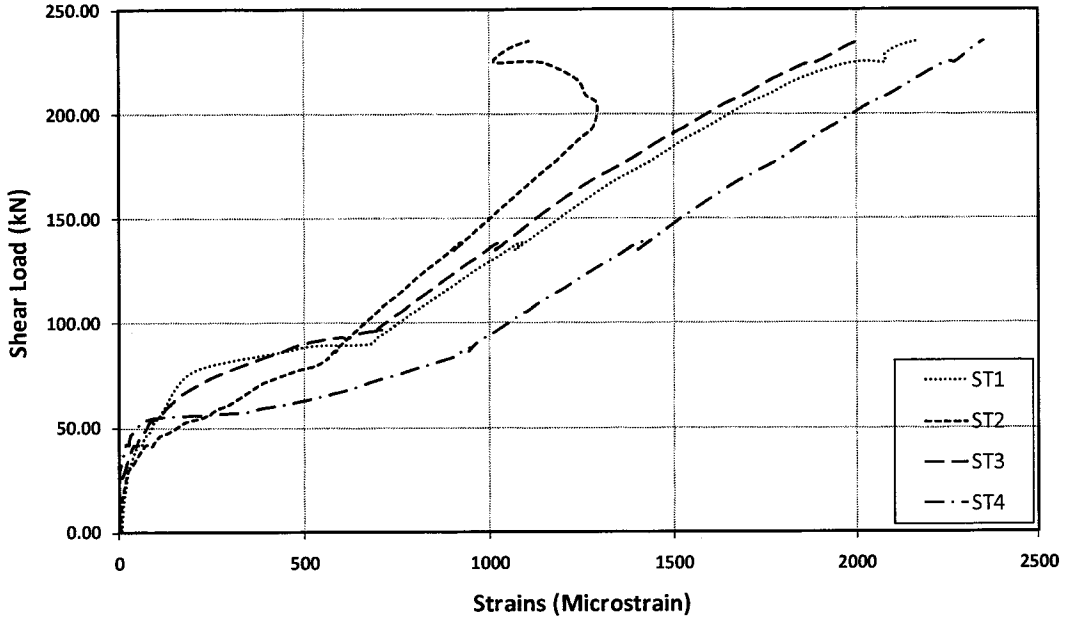

Figure 6.6 Load versus strain in steel stirrups in beam B-1

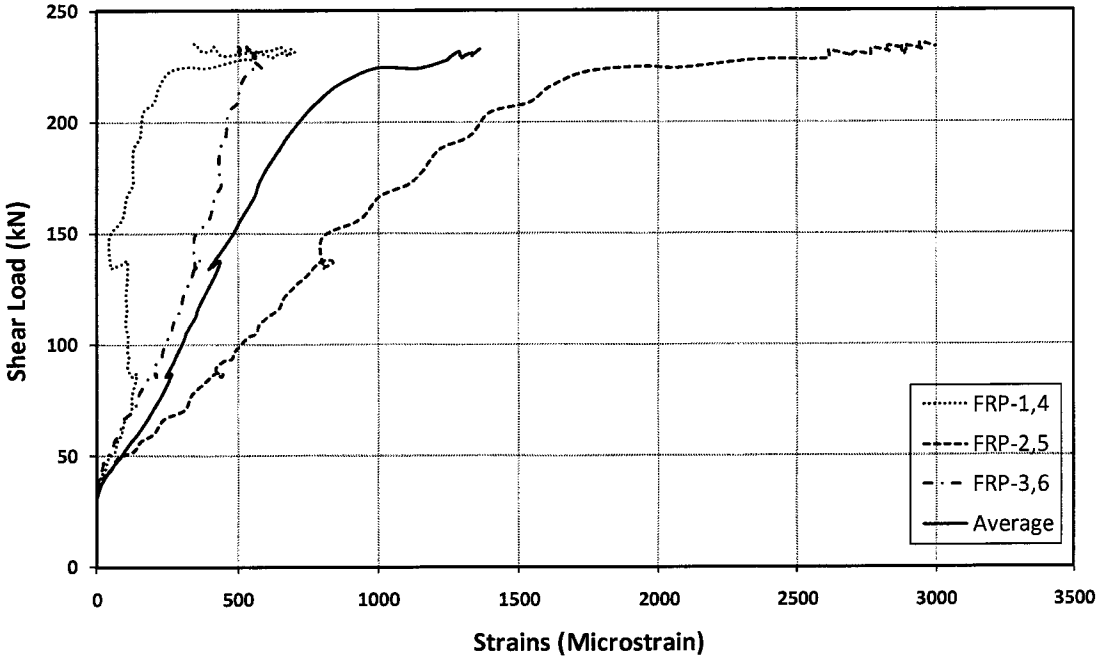

Figure 6.7 Load versus strain in CF sheet of Beam B-1

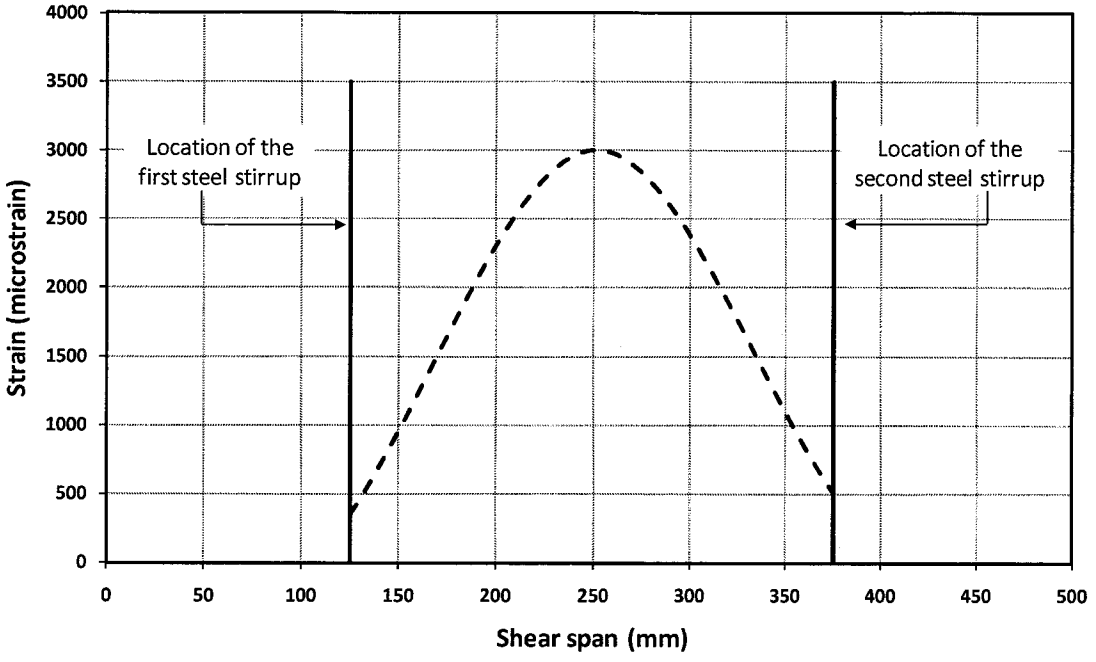

Figure 6.8 Strain distribution in CF sheet of Beam B-1 along the shear span

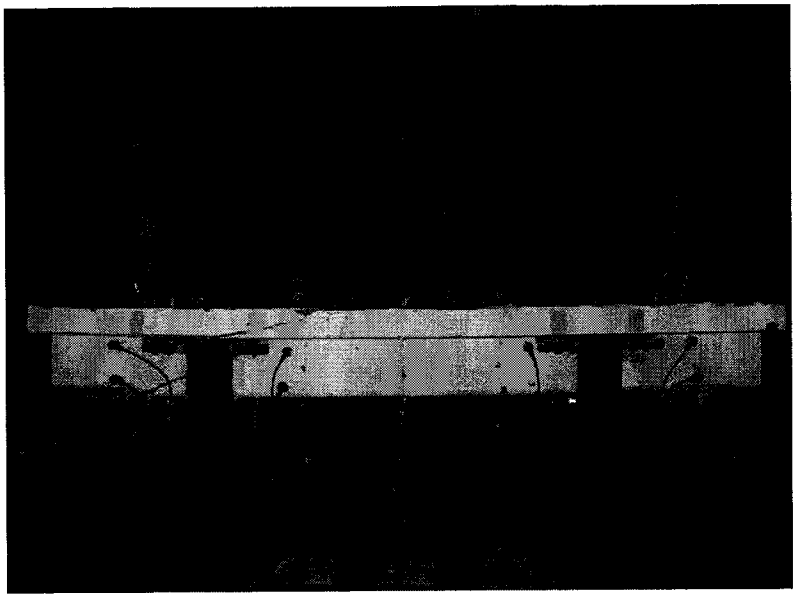

(a)

(b) (c)

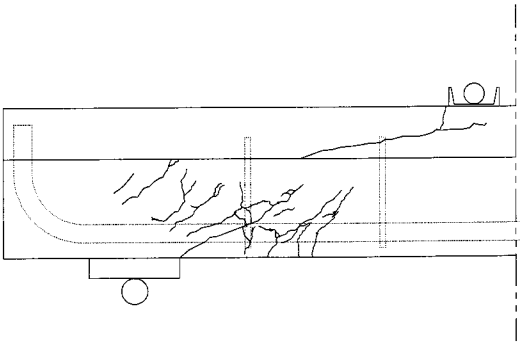

(d)

Figure 6.9 Beam B-2 after failure: (a) Global view, (b) Close view, (c) Failure pattern after removing the CF sheets, (d) Schematic cracks pattern

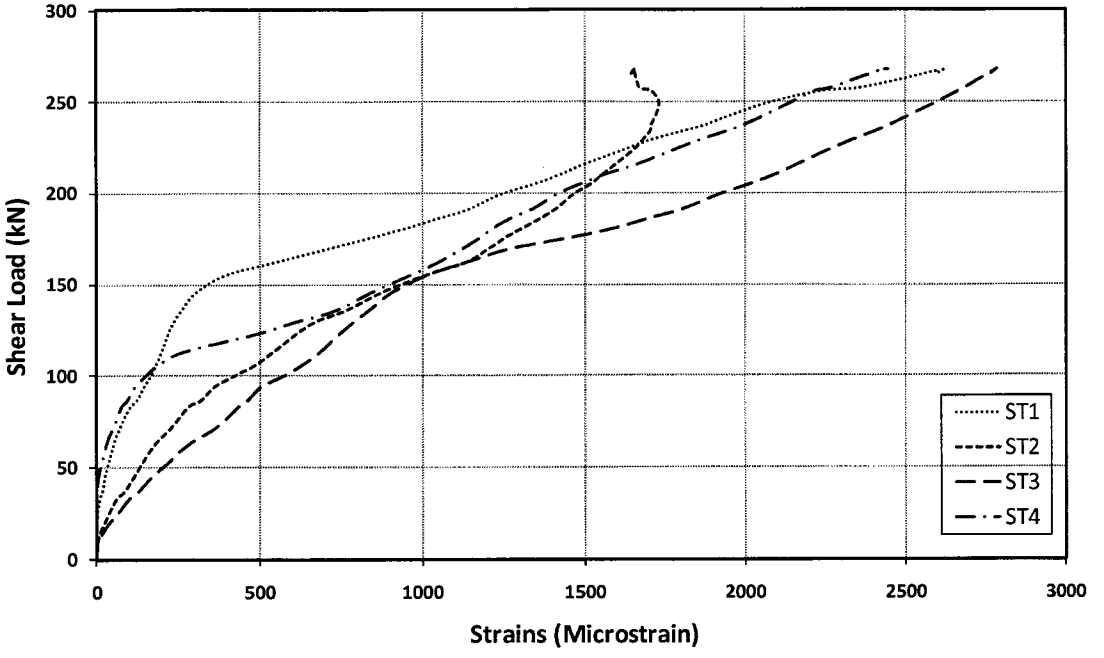

Figure 6.10 Load versus strain in steel stirrups in beam B-2

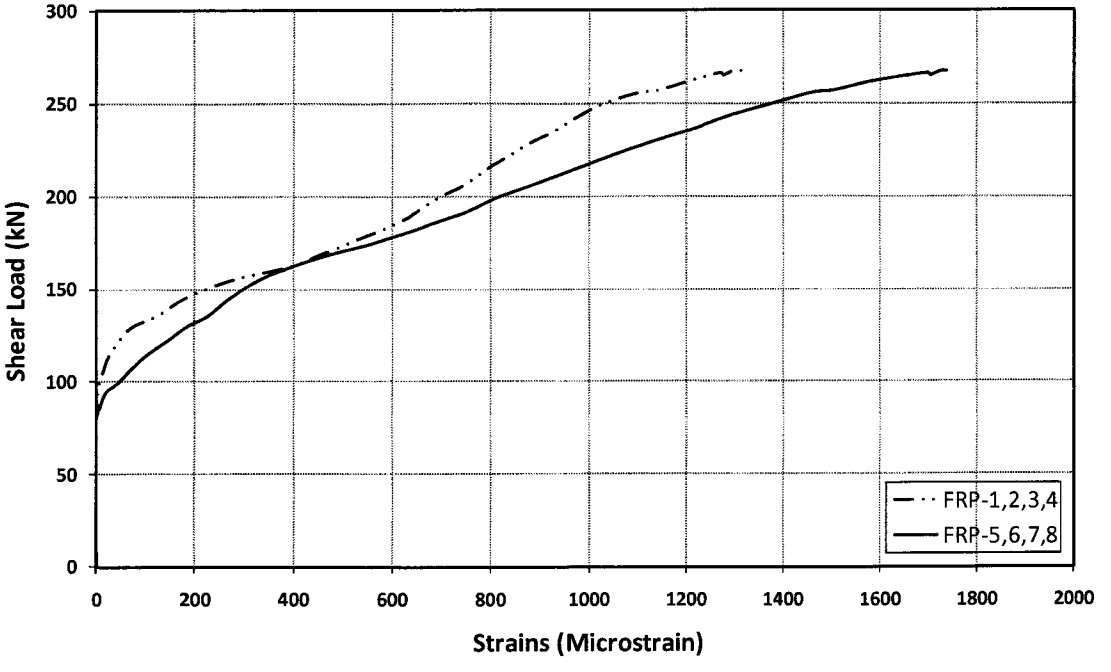

Figure 6.11 Load versus strain in CF sheet of Beam B-2

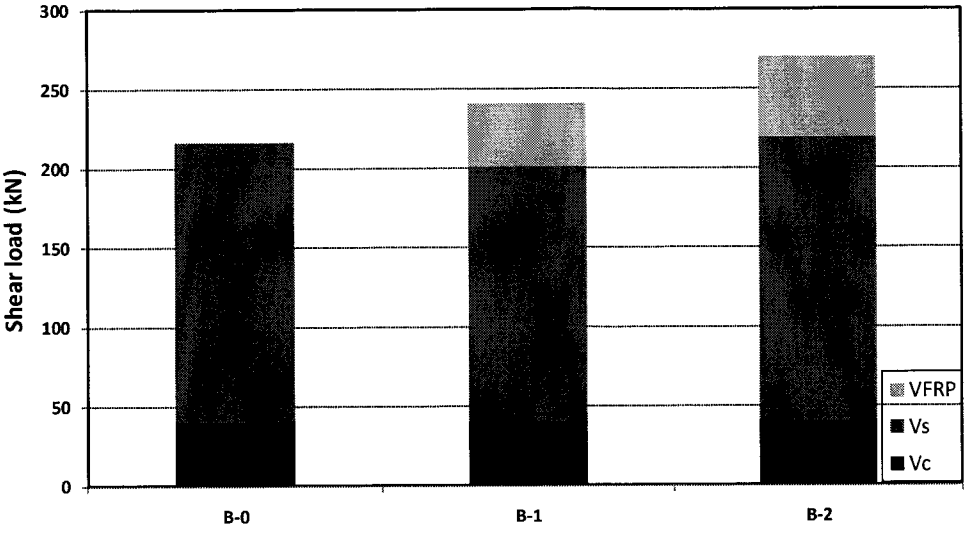

Figure 6.12 Comparison between the contribution of the concrete, steel stirrups, and CF sheets to the shear strength of all beams strengthened in shear

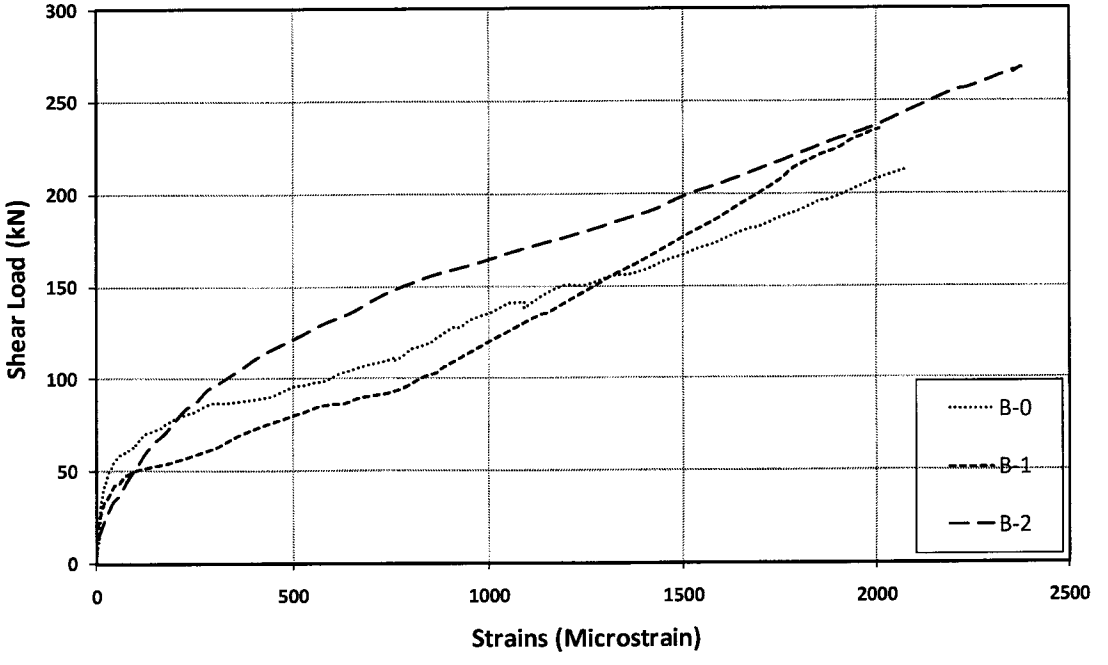

Figure 6.13 Load versus average strain in steel stirrups of all beams tested in shear

CHAPTER 7

CONCLUSIONS AND RECOMMENDATIONS

7.1 Summary

Two new applications of using FRP materials and techniques were experimentally examined in this study. One application is using newly developed thermoplastic bendable CFRP rebars for reinforcing new concrete structures. The other application is using mechanically anchored CF sheets in shear strengthening of existing RC structures. Moreover, acoustic emission monitoring of RC structures was examined as a method of monitoring of existing structures under service loading conditions.

7.2 Conclusions

7.2.1 New thermoplastic CFRP rebars for new structures

An experimental study was carried out to evaluate the performance of straight and bent new CFRP thermoplastic rebars. This study consisted of three sets of standard tests: mechanical properties test, pullout and development length test, and bent bars and stirrups test. A comparison was conducted between the new CFRP rebar, and other FRP rebars available in the market and literature. Based on the results and the test observations, the following conclusions were drawn:

- The new CFRP rebars exhibited a linear behaviour up to failure when subjected to tension. The tensile strength of the tested rebars reached 825 MPa, and the modulus of elasticity was 91 ± 2.6 MPa.

- The maximum bond stress was 9 MPa, but no debonding failure occurred due to the premature failure of the tested rebars. The bond strength of the rebars was not evaluated in this research due to the premature failure of the tested rebars.
- The strength of the bent rebars was 37 % of the strength of the straight rebars.
- Although some of the rebars had a premature failure, the results of the three conducted tests are promising compared to the other available rebars.
- The modulus of elasticity of the CONCOM rebar is 85%, 180 to 200%, 180 to 248 %, and 153 % of the modulus of elasticity of the Pultrall CFRP, Pultrall GFRP, FULCRUM, and Schöck COMBAR rebars, respectively.
- In terms of tensile strength, the test results of CONCOM rebars show that they have less tensile strength compared to Pultrall (CFRP), Schöck COMBAR, and FULCRUM; while it has higher tensile strength than Pultrall (GFRP).
- CONCOM bent rebars have better properties compared to the results of the thermoplastic rebars tested by Currier *et al.* (160%), while it is 63% to 84 % of the GFRP and CFRP Pultrall bent rebars.
- With some improvements of the geometric design of the new CFRP, the behaviour of the straight and bent rebars is expected to be higher.

7.2.2 Strengthening of existing RC T-beams in shear using mechanically anchored CF sheets

Three RC T-beams were tested in four-point bending under a monotonic load up to failure. The beams were deficient in shear and does not meet the current code requirements and thus need to be strengthened. The tests were an extension of the

previous work done by Mofidi (2008) on similar RC T-beams strengthened using similar anchoring system. Previous tests explored the feasibility of strengthening RC beams in shear by wrapping the full shear span zone with a U-shaped dry carbon fibre (CF) sheet that is anchored to the beam. The previous tests showed the effectiveness of the strengthening system in increasing the shear capacity of the RC beams. However, it showed that a small portion of CF sheet was stretched and contributed to the shear capacity of the beam. In an effort to maximize and fully utilize the benefits of the high modulus dry CF sheets, the mechanical anchoring system was improved in this experimental program. Moreover, the strains of the CF sheets were monitored along the shear span for better understanding of the behaviour of the CF sheets.

The three tested RC T-beams are denoted as: B-0 is a control beam; B-1 is a beam strengthened with one layer of dry CF sheet which was wrapped the whole shear span zone; and B-2 is a beam strengthened with double layers of CF sheets which was only 150 mm in width. Based on the results and observations of this study, the following conclusions were reached:

- The contribution of the dry CF sheets (V_{CF}) to the shear strength of beam B-1 and B-2 was 34 kN and 48 kN, respectively. That is equivalent to an increase of 16.9 and 22 % of the shear strengths of beams B-1 and B-2, respectively.
- No signs of problems or deficiencies were observed in the design of the anchoring system of the two tested beams for both the single and double layer systems.
- The strains of the CF sheets of beam B-1 were minimum at the location of the steel stirrups (500 microstrain), and maximum at the middle of the two steel stirrups (3000 microstrain).

- According to the strain distribution of the CF sheets obtained from beam B-1, the contribution of the CF sheet to the shear strength of beam B-2 was predicted.
- Because no epoxy is used to bond the dry CF sheets to the concrete surface, the CF strengthening system can be manufacture in a factory, then installed later in the site. As such, this would result in a better quality control of the strengthening system.

7.2.3 AE monitoring of concrete cylinders and RC T-beams

A testing program has been conducted by Concordia University and WINS LLC. to study the acoustic emission generated by concrete structures under loading. AE monitoring is efficient in detecting activity by hit rates and intensity by signal analysis. AE monitoring can detect and locate cracks, leaks, or corrosion in structures. Moreover, AE can identify which cracks are propagating that can cause failure of the structure.

The aim of this collaborative research work is to: establish the working procedures and parameters for AE monitoring to evaluate the structural integrity of concrete structures; compare AE data with the data acquired by the conventional data acquisition system and eye inspection; evaluate ranking system used for steel structure to be used for long term concrete monitoring application; and testing 3D AE location algorithms. The acquired and recorded data were collected using AE monitoring technologies during controlled loading until failure of three standard concrete cylinders, and three RC T-beams tested in shear. Based on the results and observations of this study, the following conclusions can be summarized:

- Monitoring concrete elements using AE was able to be detect most of the events occurred during the tests.
- The located AE events along the length of cylinder #2 and cylinder #3 were consistent with the visual observations made during the test for both cylinders.
- The AE data were consistent with the crack pattern and locations inspected during the test of beam B-0.
- The location of the critical crack that caused the failure was predicted and precisely located before the failure of beam B-1 using the 3D AE algorithm.

7.3 Recommendation for future work

7.3.1 New thermoplastic CFRP rebars

The typical modes of failure of the tested straight rebars were: (1) splitting failure, (2) splitting failure with wavy fibres, and (3) rupture. The modes of failure show the need of some modifications to improve the structure of the fibres of the CONCOM rebar and to prevent such modes of failure. In order to prevent the premature failure with wavy fibres, the yarns should be under tension during the molding process. This can be achieved by tying the two ends of the yarns and apply small tension force to the yarns to ensure that none of the yarns is loose. Moreover, the geometry of the rebars should be modified in order to prevent the splitting mode of failure. The existing geometry makes the rebar behave as two rebars connected to each other. Accordingly, the rebar should have a symmetric cross section to avoid the longitudinal splitting between its two halves.

One of the improvements of the geometry design is by having the two ellipsoidal ribs symmetrical to prevent the splitting failure between the two halves of the rebar. As

shown in Figure 8.1 (option1), additional fibres are needed to be wound around the rebar to reduce the splitting forces that exist due to the inclined fibres in the ellipsoidal ribs. This geometric design can be manufactured using the compression molding technique.

Another design could be used in manufacturing the rebars using the pultrusion technique. In this design the rebar will be pultruded in a circular cross section, then additional fibres are wounded around the rebar to increase the bond stress of the rebar and to improve the strength of the bent rebars as shown in Figure 8.1 (option 2).

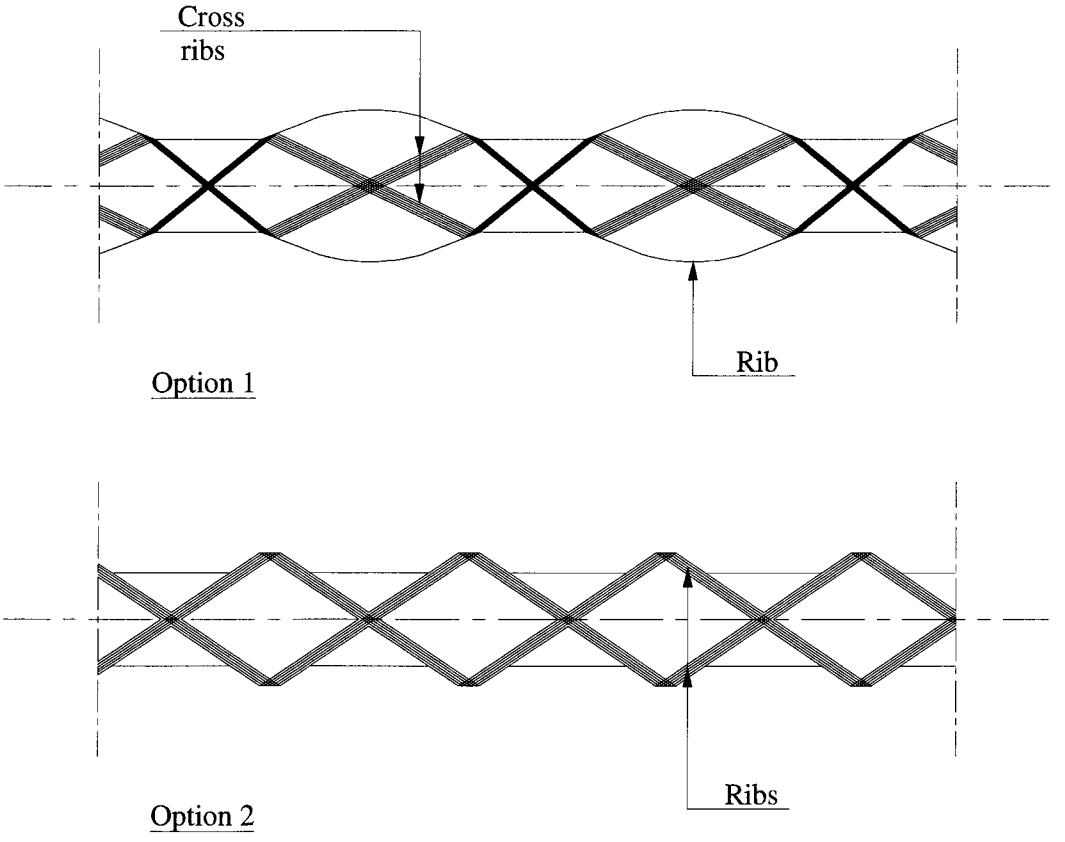

Figure 7.1 Recommended new design for CONCOM thermoplastic CFRP rebar

7.3.2 Concrete T-beams strengthened in shear using mechanically anchored CF sheets

The behaviour of the improved mechanical anchor system was satisfactory upon loading of the beams until failure. Yet, more comprehensive tests should be made to examine the effect of fatigue and long term on the behaviour of the mechanical anchor system. Moreover, the effect of using non-corrosive materials should be evaluated.

Although the CF sheets are easier than the wet CFRP laminates in terms of installation and quality control, but it can be torn off easily on any sharp edge. Thus, the protection of the CF sheets using appropriate materials should be studied.

More specimens should be tested for comprehensive understanding and prediction of the ultimate shear capacity of beams strengthened in shear with such system.

7.3.3 AE monitoring of concrete beams

Although the failure of beam B-1 was predicted and the cracks were precisely located, the estimation of the failure of beam B-2 was not accuretly located. More specimens should be tested in order to: obtain the best array of AE sensors that can predict all of the AE events, and evaluate WINS's steel maintenance system.

Monitoring using AE of the plain concrete, concrete reinforced with steel and FRP rebars should be studied. Moreover, different structural elements should be monitored to be able to predict the defferent modes of failure.

REFERENCES

1. ACI440.3R-04 American Concrete Institute (ACI), 2004, "Guide test methods for fiber reinforced polymers FRPs for reinforcing or strengthening concrete structures", ACI 440.3R-04, Committee 440, Farmington Hills, Mich.

2. Adhikary, B., Mutsuyoshi, H, 2004, "Behavior of concrete beams strengthened in shear with carbon-fiber sheets", Journal of Composites for Construction, v 8, n 3, p 258-264.

3. Adhikary, B., Mutsuyoshi, H., Ashraf, M., 2004, "Shear strengthening of reinforced concrete beams using fiber-reinforced polymer sheets with bonded anchorage", ACI Structural Journal, v 101, n 5, p 660-668.

4. Ahmed, E., El-Sayed, A., El-Salakawy, E., Benmokrane, B., 2010 "Bend Strength of FRP Stirrups Comparison and Evaluation of Testing Methods" Journal of Composites for Construction, v 14, n 1, p 3-10.

5. Ahmed, E.A., El-Sayed, A. K., El-Salakawy, E., and Benmokrane B. 2007. Mechanical and Structural Characterization of New Carbon FRP Stirrups for Concrete Members. ASCE Journal of Composites for Construction, V.11, n. 4, p 352-362.

6. Amleh, L., Mirza, M.S., (2004). "Corrosion response of decommissioned deteriorated bridge deck", Journal of Performance of Constructed Facilities, Vol. 18, No. 4, p 185-194.

7. Barros, J., Dias, S., Lima, J, 2007, "Efficacy of CFRP-based techniques for the flexural and shear strengthening of concrete beams", Cement and Concrete Composites, v 29, n 3, p 203-217.

8. Benmokrane, B., Zhang, Burong, Laoubi, K., Tighiouart, B., Lord, I., 2002 "Mechanical and bond properties of new generation of carbon fibre reinforced polymer reinforcing bars for concrete structures", Canadian Journal of Civil Engineering, v 29, n 2, p 338-343.

9. Canadian Standard Association (CSA), 2002, "Design and construction of building components with fibre reinforced polymers". CAN/CSA-S806-02, Rexdale, Ont.

10. Cao, S., Chen, J., Teng, J., Hao, Z., Chen, J, 2005, "Debonding in RC Beams Shear Strengthened with Complete FRP Wraps", Journal of Composites for Construction, v 9, n 5, p 417-428.

11. Castro, P., Carino, N., 1998, "Tensile and nondestructive testing of FRP bars", Journal of Composites for Construction, v 2, n 1, p 17-27.

12. Christophe, D., Cheng, J, 2001, "Shear behavior of reinforced concrete T-beams with externally bonded fiber-reinforced polymer sheets", ACI Structural Journal, v 98, n 3, p 386-394.

13. Currier, J., Fogstad, C., Walrath, D., and Dolan, C. 1994. "Bond development of thermoplastic FRP shear reinforcement stirrups", The 3rd Materials Engineering

Conference, ASCE, San Diego, CA, USA, 6 pages, paper in CD-ROM proceeding.

14. Eshwar, N., Nanni, A., Ibell, T., 2001, "Performance of two anchor systems of externally bonded fiber-reinforced polymer laminates", ACI Materials Journal, v 105, n 1, p 72-80.

15. FULCRUM Thermoplastic Composites, 2005, FULCRUM Thermoplastic Composites technical data sheet, http://www.fulcrumcomposites.com/literature /technical.pdf, retrieved 2010.

16. Galal, K., Mofidi, A., 2010 "Shear Strengthening of RC T-Beams using mechanically-anchored unbonded dry carbon fiber sheets", Journal of Performance of Constructed Facilities, v 24, n 1, p 31-39.

17. Higgins, C., Potisuk, T., Farrow, W., Robelo, M., McAuliffe, T., Nicholas, B., 2007, "Tests of RC deck girders with 1950s vintage details", Journal of Bridge Engineering, v 12, n 5, p 621-631.

18. Hoult, N., Lees, J., 2009, "Efficient CFRP strap configurations for the shear strengthening of reinforced concrete t-beams", Journal of Composites for Construction, v 13, n 1, p 45-52.

19. Kesse, G., Lees, J., 2007,"Experimental behavior of reinforced concrete beams strengthened with prestressed CFRP shear straps", Journal of Composites for Construction, v 11, n 4, p 375-383.

20. Larralde, J., Silva-Rodriguez, R., 1993, "Bond and slip of FRP rebars in concrete", Journal of Materials in Civil Engineering, v 5, n 1, p 30-40.

21. Lees, J., Winistörfer, A., Meier, U., 2002, "External prestressed carbon fiber-reinforced polymer straps for shear enhancement of concrete", Journal of Composites for Construction, v 6, n 4, p 249-256.

22. Leung, C., Chen, Z., Lee, S., Ng, M., Xu, M., Tang, J., 2007, "Effect of size on the failure of geometrically similar concrete beams strengthened in shear with FRP strips", Journal of Composites for Construction, v 11, n 5, p 487-496.

23. Manav, M.O, 2002, "Mechanical properties of fiber-reinforced polymer (FRP) composites for concrete bridge deck reinforcement", M.S. thesis, Florida Atlantic University, Boca Raton, Florida, USA.

24. Mehrabi, B., Elremaily, A., Vanderpool, D., 2003, "Mechanical performance of thermoplastic fiber reinforced polymer rebars", Proceedings of the Sixth International Symposium on FRP Reinforcement for Concrete Structures (FRPRCS-6), Singapore, p79-88.

25. Micelli, F., Nanni, A, 2003, "Tensile characterization of FRP rods for reinforced concrete structures", Mechanics of Composite Materials, v 39, n 4, p 445-463.

26. Mirza, S. M. and Haider, M., 2003, "The State of Infrastructure in Canada: Implications for Infrastructure Planning and Policy". A study prepared for Infrastructure Canada, McGill University, 817 Sherbrooke Street west, Montreal, Quebec, H3A 2K6

27. Moon, D., Sim, J., Oh, H., Benmokrane, B., 2007, "An exploratory study of GFRP rebar with ribs containing milled glass fibers", Composites Part B: Engineering, v 39, n 5, 882-890.

28. Pultrall Inc., 2004, "V-ROD™ Technical data sheet", Thetford Mines, Quebec, Canada, http://www.pultrall.com/Site2008/eng/V-ROD.htm, retrieved January 2010.

29. Schöck COMBAR,. 2007, Schöck COMBAR Technical information. http://www.schoeck-combar.com/upload/Files/Documents/1192008021.pdf, retrieved January 2010.

30. Shehata, E., Morphy, R., Rizkalla, S., 2000, "Fibre reinforced polymer shear reinforcement for concrete members Behaviour and design guidelines", Canadian journal of civil engineering, v 27, n 5, p 859-872.

31. Sundarraja, M., Rajamohan, S., 2009, "Strengthening of RC beams in shear using GFRP inclined strips - An experimental study", Construction and Building Materials, v 23, n 2, p 856-864.

32. WINS, and Concordia University, March 2010, "Acoustic emission testing of carbon wrapped T-section beam failures", Montreal, WINS, 15 pages.

33. WINS, and Concordia University, May 2009, "Acoustic emission monitoring of concrete", Montreal, WINS, 15 pages.

34. Zhang, Z., Hsu, C., 2005, "Shear strengthening of reinforced concrete beams using carbon-fiber- reinforced polymer laminates", Journal of Composites for Construction, v 9, n 2, p 158-169.

APPENDIX A: AE MONITORING OF CONCRETE CYLINDERS AND RC T-BEAMS

A.1 Introduction

A testing program has been initiated by Concordia University and WINS LLC. to study the acoustic emission generated by concrete structures under loading. WINS is a specialized company experienced in field non-destructive testing and has an extensive AE experience of over 300 steel bridges inspected.

AE monitoring is efficient in detecting activity by hit rates and intensity by signal analysis. AE monitoring can detect and locate almost everything that release acoustic energy such as cracks, leaks, or corrosion. Moreover, AE can identify which cracks are growing and which are not. The very active micro-cracks release a great amount of AE energy, and are more susceptible to cause failure of the structure.

The aim of this collaborative research work is to: establish the working procedures and parameters for AE monitoring to evaluate the structural integrity of concrete structures; correlate and compare AE data with the data acquired by the conventional data acquisition system and eye inspection; evaluate ranking system used for steel structure to be used for long term concrete monitoring application; and testing 3D AE location algorithms. The acquired and recorded data were collected using AE monitoring technologies during controlled loading until failure of three standard concrete cylinders, and three RC T-beams tested in shear.

A.2 Test setup and instrumentation of the concrete cylinders

Three standard concrete cylinders were tested up to failure to obtain the concrete strength of age of 14 days. The diameter of the cylinders was 200 mm, while the height was 100 mm.

The cylinders were loaded with increasing monotonically up to failure. The applied load was monitored using a digital pressure transducer connected to the conventional data acquisition system. AE of the cylinders were monitored using two sensors mounted on each end of the two cylinders, which were used to enable linear source location along the length of the cylinder. Figure A.1 shows the locations and arrangements of the sensors.

The AE sensors were mounted using hot glue gun and calibrated using standard pencil breaking method. The setup, the calibration, and the data collecting were done by WINS's professional engineer and technician.

A.2.1 Results and discussion

The data of the first concrete cylinder was not recorded due to technical problems. The AE activity of cylinder # 2 and # 3 are shown in Figure A.2 and A.3. It can be observed that the located AE events in cylinder # 2 was linearly increasing with time up to 75% of the ultimate load then the rate decreased. The AE can be rated as critically active, while the intensity can be rated as intense active. In cylinder # 3 It can be observed that the AE activity was linearly increasing with time up to failure. The AE can be rated as critically active, while the intensity can be rated as critically intense. By using the WINS steel maintenance ranking system, the reults show that cylender #2 needs

maintenance and continous monitoring, while cylinder #3 needs immediate maintenance. As the two concrete cylinderes were tested up to failure, the AE of the two concrete cylinders should have indicate that they need immediate maintenance. It can be remarked that the WINS steel maintenance ranking system may not suitable for concrete and a new system could be needed to be develpoed.

Figure A.4 shows the AE located events along the length of cylinder #2 and cylinder #3. The located events are very close to the visual observations made during the test for both cylinders.

The difference in the behaviour of samples 2 and 3, emphasize the need for testing more specimens to obtain a satisfactory database that can be used to develop maintenance system similar to WINS's steel system.

A.3 Test setup and instrumentation of the concrete T-beams tested in shear

The beams monitored in this study were tested in four point bending test to create a constant shear zone. The test setup and conventional instruments of the tested beams are described in section 5.6.

The sensors were mounted to the desired locations using hot glue gun and calibrated using the standard pencil breaking method. The setup, calibration, and the data collecting were done by WINS's professional engineer and technician. Figures A.5, A.6, and A.7 show the test setup, locations and arrangements of the sensors of beams B-0, B-1, B-2, respectively.

The loading was applied gradually by a manually controlled pump with a constant rate up to failure. The readings were collected using the conventional data acquisition system, and a multiple-channel AE workstation.

A.3.1 Results and discussion of Beam B-0

As shown in Figure A.8, the AE activity of beam B-0 was critically active as the rate of increase of the AE hits increase with time. It was observed that the locations of AE events were high in the constant moment zone at the begining of the test, then some AE events occured in the shear zones. It was noticed that the AE events in the right shear zone were significantly higher than the ones in left shear zone. These data were consistent with the cracks inspected and the crack intensity observed of beam B-0. The eye inspections showed that some flexural cracks initiated first at the constant moment zone. Then Some cracks appeared in the right and left shear zones. The cracks in the right shear zone developed, propagated and caused a shear failure of the beam. The AE located events are shown in Figure A.9 and plotted on top of the beam's picture for better visualizing and understanding of the AE locations.

A.3.2 Results and discussion of Beam B-1

The located AE events were monitored during the test on the computer screen. The location of the critical crack that caused the failure was predicted and located before the beam failed . Figure A.10 shows the located AE events plotted on top of the beam for better understanding and visualizing of the results. It was observed that the pattern of the located AE events of beam B-1 are defferent than in beam B-0. In beam B-1 high events

occured in the shear zone, while in beam B-0 high AE events located in both the shear zone and the constant moment zone. However the flexural strains on beam B-1 were higher than in beam B-0.

A.3.3 Results and discussion of Beam B-2

It was observed that some AE events occured first in the constant moment zone (near the right point load), then at later stages of loading some AE events were located in the left shear zone.

During the test and just before the failure, a shear crack was formed in the concrete flange in the left shear zone. It was expected that this crack will release high ammount of AE energy that was not detected by the sensors. Figure A.11 shows the located AE events plotted on top of the beam for better understanding and visualizing of the results.

As indicated in section A.2.1, the deference of the located AE events in the tested beams emphasise the need for testing big number of specimens to have better understanding of the acoustin emissions of the concrete structures and to develop maintenance system similar to WINSC's steel system.

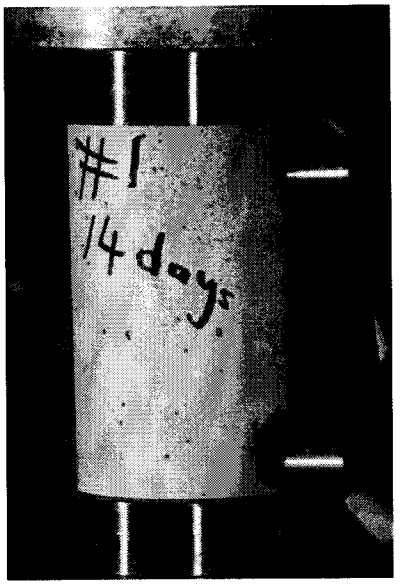

Figure A.1 Sensors distribution of tested cylinders

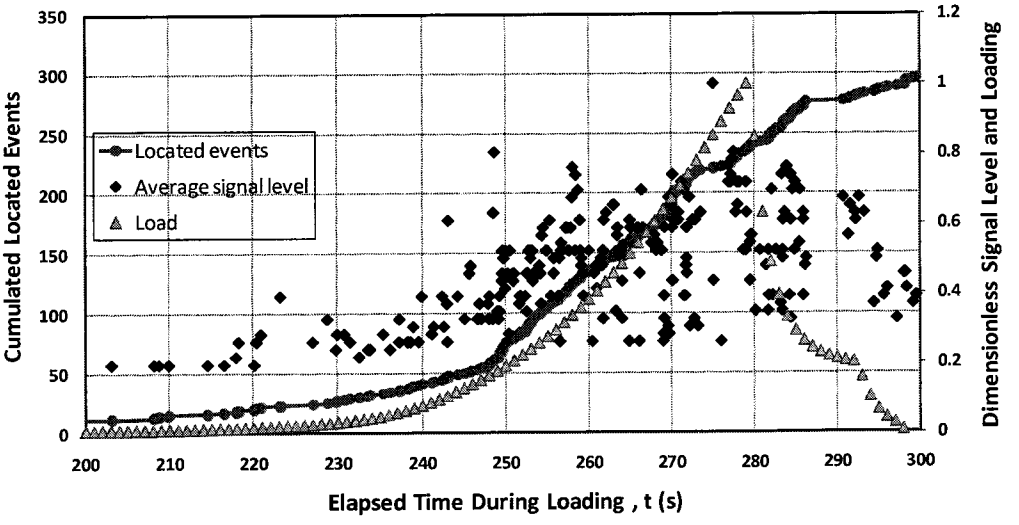

Figure A.2 AE activity of cylinder #2 (WINS, May 2009)

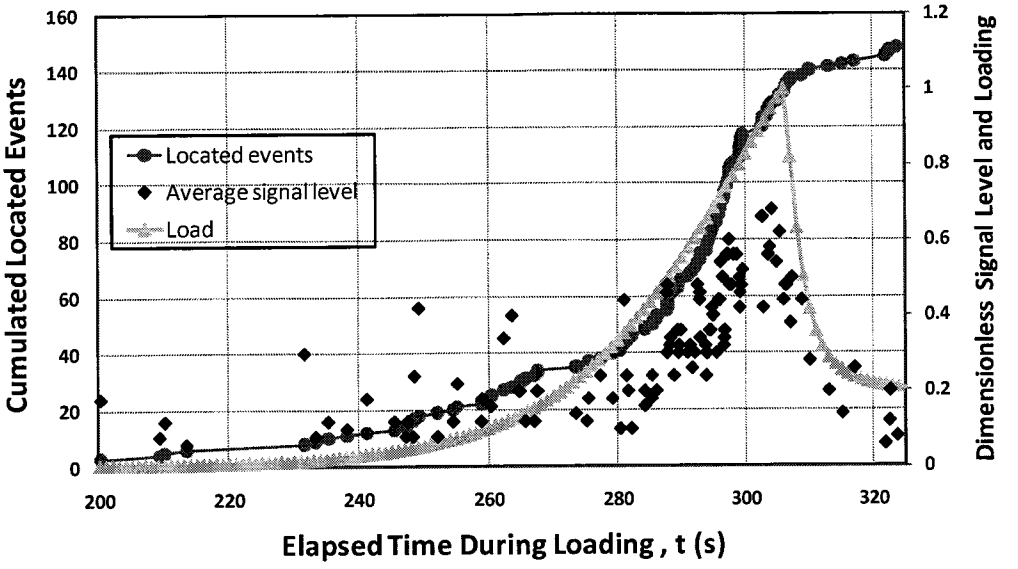

Figure A.3 AE activity of cylinder #3 (WINS, May 2009)

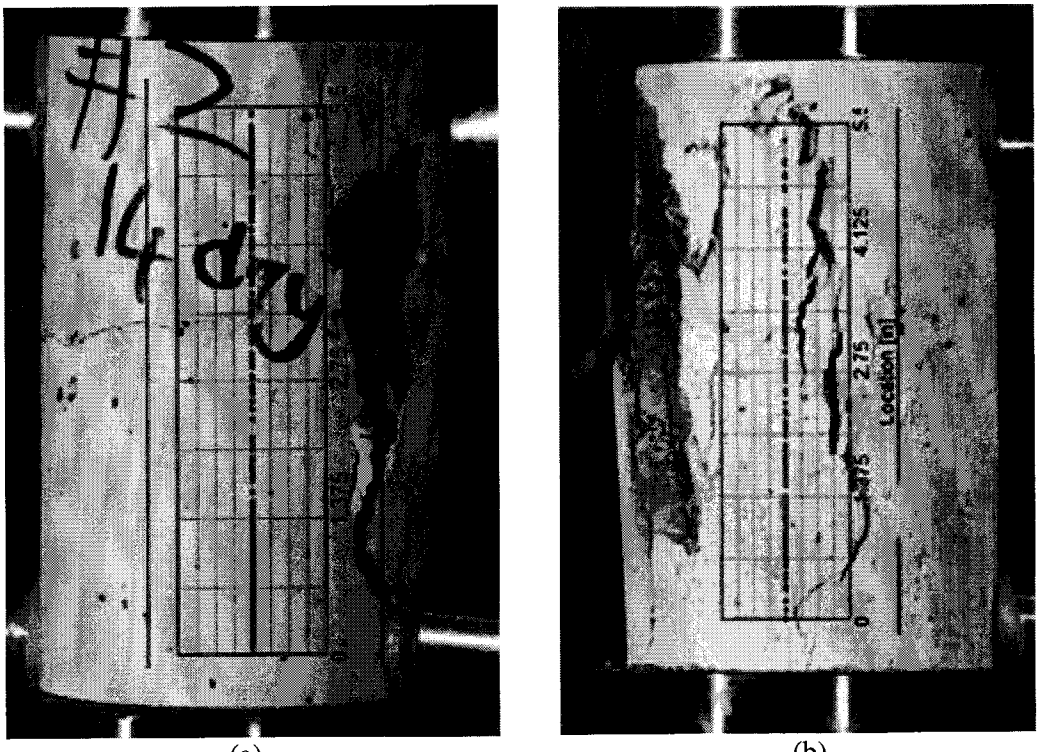

(a) (b)

Figure A.4 AE located activity of: (a) cylinder #2, (b) cylinder #3

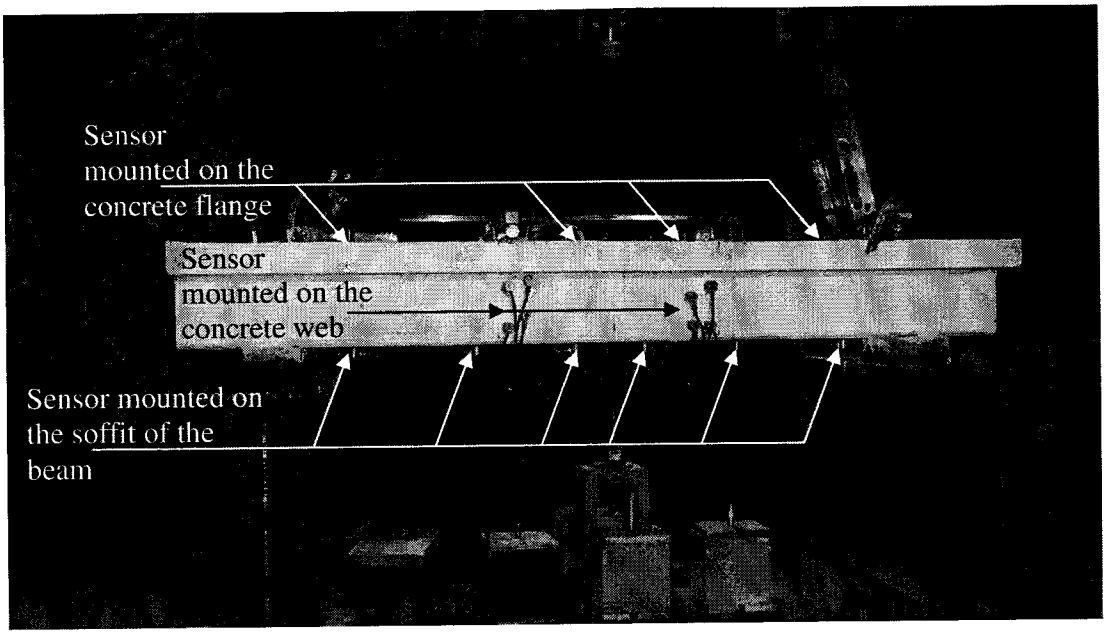

Figure A.5 Sensors distribution of beam B-0

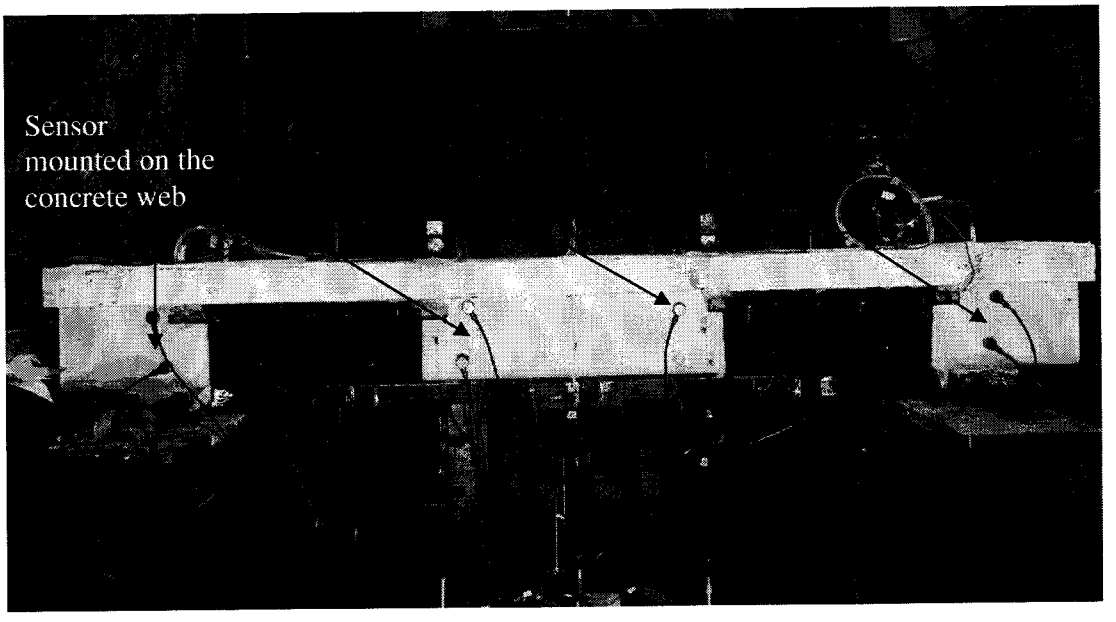

Figure A.6 Sensors distribution of beam B-1

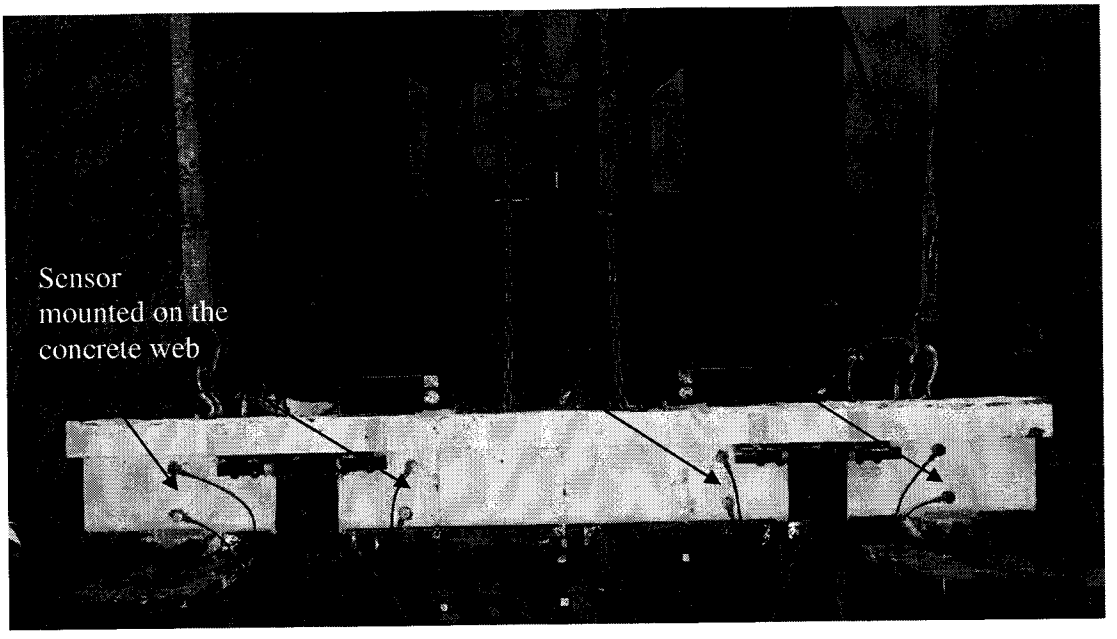

Figure A.7 Sensors distribution of beam B-2

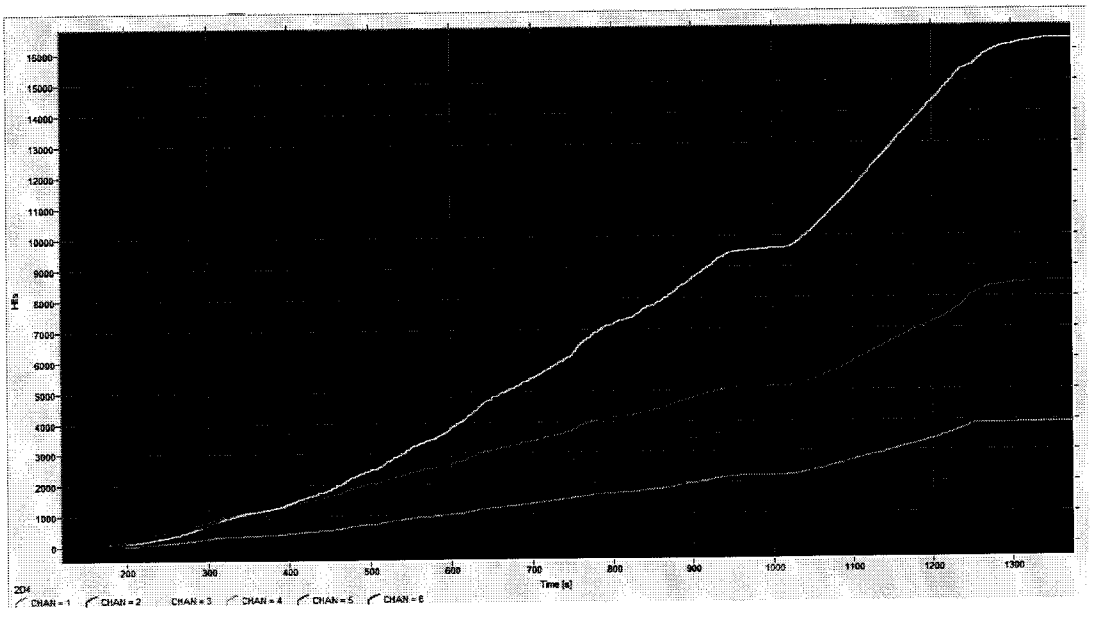

Figure A.8 Instantaneous hits on all channels versus time of beam B-0 (WINS, March 2009)

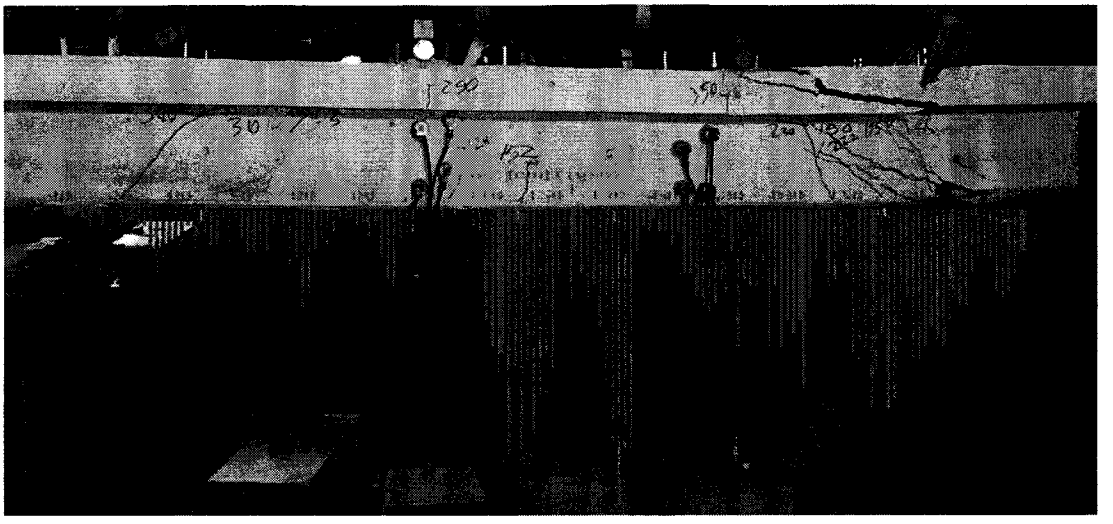

Figure A.9 Located AE activities of beam B-0

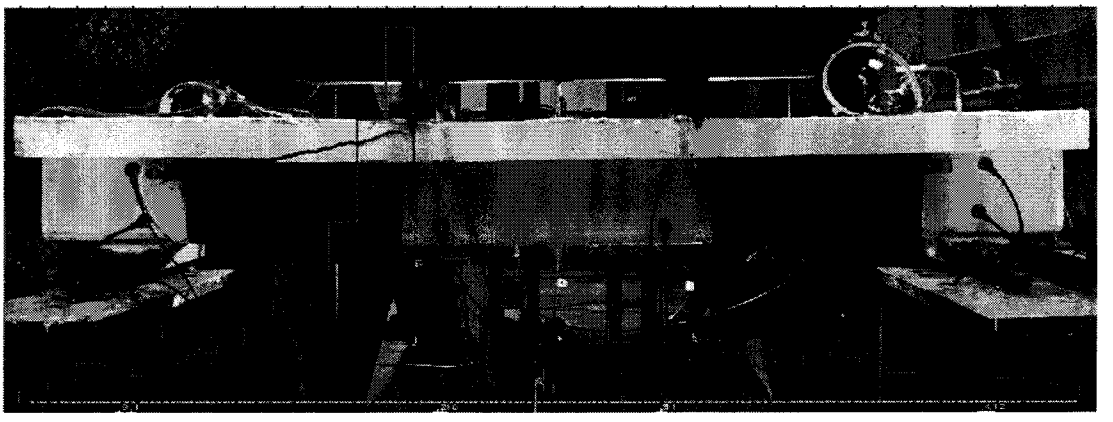

Figure A.10 Located activities of beam B-1

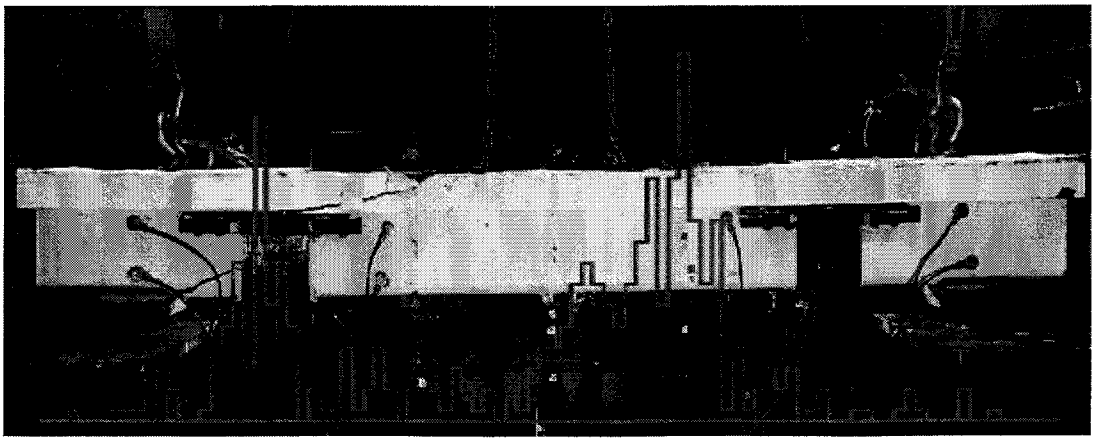

Figure A.11 Located activities of beam B-2